



Forschungszentrum Karlsruhe
in der Helmholtz-Gemeinschaft

Wissenschaftliche Berichte
FZKA 7336

Investigation of a Physical Disinfection Process Based on Pulsed Underwater Corona Discharges

S. B. Gupta

**Institut für Hochleistungsimpuls- und
Mikrowellentechnik**

September 2007

Forschungszentrum Karlsruhe

in der Helmholtz-Gemeinschaft

Wissenschaftliche Berichte

FZKA 7336

**INVESTIGATION OF A PHYSICAL DISINFECTION
PROCESS BASED ON PULSED UNDERWATER
CORONA DISCHARGES**

Suryakant Balkrishan Gupta

Institut für Hochleistungsimpuls-
und Mikrowellentechnik

Von der Fakultät für Elektrotechnik und Informationstechnik
der Universität Karlsruhe (TH) genehmigte Dissertation

Forschungszentrum Karlsruhe GmbH, Karlsruhe
2007

Für diesen Bericht behalten wir uns alle Rechte vor

Forschungszentrum Karlsruhe GmbH
Postfach 3640, 76021 Karlsruhe

Mitglied der Hermann von Helmholtz-Gemeinschaft
Deutscher Forschungszentren (HGF)

ISSN 0947-8620

urn:nbn:de:0005-073362

INVESTIGATION OF A PHYSICAL DISINFECTION PROCESS BASED ON PULSED UNDERWATER CORONA DISCHARGES

Zur Erlangung des akademischen Grades eines

DOKTOR – INGENIEURS

von der Fakultät für
Elektrotechnik und Informationstechnik
der Universität Karlsruhe (TH)

genehmigte

DISSERTATION

von

Suryakant Balkrishan Gupta MSc.
aus Ahmedabad (India)

Tag der mündlichen Prüfung:

28. Juni 2007

Hauptreferent:

Prof. Dr. -Ing. H. Bluhm

Korreferent:

Prof. Dr. -Ing. T. Liebfried

Investigation of a physical disinfection process based on pulsed underwater corona discharges

Abstract

To overcome the side effects of commonly used water disinfection methods based on chemicals, advanced oxidation processes (AOP's) are presently considered as an alternative. These processes are based on the effect of highly reactive oxidants (like ozone, OH radicals, H₂O₂, et.) on microorganisms and toxic organic compounds. In this work the effects and products from pulsed underwater corona discharges have been investigated for their potential to remove contaminants from the water. Pulsed underwater corona discharges create oxidative and reductive species, UV radiation, shock waves and strong electric field at the tip of propagating streamers. It has been supposed that the combined appearance of these effects leads to an effective destruction of contaminants in the water.

It was the aim of this work to quantify the production rates of oxidants and the intensity of other effects from underwater corona discharges, to demonstrate their effectiveness for the inactivation of microorganisms and to propose a suitable corona reactor that is scalable to large throughputs.

For that purpose a coaxial corona reactor was designed with a central anode covered by a thin (200-300 μm) porous ceramic layer. The conductive porous ceramic and the anode cathode water gap form a parallel resistive-capacitive voltage divider. For times greater than the dielectric relaxation time of the water ($\tau = \epsilon\epsilon_0/\sigma$) resistive voltage division dominates and the electric field at the ceramic layer can be more enhanced than in the case of capacitive voltage division. Applying a pulsed voltage of 30-50 kV for a duration of 200-400 ns to the anode a large number of streamers is launched homogeneously from the ceramic surface extending up to 10 mm into the anode cathode water gap. An L-C chain Blumlein configuration has been selected to generate the pulses. By changing the number and the values of the LC elements the impedance of the generator and its pulse width could easily be adapted to the requirements of the experiment. Different ceramic layers were tried, but the best results were obtained with almandine which has a very low pH value at its isoelectric point.

The number and the length of streamers increased linearly with the anode voltage. The reactor impedance was mainly determined by the water conductivity. Little influence from the appearance of streamers was observed.

A large number of chemical probes have been selected to measure the oxidant production quantitatively. OH and H radicals created in core of a streamer channel are the most important primary products. As the channel cools down they recombine or form secondary products like H_2O_2 and H_2 . H_2O_2 accumulates in the bulk water and becomes a source of additional OH radicals due to the interaction with UV radiation and the liberation of Fenton reagents from the anode. Therefore, H_2O_2 plays an important role in the disinfection process. Using DNTA as a chemical probe for OH radicals combined with an OH scavenger and measuring the H_2O_2 yield simultaneously the initial OH radical concentration at the position of the cold streamer was found to be 30 mM.

Different gases were percolated through the reactor to enhance the oxidant production. Saturating the water with N_2O it was also possible to prove the existence of solvated electrons in the water after the formation of streamer discharges. In addition it was shown that that shock waves launched from propagating streamer channels also contribute to the production of OH radicals.

Exposing gram negative bacteria (*Pseudomonas putida*) to the corona discharges it was demonstrated that they can be successfully used for water disinfection. With the experimental reactor set-up used in this thesis an inactivation by 6 logsteps was achieved for a specific energy deposition of 20 J/cm^3 . It is suggested that an optimised system exploiting the effects from percolating gases or Fenton's reagents can lower this value appreciably.

Untersuchungen zu einem physikalischen Desinfektionsverfahren auf der Basis gepulster Unterwasserkoronaentladungen

Zusammenfassung

Um die unerwünschten Nebeneffekte herkömmlicher chemischer Verfahren zur Desinfektion von Wasser zu vermeiden, werden gegenwärtig sogenannte fortgeschrittene Oxidationsverfahren (advanced oxidation processes AOP's) als Alternative entwickelt. Diese Verfahren basieren auf der Wirkung starker Oxidationsmittel wie Ozon, OH-Radikale, Wasserstoffsuperoxid etc., auf Mikroorganismen und toxische organische Verbindungen. In dieser Arbeit wurde das Potential der Produkte und Effekte gepulster Unterwasserkoronaentladungen für die Beseitigung von Kontaminanten in Wasser untersucht. Gepulste Unterwasserkoronaentladungen erzeugen oxidierende und reduzierende Substanzen, UV-Strahlung, Stoßwellen und starke elektrische Felder an der Spitze der propagierenden Streamer. Es wurde vermutet, dass das kombinierte Auftreten dieser Effekte zu einer wirksamen Zerstörung der Kontaminanten in Wasser führt.

Ziel dieser Arbeit war es, die Produktionsrate der Oxidantien und die Stärke der anderen Effekte zu quantifizieren, ihre Wirksamkeit für die Inaktivierung von Mikroorganismen zu demonstrieren und einen geeigneten, zu großen Durchsätzen skalierbaren Koronareaktor, vorzuschlagen.

Zu diesem Zweck wurde ein koaxialer Koronareaktor mit einer keramisch beschichteten Anode entworfen. Dabei hatte die poröse Keramiksicht eine Stärke von 200-300µm. Die leitfähige poröse Keramiksicht und der Wasserspalt zwischen Anode und Kathode bilden einen parallelen kapazitiven und resistiven Spannungsteiler. Für Zeiten, die größer als die dielektrische Relaxationszeit des Wassers ($\tau = \epsilon\epsilon_0/\sigma$) sind, dominiert die resistive Teilung und das elektrische Feld in der Keramiksicht ist stärker erhöht als im Falle einer rein kapazitiven Teilung. Mit einer Pulsspannung von 30-50kV und einer Pulsdauer von 200-400 ns kann eine große Anzahl von Streamern, homogen über der Anodenoberfläche verteilt

und mit einer Ausdehnung von ca. 10 mm in den Anoden-Kathoden-Wasserspalt, hervorgerufen werden. Für die Erzeugung dieser Pulse wurde ein LC-Kettenleiter in einer Blumlein-Anordnung gewählt. Durch Änderung der Anzahl und der Werte der LC-Elemente konnten die Impedanz des Generators und die Pulsdauer einfach den Erfordernissen des Experiments angepasst werden. Es wurden verschiedene Keramiksichten untersucht, aber die besten Ergebnisse wurden mit Almandine erzielt, das einen sehr niedrigen pH-Werts an seinem isoelektrischen Punkt aufweist.

Die Anzahl und die Länge der Streamerkanäle wächst linear mit der Anodenspannung. Die Reaktor-Impedanz ist hauptsächlich durch die Leitfähigkeit des Wassers - bestimmt, das Auftreten der Streamer besitzt einen nur geringen Einfluss.

Eine Vielzahl chemischer Sonden wurde eingesetzt, um die Produktion der Oxidantien quantitativ zu messen. OH und H Radikale, die im Inneren des Streamerkanals gebildet werden, sind die wichtigsten Primärprodukte. Wenn sich der Kanal abkühlt, rekombinieren sie oder bilden Sekundärprodukte wie H_2O_2 und H_2 . H_2O_2 reichert sich im Wasser an und wird dadurch zu einer zusätzlichen Quelle für OH-Radikale aufgrund der Wechselwirkung mit UV-Strahlung und der Freisetzung von Fenton-Reagenzien aus der Anode. Daher spielt H_2O_2 eine wichtige Rolle im Desinfektionsprozess. Durch Verwendung von DNTA als chemische Sonde für OH-Radikale in Kombination mit einem Fänger für OH-Radikale und durch gleichzeitige Messung der H_2O_2 -Ausbeute konnte die anfängliche Konzentration der OH-Radikale an der Position des kalten Streamers zu 30 mM bestimmt werden.

Unterschiedliche Gase wurden durch den Reaktor geleitet, um die Ausbeute an Oxidantien zu erhöhen. Durch Sättigung des Wassers mit N_2O war es auch möglich, die Existenz hydratisierter Elektronen im Wasser nach Streamerentladungen nachzuweisen. Zusätzlich konnte gezeigt werden, dass die von propagierenden Streamerkanälen ausgesandten Stoßwellen ebenfalls zur Erzeugung von OH-Radikalen beitragen.

Der Wirkung von Koronaentladungen ausgesetzte gram-negative Bakterien (*Pseudomonas putida*) konnten effektiv abgetötet werden. Mit dem in dieser Dissertation verwendeten experimentellen Reaktoraufbau konnte eine Inaktivierung von 6 Logstufen bei einem spezifischen Energieeinsatz von 20 J/cm^3 erreicht werden. Es ist anzunehmen, dass ein optimiertes System, das die Effekte durch strömende Mikrogasblasen oder Fenton-Reagenzien ausnutzt, diesen Wert noch erheblich reduzieren kann.

CONTENTS

1. Introduction	1
2. Physical and Chemical Processes in Underwater Streamer Discharges	6
2.1 Physical processes	6
2.2 Chemical processes	18
3. Experimental Methods	24
3.1 The pulse generator	24
3.2 Electrical diagnostics	26
3.3 The corona reactor	27
3.4 Anode coatings	29
3.5 Diagnostics of oxidants	31
3.5.1 Photometric diagnostics	31
3.5.2 Hydroxyl radicals	31
3.5.3 Hydrogen peroxide	39
3.5.4 Ozone	40
3.6 Diagnostic for reductive species	43
3.6.1 <i>Solvated electrons</i>	43
3.6.2 <i>Super oxide ions</i>	43
3.7 UV diagnostics	44
3.7.1 <i>Spectroscopy</i>	45
3.7.2 <i>Chemical actinometry</i>	47
3.8 Diagnostics of bactericidal effectiveness	49
3.8.1 <i>Epifluorescence microscopy</i>	50
3.8.2 <i>Heterotrophic plate counting (HPC)</i>	51
4. Results	53
4.1 Electrical and optical observations	53
4.2 Oxidant production	70

4.2.1.	<i>OH radicals</i>	70
4.2.2.	<i>Influence of reagent concentration</i>	72
4.2.3.	<i>Relation between oxidant yield and streamer volume</i>	79
4.2.4.	<i>Effect of anode material</i>	81
4.2.5.	<i>Influence of ceramic coatings</i>	84
4.2.6.	<i>Anode aging</i>	85
4.2.7.	<i>Effect of electrode surface area</i>	86
4.2.8.	<i>Effect of dissolved and percolating gases</i>	88
4.2.9.	<i>Distribution of oxidants</i>	90
4.2.10.	<i>Combination with Fenton's reaction</i>	93
4.2.11.	<i>Oxidation of organic molecules</i>	95
4.2.12.	<i>Comparison of H₂O₂ yields</i>	96
4.2.13.	<i>Dependence of H₂O₂ production on conductivity and pH</i>	96
4.2.14.	<i>Ozone yield</i>	98
4.3	Reductive species	99
4.3.1.	<i>Aqueous electrons</i>	99
4.3.2.	<i>Super oxide ions</i>	100
4.4	UV measurements	101
4.4.1.	<i>Spectroscopy</i>	101
4.4.2.	<i>Actinometry</i>	102
4.5	Cavitation effects	104
4.6	Disinfection experiments	107
4.6.1	<i>Epifluorescence microscopy</i>	107
4.6.2	<i>Heterotrophic plate counting (HPC)</i>	108
5.	Discussion	111
6.	Conclusions	122
7.	References	126
8.	Appendix	134

List of Abbreviations

AOP	Advanced oxidation processes
CCA	Coumarine-3-carboxylic acid
CFU	Colony forming unit
CTC	5-cyano-2, 3-ditoly tetrazolium chloride
DAPI	4', 6-diamidino-2-phenylindole
DBP	Disinfection by-product
DNA	Deoxyribonucleic acid
DNTA	Terephthalic acid di-sodium salt
HAA	Haloacetic acid
HPC	Heterotrophic plate counting
HPLC	High performance liquid chromatography
HTA	Hydroxyterephthalic acid
IEP	Isoelectric point
NBT	Nitro blue tetrazolium chloride
NDMA	<i>N</i> -nitrosodimethylamine
PBS	Phosphate buffer saline
pCBA	Para-chlorobenzoic acid
PTFE or Teflon	Polytetrafluoroethylene
SEM	Scanning electron microscope
THM	Trihalomethanes
tBuOH	Tertiary Butanol
UV	Ultraviolet
UV-VIS	Ultraviolet visible
XRD	X-ray diffraction

List of symbols

Φ_{λ}	Quantum yield
$\bullet\text{H}$	Atomic hydrogen
$\bullet\text{HO}_2$	Hydroperoxyl radical
O	Atomic oxygen
$\bullet\text{OH}$	Hydroxyl radical
A	Absorbance
Al_2O_3	Alumina oxide
C	Concentration of absorbing molecules in the sample
C	Capacitance
C_{ceramic}	Capacitance of porous ceramic layer
C_{water}	Capacitance of water layer
E	Spectral irradiance
e_{aq}^-	Aqueous electrons
$\text{Fe}_3\text{Al}_2(\text{SiO}_4)_3$	Ferrous aluminium silicate (Almandine)
$G_{\text{H}_2\text{O}_2}$	Hydrogen peroxide production yield
G_{OH}	OH radicals production yield
G_{Ozone}	Ozone production yield
H_2O_2	Hydrogen peroxide
I	Transmitted light
I_0	Incident light
J	Joule
k	Reaction rate constant
l	Length
L	Inductance
L	Liter
$\text{O}_2^{\bullet-}$	Super oxide ions
Pa	Pascal
pKa	Acid dissociation constant
T	Time
Ti	Titanium
TiO_2	Titanium oxide
ϵ	Absorption coefficient
λ	Wavelength
λ_{em}	Emission wavelength
λ_{ex}	Excitation wavelength
σ	Conductivity

1. INTRODUCTION

Water and wastewater processing technologies become increasingly important with diminishing natural water resources, the gradual increase of chemical pollutants in aqueous systems, and the rapid growth of population & industrial activities. Biological methods are most commonly used for wastewater treatment. However toxic and non-biodegradable pollutants cannot be treated by these methods alone. Still the most widely used water disinfection method is chlorination. Its technology is well established and it is very cost effective. However, by using chlorine as a disinfection tool harmful secondary carcinogenic disinfection by-products (DBP) can be formed which are not easily biodegradable. This is especially true if the water contains a large organic freight. Based on various studies it is confirmed that disinfection by-product (DBP) chemicals, including *N*-nitrosodimethylamine (NDMA), trihalomethanes (THMs) and haloacetic acids (HAAs), are formed from naturally occurring organic substances. Studies have shown that regular consumption of these DBPs can cause bladder or rectal cancer, increase the risk of miscarriage in women, birth defects and fetal growth restriction, and it can adversely affect the brain, eyes and other major organs as well [1-5].

Advanced oxidation processes (AOP): Advanced Oxidation Processes (AOP) are considered to be an alternative method to chlorination. In an Advanced Oxidation Process, chemical, electrical or radiative energy is supplied to the water matrix to produce highly reactive oxidants, which can attack and destroy the target compound(s) [6]. Usually AOPs are ambient temperature treatment processes which are primarily based on the formation of highly reactive radicals. Especially the OH radical plays an important role as the primary oxidant in these processes. The OH radical is the strongest oxidizing specie used in water and wastewater treatment. Because of its large redox potential it greatly accelerates the rate of contaminant oxidation (Table 1).

Table 1. Redox potential of different oxidants used in water treatment.

Oxidants Species	Redox potential (V)
Hydroxyl radicals	2.80
Ozone	2.07
Hydrogen peroxide	1.78
Permanganate	1.69
Chlorine dioxide	1.56
Chlorine	1.36
Oxygen	1.23

The major AOPs for water treatment are UV radiation, ozone, H₂O₂, and various combinations of UV, ozone, and H₂O₂ [7]. In addition cavitation by ultrasound (sonolysis) [8, 9], high energy electron beams [10, 11] and underwater discharges [12] have been applied. Membrane filtration, which does not fall into the category of AOPs, is also an emerging disinfection process free of chemicals [13]. A brief comparison of these methods is discussed in the following.

UV: UV radiation for industrial water treatment is produced by large arrays of UV-lamps. It is absorbed by the DNA of microorganisms present in the water. The absorbed UV radiation can disrupt the “basic pair” structure of the DNA in such a way that the DNA can not replicate in cell mitosis (nuclear division) and thus eventually leads to cell death [14, 15]. But the penetration depth of UV radiation in turbid water is limited and a low dosage of UV is not effective for some microorganisms and some studies have shown that self repair of DNA damage can occur [16].

Ozone: Ozone gas, externally produced by electrical discharges in oxygen, is injected into the aqueous system. Ozone is formed through a combination of atomic oxygen (O) and molecular oxygen (O₂). The reaction is endothermic and requires a considerable amount of energy. More than two thirds of the electrical energy applied to an ozone generator is lost as heat.



It is a powerful disinfectant that destroys microorganisms through direct oxidation. Typical contact times necessary for water disinfection are between 10 and 30 minutes. But ozone has a low solubility in water and besides the ozonizer an efficient gas mixing system is required, which further consumes energy. Higher temperatures reduce the solubility of ozone in the water.

The ozone gas leaving the water needs to be reprocessed. Low ozone dosage may not effectively inactivate some microorganisms. Due to its toxicity and instability, ozone is usually generated at the treatment site. Ozone is very reactive and corrosive. Therefore corrosion – resistant materials have to be used. Moreover at alkaline pH and at elevated temperatures it decays very fast. The effectiveness of ozone can be increased by combining it with hydrogen peroxide or/and UV-radiation [17, 18].

Ozone + H₂O₂ [Peroxone]: H₂O₂ reacts with ozone, and produces OH radicals. At higher pH, the OH radical yield increases [19]. An ozone reprocessing system is required to recycle the unused gas. Being a strong oxidant special storage tanks are needed for hydrogen peroxide. Moreover it gradually deteriorates during storage.

Ozone + UV-radiation: UV radiation can lead to excitational decomposition of ozone into O_2 and atomic oxygen O . Atomic oxygen can further react with water molecules and create OH radicals. [20] This process is however less economical than the O_3/ H_2O_2 or the H_2O_2 / UV process.

H_2O_2 + UV-radiation: When UV photons are absorbed by H_2O_2 dissolved in water hydroxyl radicals can be formed, again by excitational decomposition. The UV/hydrogen peroxide process (or UV-oxidation), is an efficient disinfection processes [21]. But water turbidity influences the OH radical production.

Ultrasound (sonolysis): Ultrasound can produce micro bubbles in water due to cavitation effects. These microbubbles implode violently, generate a hot plasma in its interior and thus produce OH radicals. Ultrasound treatment is simple in operation and byproducts are absent. But this process has a low energetic efficiency for water disinfection. According to pilot plant studies supplemental oxidants such as UV, ozone or hydrogen peroxide are required [22-25].

High energy electron beams: Using intense electron beams with particle energies of several MeV water disinfection can be achieved by two mechanisms: Energetic electrons can either interact directly with microorganisms and destroy their DNA or other vital cell structures or they can break-up the water molecules and form radicals. Electron beam treatment is considered to be an environmentally friendly disinfection technology which does not require any additional external chemicals. At present pilot plants are in operation in the United States, Russia, Brazil, and a few other countries [26-28]. The depth of treatment depends on the electron range in water which for 10 MeV electrons is of the order of several centimetres. This electron range limits the thickness of water layers that can be treated. However, unlike in UV-treatment water turbidity is of minor importance. But electron beams require special radiation shielding arrangements.

Membranes: The use of membranes for water disinfection is a new emerging technology. [29] Like the AOPs described before it is a method free of additional chemicals. Membrane filtration can be broadly defined as a separation process that uses semi-permeable membranes to divide the feed stream into two portions: a permeate flux that contains the material passing through the membranes and a retentate, consisting of species being left behind. The ability of membrane filters to remove various pathogenic bacteria from drinking water depends upon the basis of size of pore present in the membrane. Typically the membrane pore size is kept below 10 μm for microbiological applications. For the finest membranes the typical pore size is $< 0.001 \mu m$ and a trans-membrane pressure of the order between 5-8 MPa is required. To avoid fouling (mineral, organic, or microorganisms) on the

membrane surfaces, regular cleaning is necessary. Also in due course of time the permeate flux declines and the membranes have to be replaced.

Ideally AOP systems are designed to completely mineralize the organic contaminants of concern to CO_2 and H_2O but this may require more energy and greater chemical dosage and ultimately may prove to be cost prohibitive in certain applications [30]. Moreover by increasing one oxidant concentration can lead to the formation of other DBPs. Also as described above each method has certain inherent limitation. Therefore, more sophisticated and efficient treatment processes are necessary to preserve the natural environment.

Pulsed underwater corona discharges promise to overcome some limitations of existing AOPs for water disinfection. This method is free of additional chemicals, and therefore environmental friendly. However its energetic efficiency needs to be assessed. In a pulsed underwater corona discharge propagating plasma channels (also termed streamers) are created. Previous researchers have shown that electrons present in the plasma channels can dissociate water molecules and produce various reactive radicals ($\cdot\text{OH}$, $\text{H}\cdot$, O , and $\text{HO}_2\cdot$) and molecular species such as H_2O_2 , H_2 , & O_3 as well. Apart from these chemical oxidants, solvated electrons, UV-radiation, and strong electric fields at the streamer tip appear. In addition, expansion of the plasma channel against the surrounding water generates intense shock waves, with pressure amplitudes of the order of hundreds of MPa. The resulting shockwaves also help to induce free radical reactions indirectly via electro hydraulic cavitations. It is supposed that a possible synergy between these effects makes pulsed corona discharge treatment of water an efficient disinfection method [31-35].

As stated earlier pulsed underwater corona discharges comprise different oxidant generation mechanisms. Oxidant formation and subsequent reactions between different oxidant species and between oxidants and water molecules or gases dissolved in water take place simultaneously. Hence to understand the complex reaction kinetics is required to control the production of desired species and their distribution in the water. The lifetime of most oxidants is so short that conventional radical detection methods cannot be used. To extend underwater corona discharges to a large-scale water purification technology the following aspects need further consideration:

- Design and development of a suitable corona reactor concept which is scalable to the treatment of large water throughputs and which gives hope of achieving a long operational life.
- Development of a robust rep-ratable high voltage pulse generator as a driver for the corona reactor.

- Quantitative measurement of oxidant production inside and outside the streamer channels. This includes:
 - Selection and verification of suitable diagnostic methods.
 - Determination of the dependence of different oxidant production rates on electrical parameters and water conditions (conductivity, pH-values, dissolved gases, etc.).
- Demonstration of the disinfection efficiency for certain selected bacteria and investigation of operating parameters on these results.

It is the aim of this thesis to contribute to the solution of these points. It is mainly based on experimental results obtained with a special corona reactor that used an anode covered by a thin porous ceramic layer:

In chapter 2 we summarize the present knowledge of pulsed underwater corona discharges, and present a model that describes the formation and propagation of streamers. Also a perception of oxidant formation inside the plasma channel and in a reaction zone surrounding it is presented.

In chapter 3 the experiment methods and the diagnostics are described. Chapter 4 presents the experimental results. In chapter 5 the results are interpreted and in chapter 6 some conclusions are drawn with respect to large scale applications of underwater corona discharges and areas that require further research and development are pointed out.

2. PHYSICAL AND CHEMICAL PROCESSES IN UNDERWATER STREAMER DISCHARGES

2.1 Physical processes

Electrical discharges: An electric discharge is defined as a passage of electric current through a dielectric material. This can happen when any dielectric material i.e. gas, liquid or solid is exposed to strong electric fields. During this process the electric conductivity of the discharge path can increase by several orders of magnitude. More precisely, in an electric discharge the free charge carriers are multiplied by a local ionization avalanches as long as the local electric field is high enough. However, conducting matter can redistribute its space charge and hence modify the externally applied electric field. Depending on the spatial distribution of the ionized areas, the ionization reaction then is enhanced at some places and suppressed at others. Generally electric discharges in gaseous or liquid media are of more interest than discharges in solids, because in gaseous or liquid media these discharges are of self-repairing nature, i.e. they can recover their previous strength after the discharge [36]. During the electric discharge process the conducting path becomes a plasma channel. Electric discharges in gases can be initiated at lower field strength than in liquids because their density is lower than that of liquids. In gaseous media electrons have longer mean free paths and ionising avalanches appear at much lower electric fields. Inducing an electric discharge in a liquid can disintegrate it into basic compounds. Water can be dissociated and oxidants may be produced. Primarily liquid discharges can be divided into spark and corona discharges.

Streamer discharges: When a sufficiently high electric field is applied to a metallic electrode streamer channels originate from its surface. These streamer channels are of gaseous nature and electron avalanches can occur in their interior creating a conductive plasma that transports the electrode potential towards the streamer tip. If the electric field at the streamer tip becomes sufficiently strong, field induced ionisation and dissociation enhances the conductivity in front of the streamer head and the streamer begins to self-propagate until the voltage drop inside the streamer channel reduces the electric field at the tip below a critical value.

Spark discharges: If a streamer channel bridges the gap between the electrodes an increasing current begins to flow through it which continuously heats the channel and reduces its resistance to very small values. Thus within a very short time a large amount of energy can be deposited along the channel leading to intense light emission and strong shock waves.

In this thesis we only deal with streamer discharges. Depending on the polarity we distinguish between negative or positive streamers originating from the cathode and anode respectively. In water positive filamentary streamers are easier to create. Therefore only positive streamers are considered in this work. One possibility to restrict the streamer length and to prevent arcing is to limit the duration of the driving voltage pulse. An important consequence of the brief pulse duration is that it minimizes energy dissipation due to ohmic losses in the conductive water.

Specifics of underwater pulsed corona discharges: Various configurations for the initiation of corona discharges in water have been described in the literature. A selection of these configurations has been reproduced in Fig. 2.1. For basic studies on streamer properties point-plane geometries (Fig. 2.1-A) are well suited [12, 37, 38]. In these set-ups a thin sharp needle is applied as one electrode and a plate or disk as the counter electrode. In general both electrodes are submerged into the liquid. In some cases a hypodermic needle has been utilized instead of a solid pin and gas was bubbled through it [39, 40]. Circulating oxygen through the needle led to an increased production of ozone in the discharge. The point plane geometry is inappropriate for industrial applications because only very restricted volumes can be treated and the lifetime of the needle is rather limited.

A variant of the point-plane geometry is depicted in Fig. 2.1-[B]. Here the needle electrode is located in the gas plenum above the water while the plate electrode sits in the water. The corona discharge originates in the gas. Oxidants that may have been created in the gas phase must migrate into the liquid to become effective [41, 42]. In the hybrid configuration of Fig. 2.1- [C] streamers result both in the liquid phase and in the gas phase [43]. Here the ground electrode is placed at the interface between gas and liquid and the needles in the gas and in the water may be supplied from the same pulse generator although care must be taken not to create an arc discharge in the gas plenum.

A different type of reactor is based on a diaphragm discharge (Fig. 2.1-[D]). In this configuration the HV electrodes are separated by an insulating disk, which is made from quartz or alumina containing a pinhole of a few μm diameters in its centre. When a high voltage pulse is applied to the electrodes, due to the ionic conductivity of the water, polarization occurs across the diaphragm, and the applied voltage drops across it leading to strong electric fields in the pinhole and finally to the development of a streamer [44, 45].

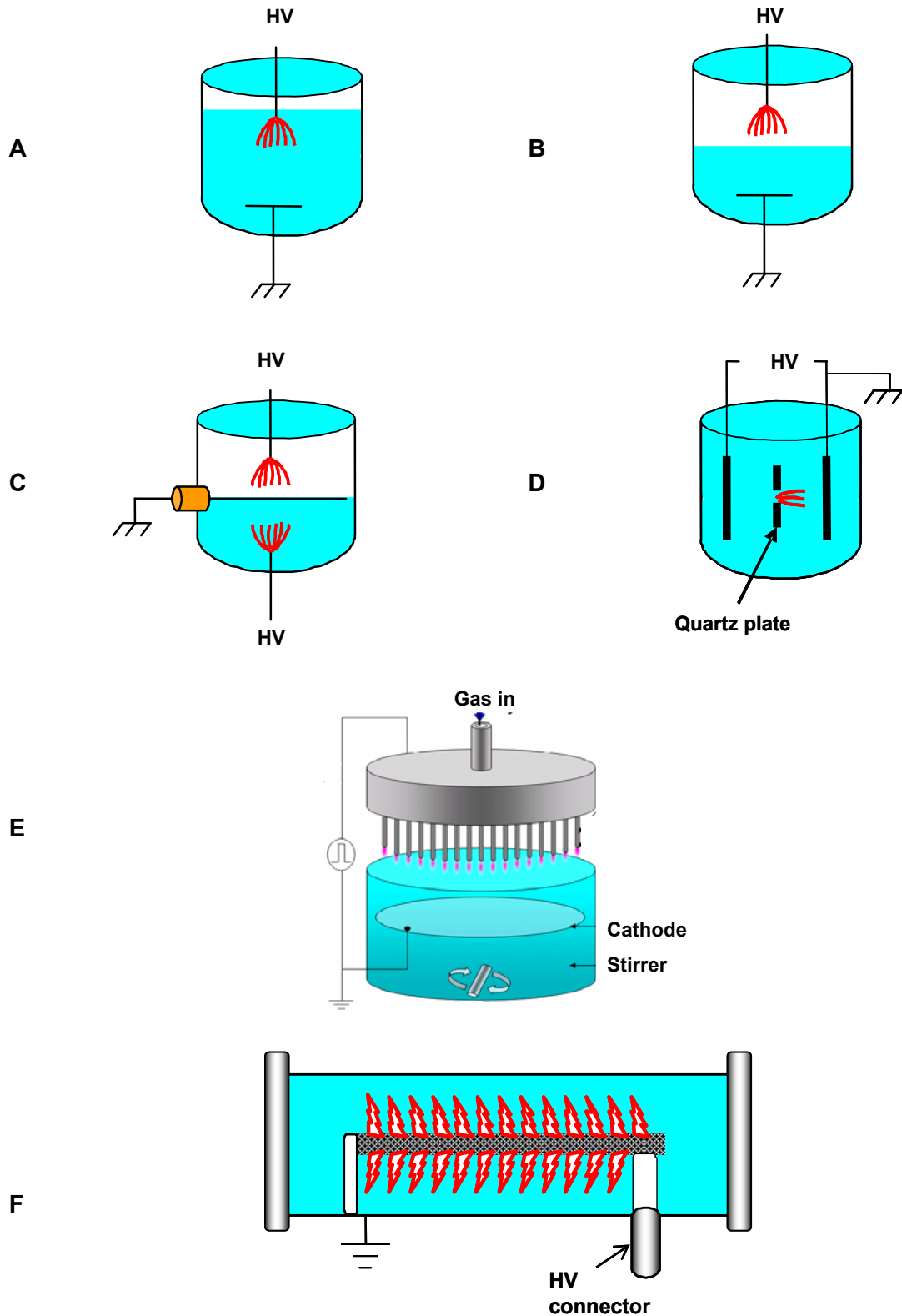


FIG. 2.1. Different configurations for the initiation of streamer discharges in water. [A] Point-plane geometry for liquid phase corona discharges. [B] Point-plane geometry for glow discharge initiation in the gas plenum above the water. [C] Hybrid geometry for simultaneous streamer discharge initiation in the water and in the gas plenum. [D] Streamer discharge originating from a diaphragm. [E] Multi-pin reactor configuration. [F] Coaxial pulsed underwater corona reactor with anode covered by a porous ceramic layer.

To overcome the wear of needle electrodes suspended in water a solution has been proposed by M/s Toshiba Corporation, Japan (Fig. 2.1-[E]) where 1000 hollow needles were mounted above the water surface and a gas mixture was passed through them [46]. Since the corona discharge took place in the gas phase it was necessary that any oxidants produced in the gas diffuse into the water through the surface to become effective. However because of the short diffusion length of oxidants in water only a thin surface layer can be affected. Generally we can conclude that pulsed corona discharges inside the water provide a more efficient utilization of oxidants.

To overcome the deficiencies of the configurations described above we have selected the set-up presented in Fig. 2.1-[F] for our investigations in this thesis. Here hundreds of streamers are created simultaneously from an anode covered by a porous ceramic layer. The oxidants as well as the other physical effects are produced inside the water and react simultaneously. The system seems scalable to large throughputs and the electrodes have the potential to operate for long time without maintenance [12]. As indicated in Fig. 2.1-[F] a large fraction of the reactor volume comes into direct contact with the effects resulting from the streamers.

Streamer model: In the streamer channel only free electrons gain energy and since the equilibration time is much longer than the active lifetime of the channel ions and neutrals remain cold. Therefore a non-equilibrium plasma is established inside the streamer channels. Electron collisions with water molecules are considered to be the main source of oxidant production inside the channels. However the details of streamer initiation and propagation in water and the concurrent and subsequent formation of active chemical species are currently not completely understood. In the following sections we summarize our present knowledge on streamer initiation and propagation in water. Initiation from metallic as well as ceramic surfaces is considered. Finally we draw some preliminary conclusions related to the production of oxidants.

Primary Streamers: If the electric field at a metallic tip exceeds a certain threshold value a tree-like filamentary structure is observed as shown in the upper left corner of Fig. 2.2. This structure is called the primary streamer. Its filaments are characterized by a very weak light emission and a negligible conductivity. They do not disturb the initial electric field configuration. The symmetry and size of this primary streamer are largely determined by the field distribution at the anode tip. High resolution images suggest that they consist of small bubbles. It is believed that these bubbles can form in the water due to field induced phase instabilities [37]. However other mechanisms have been discussed as well in the literature [47-52]. The bush like hemispherical primary streamer shown in Fig. 2.2 consists of 100-200 radial filaments which expand at a supersonic speed of 2.5 km/s.

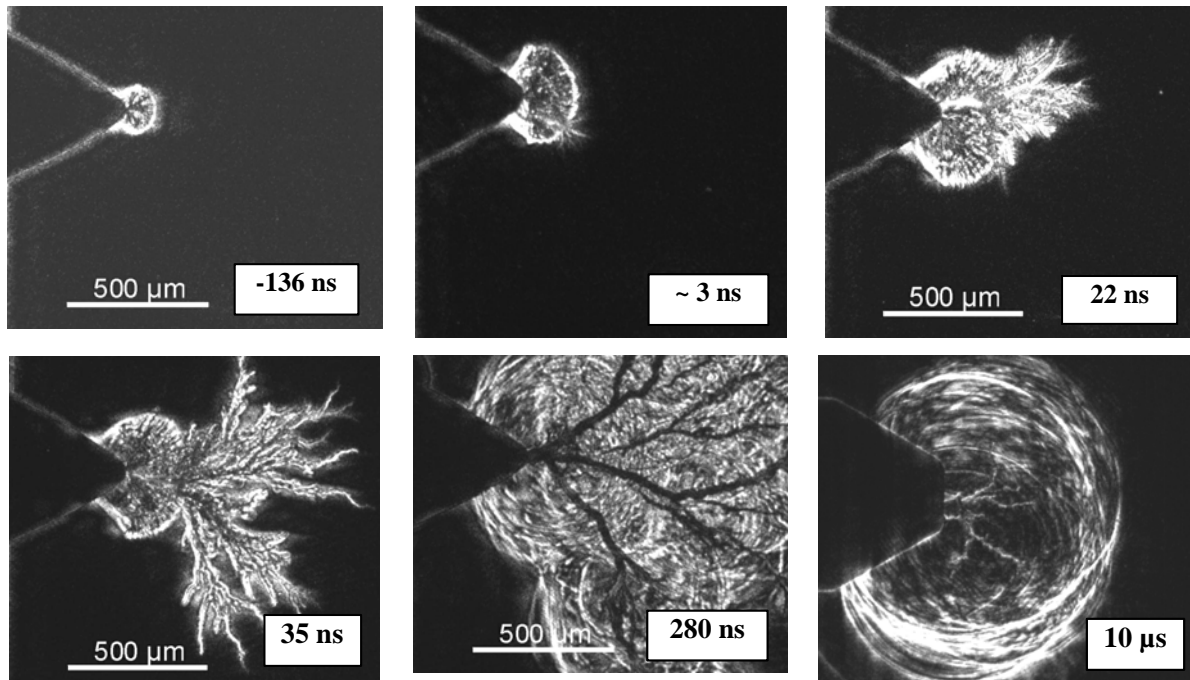


FIG. 2.2. Schlieren images of streamer development from a point anode. Here $t=0$ is the time when the secondary streamer starts. [a – sign represents the time before the initiation of the secondary streamer [37].

Secondary streamers: As time progresses the primary streamer filaments expand and the density inside the channels reduces. At some point the conditions for electron avalanche formation are reached. This appears first at the foot (i.e. base) where the field strength is highest and the density is lowest and then propagates in one of the filamentary channels offering the most favourable conditions towards the rim of the primary streamer. Electron avalanching in the channel increases the conductivity and transports the potential of the metallic tip to the head of the channel. In general this is accompanied by a strong field enhancement establishing conditions for the initiation of a self-propagating secondary streamer.

Streamer initiation from a porous ceramic layer: Macroscopic electric fields above $1\ \text{MV/cm}$ are needed to initiate a primary streamer in water, which is the less stringent pre-condition for secondary streamer formation and propagation. Manageable voltages can reasonably realize such high field strengths only by using field enhancement effects at point tips, thin wires, or across a thin layer of porous dielectric material [12]. At spherical point tips the electric field strength E is proportional to U/r_c (here U is the applied voltage, and r_c is the radius of the wire tip). It has already been pointed out that sharp needles cannot be used for industrial water processing because of limitations in the needle erosion and in the treatable volume. A more suitable solution seems to launch the streamers from an anode, coated with a thin layer of porous ceramic.

For pulse duration τ shorter than the dielectric relaxation time $\varepsilon\varepsilon_0/\sigma$, water behaves like a dielectric but for $\tau \gg \varepsilon\varepsilon_0/\sigma$ it can be considered as a resistive medium. In the frequency range of interest here the permittivity of water is 81 while it becomes 8 to 10 for ceramic [53, 54]. The conductivity of porous ceramic is determined by the geometry and the number of water filled pores connecting the metallic anode surface with the bulk water. Since this conductivity can be kept small we obtain a field enhancement in both time domains considered above.

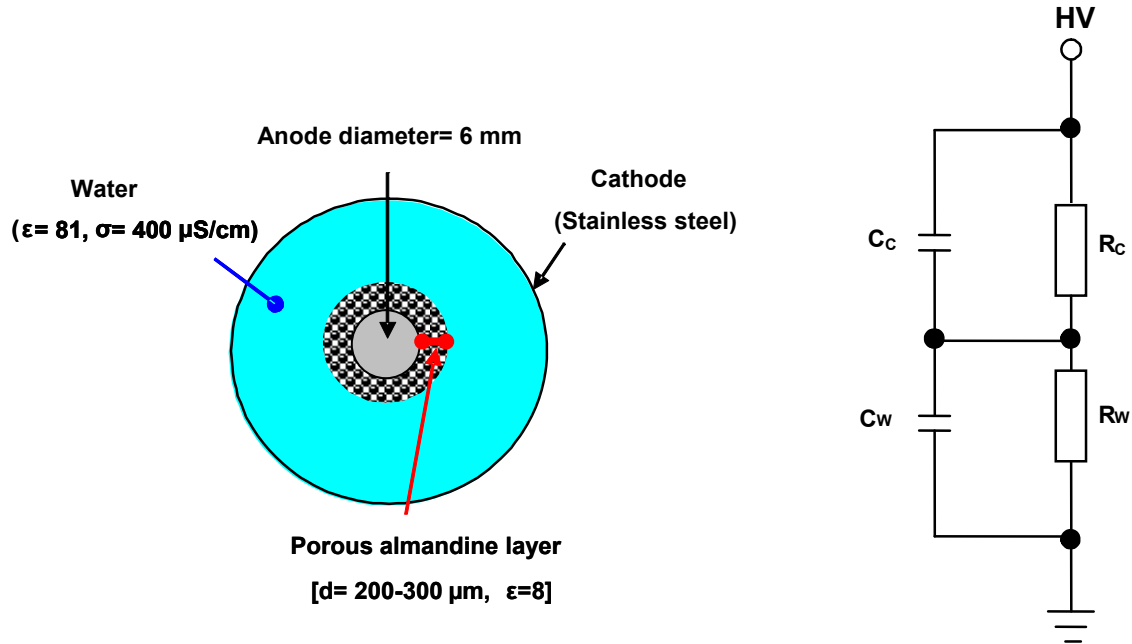


FIG. 2.3. Cross sectional cut through a coaxial pulsed underwater corona reactor and corresponding equivalent circuit. (R_c = resistance of porous ceramic coating, R_w = resistance of conducting water layer, C_c = capacitance of ceramic coating, C_w = capacitance of water layer).

However, for the ceramic layers applied in this thesis the field enhancement due to resistive voltage division between the water and the ceramic was much larger. An equivalent circuit of the coaxial reactor with an anode covered by a thin ceramic layer is presented in Fig. 2.3. Due to this field enhancement a much lower voltage than for the bare anode case is required to initiate a streamer discharge. A pictorial representation of streamer initiation from an anode coated with a porous ceramic layer is shown in Fig. 2.4. The enhancement of the electric field due to the differences in permittivity and resistivity are given by the following expressions:

(A) Effect of differences in permittivity:

$$E_{Cl} \approx \left[\frac{\varepsilon_w}{\varepsilon_c} \right] E_a \approx 10E_a$$

where

E_{C1} = Electric field at the ceramic surface

ϵ_W = Permittivity of water ~ 81

ϵ_C = Permittivity of ceramic $\sim 8-10$

E_a = Electric field at the anode surface without coating

(B) Influence of differences in resistivity:

$$E_{C2} \approx \left[\frac{V_A R_C}{d (R_W + R_C)} \right]$$

where

E_{C2} = Electric field at the ceramic surface

R_W = Resistance of water layer

R_C = Resistance of porous ceramic coating

d = Thickness of ceramic coating

V_A = Anode voltage

V_C = Voltage across ceramic coating

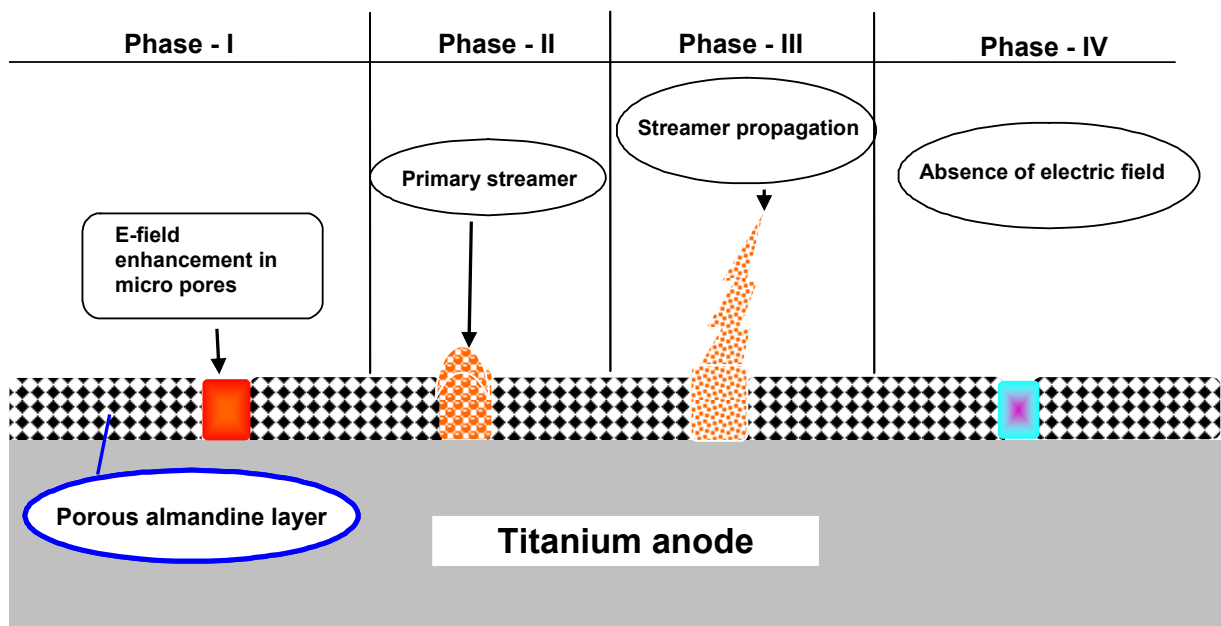


FIG. 2.4. Model of streamer initiation from micro pores in the ceramic coating.

R_C is mainly determined by the porosity of the ceramic layer and the conductivity of the water filling the pores and must be determined experimentally. A rough estimate can be obtained by assuming that the conductivity of the ceramic layer is given by the conductivity of the water used in the reactor multiplied by the porosity percentile.

Secondary streamer (from ceramic layer): Secondary streamer propagation does only occur if the electric field at the tip is sufficient to initiate a local micro-discharge in the water. It has been concluded from measurements of the channel diameter at the tip that field strengths much above 20 MV/cm appear in the water in front of the streamer head. Such field strengths are sufficient to create field induced dissociation (into OH^- and H^+) and ionisation of water molecules increasing the water conductivity by several orders of magnitude. It is well known that both the dissociation and the ionization of water molecules increase exponentially with the applied electric field [47, 48]. The subsequent current flow charges the new segment, heats the water instantaneously and launches a strong shock wave into the water [37]. The analysis of shock waves resulting from the streamer discharge channel strongly supports the conclusion that the initial electric breakdown occurs in the high-density water and not as previously assumed in a low-density region [55-57]. The new section becomes part of the streamer channel after expansion and complete polarisation. Secondary streamers advance with a velocity of 30 km/s. Their advancement stops if the voltage drop along the streamer reduces the effective voltage at the streamer tip below the inception voltage required for self-propagation.

Shock wave analysis demonstrates that during streamer propagation a very short (2- 3 ns) pressure pulse of 2-3 GPa amplitude expands into the surrounding water. The initial streamer radius is estimated to be less than 4 μm . The propagation velocity of streamers was found to be constant over a wide voltage range while the number of streamer branches increased with voltage. The measured electron density at the streamer tip is of the order of 1.5×10^{19} per cm^3 . It reduces to less than $10^{18}/\text{cm}^3$ at the streamer foot. From spectroscopic data molecular rotational temperatures of $T_{\text{rot}} = 5000$ K have been inferred [37]. Since much lower vibrational temperatures were obtained it was concluded that the streamer plasma was not in equilibrium. It was also observed that at lower water conductivity the streamer growth occurred in steps. During each streamer growth step a current pulse was recorded co-related with intense light emission. Between pulses an intermission was observed whose duration depended upon the conductivity of the liquid. The fact that the streamer channels became visible only during current flow indicated that the channel plasma remained cold and resistive. Only during the active phase of streamer advancement the plasma inside the channel is heated by the polarization current. At higher water conductivity a continuous ion flux through the streamer surface contributed to the current inside the channel which kept the channel plasma hot and sufficiently conductive. Therefore at a conductivity $> 600 \mu\text{S}/\text{cm}$ the pulsed or intermittent behaviour of streamer current disappeared.

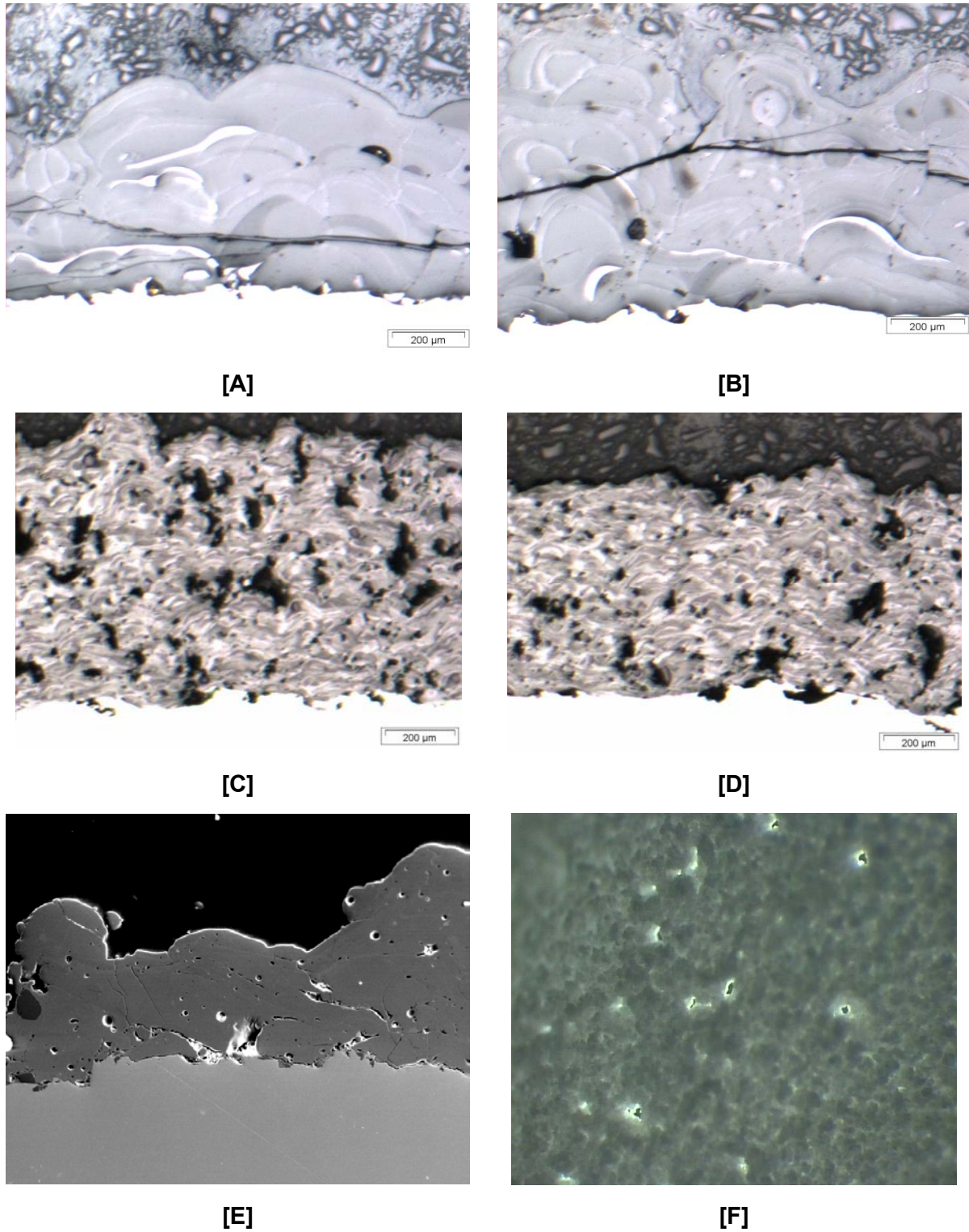


FIG. 2.5. Electron microscopic (SEM) images of cross sectional cuts through different ceramic coatings used in this thesis. [A] TiO_2 ceramic layer without porosity. [B] Almandine ceramic layer without porosity. [C] Al_2O_3 ceramic layer with increased porosity. [D] Al_2O_3 ceramic layer with 6-8 % porosity. [E] Almandine ceramic layer with 4-6 % porosity. [F] Micropores in a thin layer of Al_2O_3 ceramic.

Effect of porosity: To select the most appropriate ceramic coatings for the corona discharge reactor different coating materials and different porosities [(Almandine, Titanium dioxide, Alumina, (layer thickness= 200 - 300 μm)] were studied. Electron microscopic images of cross sectional cuts through these coatings are presented in Fig. 2.5. As expected, from coatings without porosity (TiO_2 and almandine) streamers could not be launched. Although the macroscopic field distribution in the reactor is nearly the same as in the case of a porous ceramic layer streamers cannot appear.

After complete polarization the electric field in the water is much reduced everywhere. Local field enhancements do not occur under these conditions. However when the voltage drop across the ceramic layer exceeds its breakdown strength the ceramic layer can be punctured. This leads to a local field enhancement from which a streamer may be launched into the water. It is most likely that another streamer will originate from the same location during the following pulse since the breakdown strength of the water now filling the breakdown channel in the ceramic is probably smaller than that of the ceramic. This behaviour was indeed observed in an experiment with an epoxy layer. After breakdown of the epoxy layer streamers always appeared at the same breakdown locations.

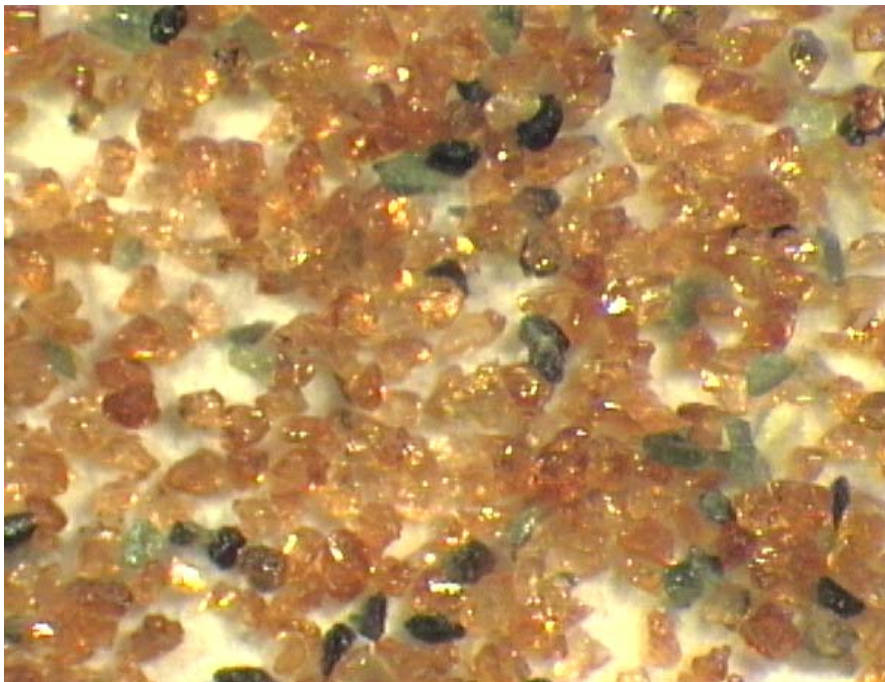


FIG. 2.6. Microscopic photograph of almandine powder used for the preparation of porous ceramic anode coatings. The different colouring is attributed to impurities and different portions of certain elements. A grain size variation is also visible.

In a range of porosities from 4-8 % almost similar streamer properties were observed with alumina and almandine coating. As it is difficult to control the porosity

accurately this result facilitates to meet the requirements. To obtain an optimum porosity a broad distribution of grain sizes is required. To obtain a porosity of between 4-6% almandine powders with a grain size variation between 5 μm and up to 215 μm was used (Fig. 2.6). The use of more uniform grain size powder caused a reduction of the porosity. Experimental results showed that the number of streamers per pulse was related to the anode voltage (section 4.1). This observation suggests that streamer initiation is also related to the pore geometry. Due to the large variety of grain geometries a correspondingly large diversity of pore geometries and orientations exists in the layer. Therefore, we expect a marked dependence of the number of streamers on the applied voltage

Alumina (Al_2O_3) an oxide and almandine ($\text{Fe}_3\text{Al}_2(\text{SiO}_4)_3$) a silicate were selected to study the streamer formation further. Using water of neutral pH, both materials initially produced streamers of similar properties (length and numbers). However in case of Al_2O_3 streamer generation stopped after longer operation time (>1000 pulses). This suggests that the initiation of the streamer discharge does not only depend on the permittivity and the porosity of the ceramic layers but also on the surface charge of the ceramic material determined by the polarity of the applied voltage, the pH-value and the ions dissolved in the water [58].

The different performance of alumina and almandine coated anodes has been explained by differences of their isoelectric points (IEP). The IEP corresponds to the pH where the net surface charge of a heterogeneous ceramic becomes zero. It is generally assumed that when a coated electrode is immersed in water its surface is covered with hydroxyl species, M-OH , where M stands for a metallic component. Hydrated surfaces possess amphoteric properties meaning that they can either adsorb or release protons. At pH values above the IEP, the predominate surface species is M-O^- , while at pH values below the IEP, M-OH^+ species predominate. This can lead to the built-up of charges on the ceramic surface whose magnitude and polarity depend on the ceramic properties and the pH of the solution. The isoelectric point of Al_2O_3 is $\text{pH}_0=9.1$, which means that in common aqueous solutions ($\text{pH} < 9.1$) it carries a positive surface charge.

If other than H^+/OH^- cations and anions are present in the solution they can cause a substantial shift in the magnitude of pH_0 . It has been found e.g. that for phosphate anions $\Delta\text{pH}_0=-4$ occurs with alumina electrodes [58].

Due to the ion exchange capacity of its crystalline lattice, sites of both polarities can appear on the surface of almandine compensating the build-up of additional surface charges over a very large range of pH-values. The isoelectric point of almandine is $\text{pH}_0=2$, meaning that almandine coated anodes can operate over a very large range of pH-values.

If a net charge is established on the surface of the ceramic layer a counter charge of equal amount must accumulate at the ceramic-water interface to maintain electrical neutrality. Thus an electrical double layer arises at the ceramic surface which strongly affects the electric field. The influence of this double layer becomes even stronger if an external electric field is applied. If the field connected with the double layer becomes opposite to the external field the resulting field may fall below the conditions for streamer initiation.

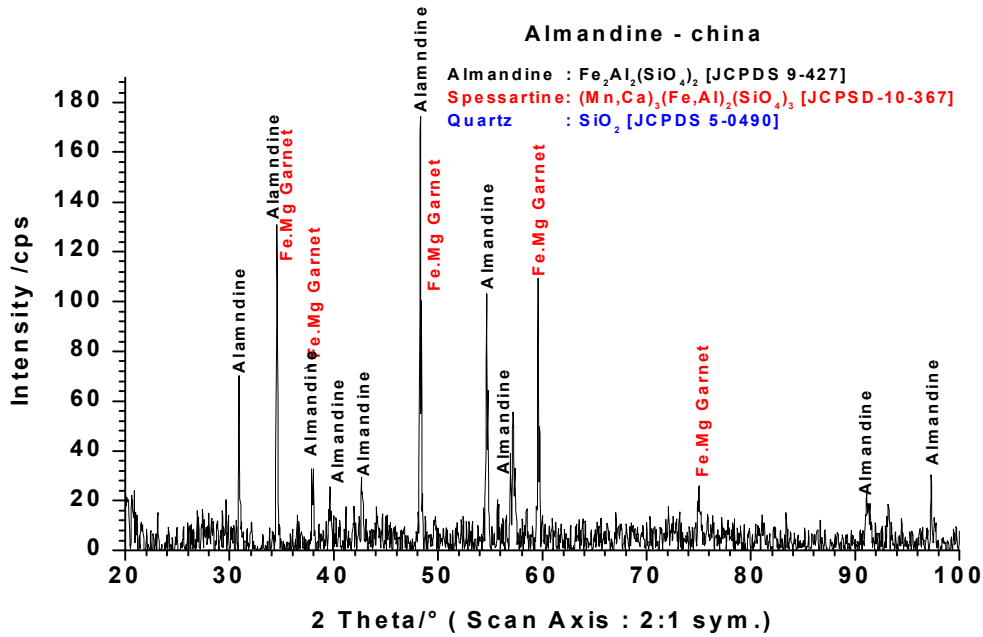


FIG. 2.7 XRD details of the almandine powder used for the production of porous ceramic coatings. Along with the almandine peaks Fe peaks are observed too.

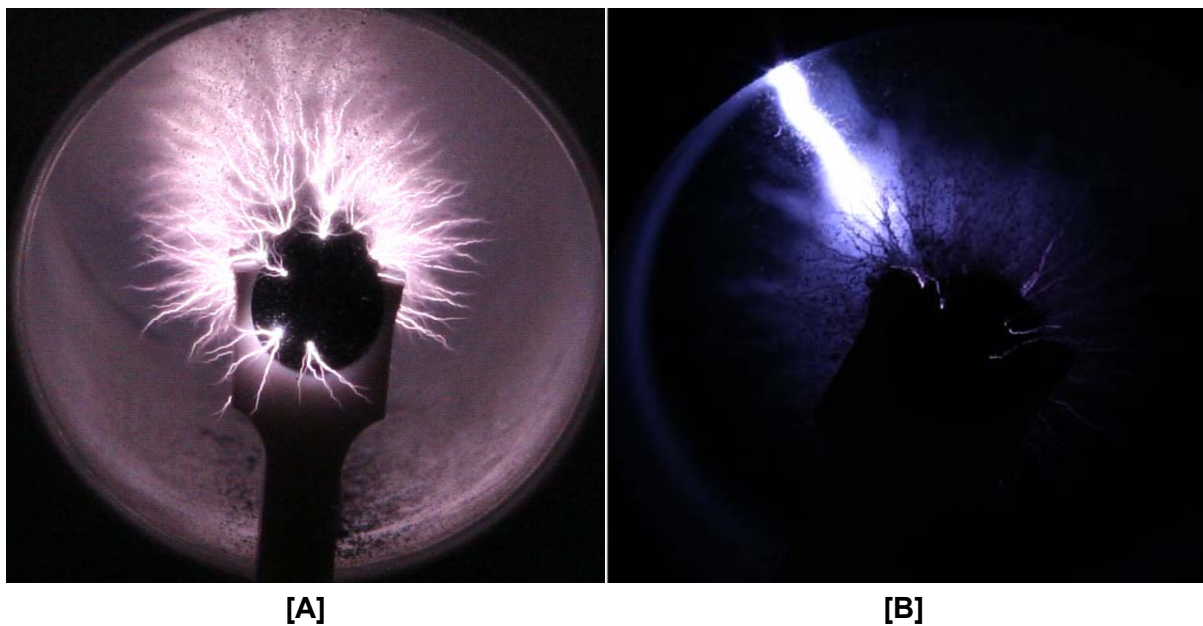


FIG. 2.8. Images of discharges in the reactor. [A] Filamentary streamer channels, distributed almost homogeneously over the anode surface [B] Arcing preventing appearance of streamers.

Moreover almandine also contains Fe^{2+} ions, which may be released into the water and facilitate the decomposition of H_2O_2 possibly present in the water. These Fe peaks are clearly visible in the XRD analysis of the almandine powder that was used to produce the coatings on the Ti anode surface (Fig. 2.7). Optimisation of various electrical parameters is required to achieve a uniform distribution of streamers in the pulsed underwater corona discharge reactor. As shown in Fig. 2.8 [A] large numbers of filamentary streamer channels, distributed almost homogeneously over the anode surface, are launched with an optimum applied pulse voltage (depending upon the reactor geometry). If this voltage is further increased then the corona channel transforms into an arc (Fig. 2.8 [B]). In this case the voltage in the reactor breaks down and prevents the formation of streamers at other position of the anode.

2.2 Chemical processes

Oxidant formation: Pulsed corona discharges in water have been previously considered as a tool for the destruction of toxic organic compounds [39, 40, 59-62] and bacteria [63, 64] as well as for the formation of shock waves [65] for different medical applications. It has been proven that significant amounts of hydrogen peroxide [63, 66, 67] are created during pulsed corona discharges in water. Also the appearance of hydroxyl radicals in the discharge channels was demonstrated by emission spectroscopy [68, 69] and by specific chemical probes [41, 70]. Kirkpatrick [43] has found that molecular hydrogen, hydrogen peroxide and molecular oxygen appeared with a stoichiometric ratio of 4:2:1. Streamer discharges in water involve complex physical and chemical processes and many of the details are still not understood. Industrial applications for water purification and disinfection however require a better understanding of the dependence of oxidant yields on electric pulse parameters and additional components dissolved in water. This has not yet been treated appropriately in the literature.

Due to the combined effect of energetic electrons, UV radiation, and shock waves inside the propagating streamer channel (Fig. 2.9-A) water molecule are dissociated and various reactive species are produced (Fig. 2.9-B). Three different reaction zones can be distinguished for the production of radicals. The first zone is the plasma channel itself. The second zone is the interfacial region between the plasma phase and the bulk liquid, where large temperature and pressure gradients exist and where molecular species can migrate from the streamer channel into the bulk water. During cool down or collapse of the channel many of the atomic and molecular species created during the hot phase recombine and react with each other forming a new composition of reactive species.

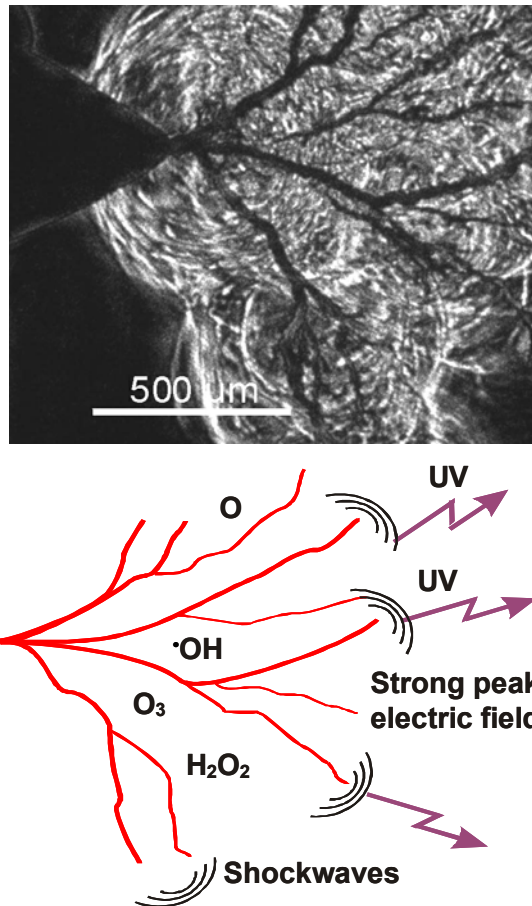
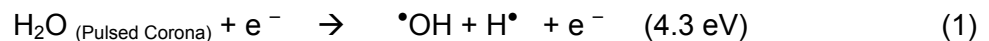


FIG. 2.9. [A] Shadowgraph of a pulsed underwater streamer discharge from a point electrode, [B] Schematic illustrating different physical effects occurring in the discharge.

The third possible reaction zone involves the bulk solution (similar to the conditions in radiation - and sonochemistry), where reactions take place between the radicals from the plasma channel and other species present in the water. In detail we can describe the radical formation by the following parts:

Inside and at the interface of plasma channel: Inside the streamer discharge channel the prime and most dominant pathway of oxidant production is the dissociation of water molecules due to collisional excitation by energetic electrons.



Dissociation of water molecules is much more likely than ionisation since it requires much less energy. Nevertheless a small fraction of water molecules must have been ionised. From measurements of the electron densities at the streamer tip we estimate that less than 1% will be ionised. Only few $\cdot\text{OH}$ and $\text{H}\cdot$ radicals will escape from the streamer channel into the surrounding water. As the channel cools down many will recombine to water or interact with themselves forming H_2O_2 and H_2 . H_2O_2 is relatively stable and long living and will

therefore accumulate in the water. This is also true for H₂. The thermal velocity of the H atom is about four times larger than that of OH radicals. Therefore it is expected that more H-atoms reach the plasma-water boundary per unit time and diffuse into the bulk water [71].



According to the findings of Fischer et al. from ultrasound experiments more than 80% of the OH radicals and H atoms initially created in the plasma recombine to reform water [72, 73].



Inside the expanding streamer channel large gradients in density and temperature exist. The final destiny of the $\bullet\text{OH}$ and H radicals not only depends on the distribution of these physical parameters but also on the species present in the plasma and in the interfacial water zone. Some of the randomly moving radicals coming to the border zone can react with chemical species present at this location. It is assumed that neither complex organic compounds nor micro organisms will survive the extreme conditions inside the plasma channel. Direct further destruction by radicals can only occur in the interface region and in the bulk water. Also the fraction of the total water volume affected by the streamer channels remains always small even after many thousands of pulses. In general the migration length of OH radicals in bulk water remains short too. It depends on the concentration of reacting species and good estimates are not available. Values of several nm cited in the literature are not very solid. Nevertheless it will be short and therefore the effective reaction zone for OH radicals around the channel will also be small.

Joshi [66] has reported a numerical solution of the set of kinetic equations describing the most important reactions in pulsed underwater corona discharges. In his model he assumed homogeneity i.e. that the reaction mechanisms were similar to those found in radiolysis (γ - or electron beam irradiation). However, besides some similarities considerable differences exist between these processes. In radiolysis the production of the primary oxidants (e_{aq}^- , $\bullet\text{OH}$, $\text{H}\bullet$ and H_2O^+) occurs rather homogeneously in a large volume determined by the beam cross section and the range of the radiation. Therefore the solution presented by Joshi is of limited value for the interpretation of reaction yields measured in pulsed underwater corona discharges.

As schematically indicated in Fig.2.10 the temperature and H₂O₂ gradients change with time. At the end of the pulse a large amount of energy has been deposited in the streamer channel. It appears in the form of particle kinetic energy and ionization and

excitation energy. During the cooling phase of the channel this energy is dissipated by evaporating water from the channel walls. As the temperature drops the equilibrium of the reaction described by equation 2 shifts to the right, i.e. H_2O_2 becomes stable and mixes with the water.

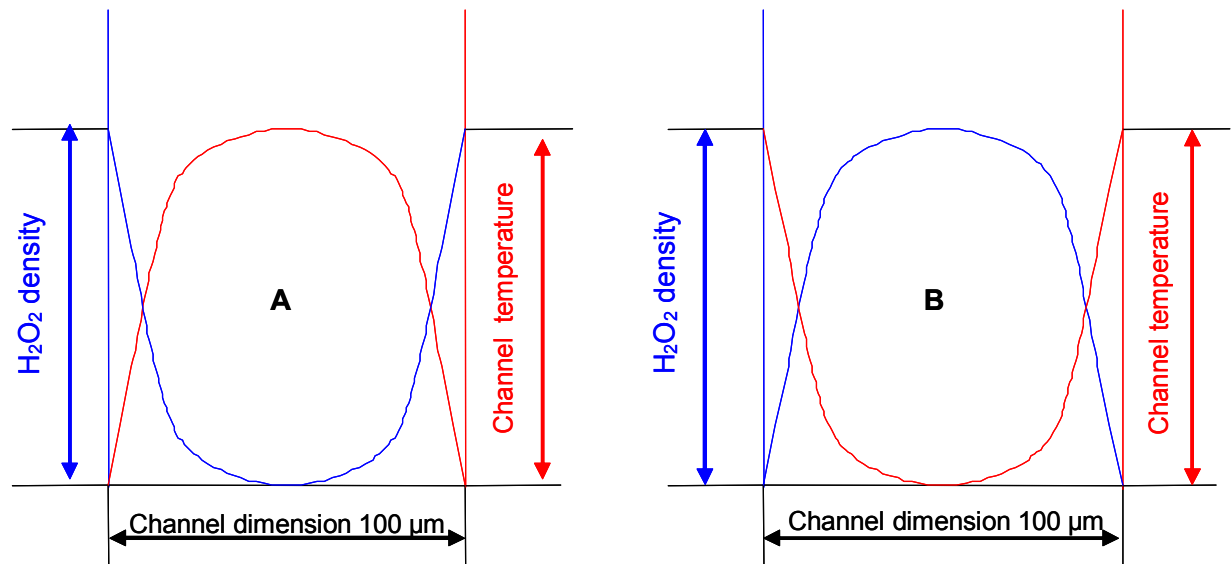


Figure 2.10: A pictorial representation of the H_2O_2 density and temperature gradients inside and at the interface of the plasma channel. [A] During the active phase of the streamer channel [B] During the cool down phase

The main stable oxidant product emerging from the streamer channel is H_2O_2 which consequently accumulates in the bulk water. However UV radiation emitted from the plasma channels [74, 75] can decompose H_2O_2 as well as water molecules and thus directly create OH radicals in the bulk water. It is supposed that these OH radicals then affect organic molecules, protein-chains and channels in the membrane of bacteria. Moreover the emitted UV radiation can also directly interact with bacteria.

It has been mentioned before that a certain fraction –probably less than 1%– of the water molecules inside the streamer channel will also become ionised.



The cation H_2O^+ of the water molecule reacts strongly acidic and rapidly gains a proton from a surrounding water molecule (reaction 6).



Due to its short migration length a very small fraction of free electrons escaping from the plasma channel into the bulk water becomes solvated (reaction 7):



In a solution saturated with oxygen an equivalent portion of oxygen will appear in the streamer channel and become dissociated into atomic oxygen (O) (equation 8):



The very reactive oxygen atoms can interact with oxygen molecules (O_2) forming ozone (O_3) (equation 9):



In the bulk solution: After the cleavage of water molecules the major species which can migrate from the plasma channel to the bulk solution are $\bullet\text{OH}$, $\bullet\text{H}$, O, free electrons, and molecular species such as H_2 , H_2O_2 , and ozone O_3 . Depending upon their concentrations and their diffusion constants, their migration length in bulk water varies. This further determines their reaction rates with other species present in the water.

Near the plasma-water interface and in bulk water, the major possible reactions are as follows,

e_{aq}^- can react with H_2O_2 and produce OH radicals:



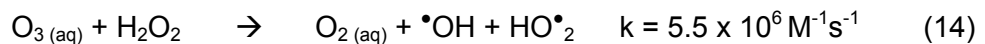
$\bullet\text{OH} + \text{OH}^-$ react together and super oxide radical is produced:



This super oxide radical $\text{O}^{\bullet-}$ can react with molecular H_2O_2 and O_2 in the following way:



Ozone diffusing into the bulk solution reacts with accumulated H_2O_2 and further OH radicals are produced. This process is also known as the Peroxone process:



In absence of other $\cdot\text{OH}$ scavengers, excess hydrogen peroxide can scavenge $\cdot\text{OH}$ as follows:



Fig. 2.11 summarizes the major reaction paths leading to the production of oxidants with bactericidal effects. From the viewpoint of applications for water disinfection OH radicals, hydrogen peroxide and ozone are the most important species. The major pathway for the formation of H_2O_2 is by combination of two OH radicals. Therefore, to create one H_2O_2 molecule, two H_2O molecules are required. Considering the volume of propagating streamer channels we can estimate the number of water molecules dissociated per pulse.

From experimentally obtained physical dimensions (i.e. length and number) of the streamer channels (initial diameter: $4 \mu\text{m}$), the calculated total volume of all plasma channels summed over 1000 pulses becomes $6.4 \times 10^{-8} \text{ m}^3$. If we assume that all water molecules within the channels were dissociated we should detect $1.7 \text{ mM H}_2\text{O}_2$. Instead a yield of $65 \mu\text{M}$ was measured. This suggests that only a few percent of the water molecules become dissociated.

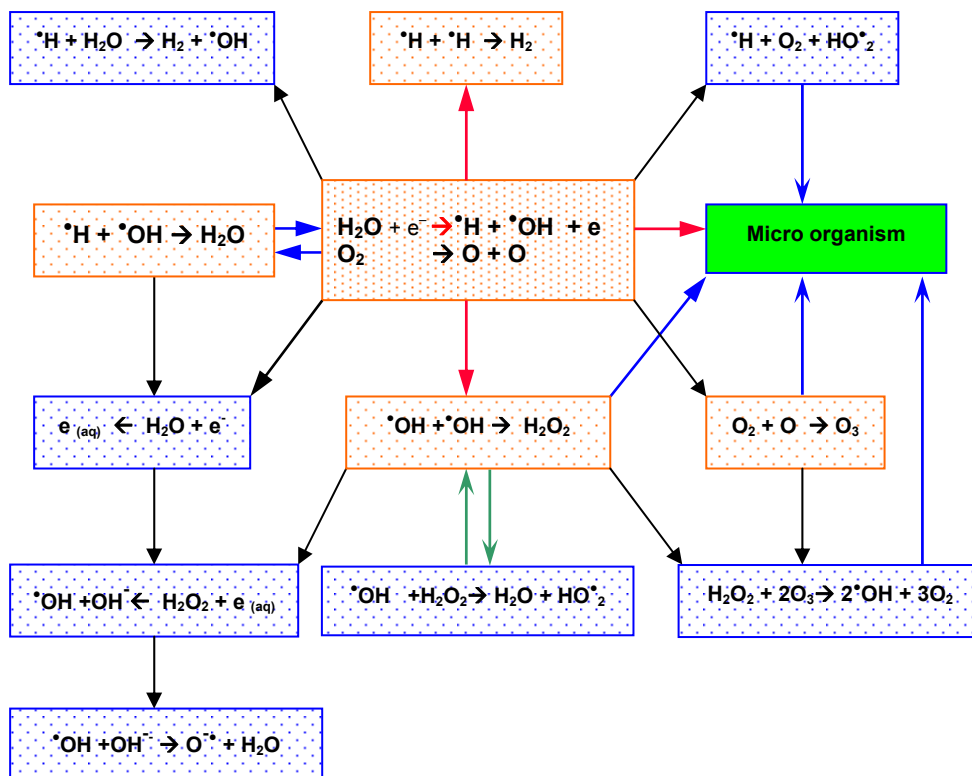


Figure 2.11: Major chemical reaction paths leading to the production of oxidants with bactericidal effects in pulsed corona discharges. (Blue dots represent reactions taking place in the bulk solution; red dots show reactions occurring at the interface and inside the plasma channel)

3. EXPERIMENTAL METHODS

3.1 The pulse generator

The high voltage pulse generator is a crucial component of a water cleaning technology based on pulsed underwater corona discharges. To achieve the desired discharge conditions in the corona reactor, the generator should meet the following demands: depending on the inter-electrode gap and the voltage amplitude a short pulse width is required; for the laboratory reactor described below it is between 200 and 400 ns; in all cases a rise time of less than 100 ns is necessary to simultaneously launching many streamers. To drive the laboratory reactor a pulse amplitude of less than 100 kV and an impedance around 50 Ω are adequate.

Such a generator can either be realized through a *LC*-chain consisting of a suitable number of *LC*-elements or through a pulse forming line. In either case a fast repetitive closing switch is necessary. For the relatively low power of the pulses required here a gas filled spark gap seems an adequate choice. These switches are robust and inexpensive and have a tolerable wear at the power levels requested. Their recovery time is fast enough to allow repetition rates of up to 50 Hz [36, 76]. We used N_2 filled self-breaking spark gaps whose ignition voltage could be adjusted by the gas pressure. The generator repetition rate was fixed by regulating the current of the high voltage charging unit.

Based on these considerations it was decided to realize the pulse generator through an *LC*-chain in a Blumlein configuration. The *LC*-chain has the advantage of providing a more convenient flexibility in changing the generator impedance or pulse width. The Blumlein configuration has the benefit that the output voltage (into a matched load) matches the charging voltage.

A schematic of the Blumlein line pulse generator and its connections to the corona reactor is shown in Fig. 3.1-[A]. This set-up comprises a high voltage power supply (0 to 120 kV/50 mA) from Hilotest, Karlsruhe and the *LC*-chain in a Blumlein configuration. The Blumlein consists of two chains each built from six *LC* ($L=0.6 \mu\text{H}$, $C=2\text{nF}$) elements. With these *LC* values the calculated generator impedance $Z_0 = 2\sqrt{L/C}$ was 35 Ohm and the pulse width $\tau = 2n\sqrt{LC}$ became 415 ns, where n is the number of *LC*-elements. The pulse generator is capable of delivering a peak voltage of up to $\sim 80\text{kV}$ to a load. A picture of this pulse generator is shown in Fig. 3.1-[B]. Some initial experiments were performed with a modified pulse generator of 50 Ohm impedance ($L=1.3 \mu\text{H}$, $C=2\text{nF}$) and 600ns pulse width.

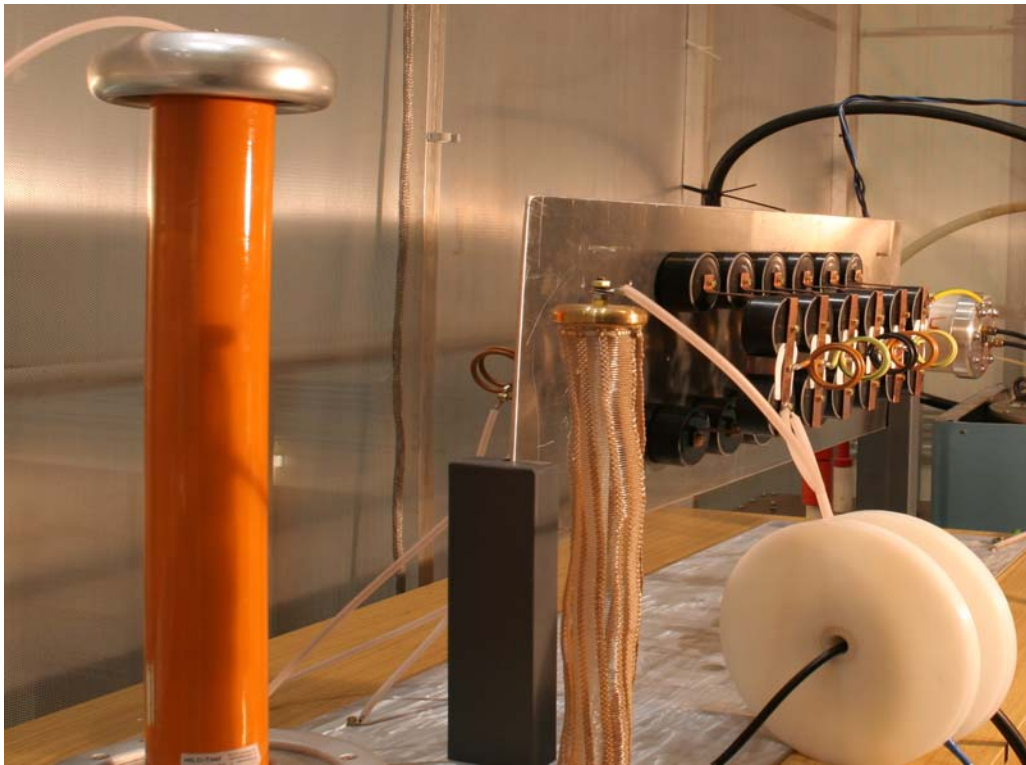
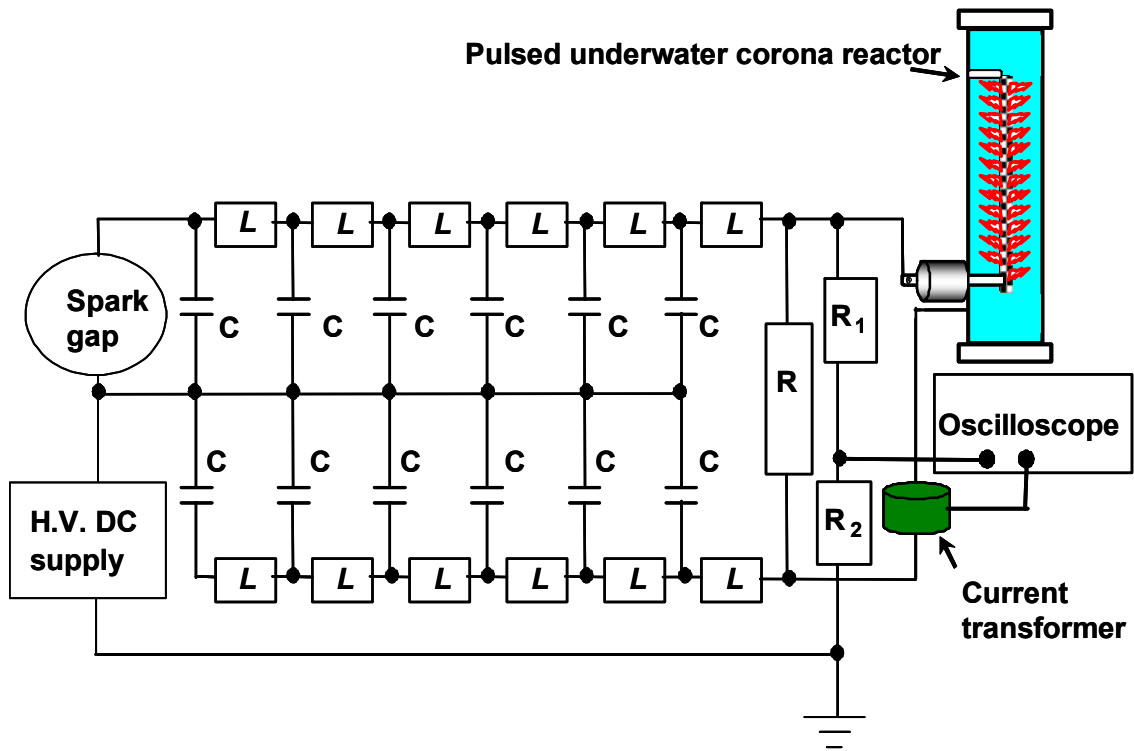


FIG. 3.1-[A]. Six section LC Blumlein generator set-up. ($L = 0.6 \mu\text{H}$, $C = 2 \text{ nF}$). $R = 50 \Omega$ is connected in parallel to the corona reactor. R_1 and R_2 represent the high resistance voltage divider. The output of the Blumlein generator is connected to the reactor through a RG/U217 coaxial cable. Nominal generator impedance = 35Ω . [B] Photograph of the pulse generator

Varying both the LC values and the number of LC elements it was found experimentally that for the laboratory reactor (70 mm (Φ) x 200 mm (l)) a pulse width of 200 - 400 ns, and a pulse amplitude of up to 65 kV led to maximum streamer lengths without arcing. For one experiment in order to obtain a shorter pulse width of 240 ns, a single LC section ($L = 2 \mu\text{H}$, $C = 9 \text{ nF}$) was also used.

3.2 Electrical diagnostics

A Pearson current transformer (Model 101) and a voltage divider HVT-80 (Hilotest GmbH, Karlsruhe), were used to measure the temporal evolution of the reactor current and the voltage at the anode respectively. Another voltage divider (HVT-120; Hilotest GmbH, Karlsruhe) was used to measure the charging voltage of the Blumlein line. The applied pulse voltage and the pulse current were recorded on a Tektronix TDS 540 digital storage oscilloscope operating with a sampling rate of up to 1 GS/s. To avoid electromagnetic interference from the pulse generator and the corona reactor, flexible copper tubes were used to carry the signal cables connecting the transducers with the oscilloscope. All electrical measurements were performed in a screen room. The number of pulses was counted using a pulse counter from Monsanto (Model 114-A). The total electrical energy delivered to the reactor was calculated by integrating the product of voltage and current over time and by summing over the number of applied pulses.

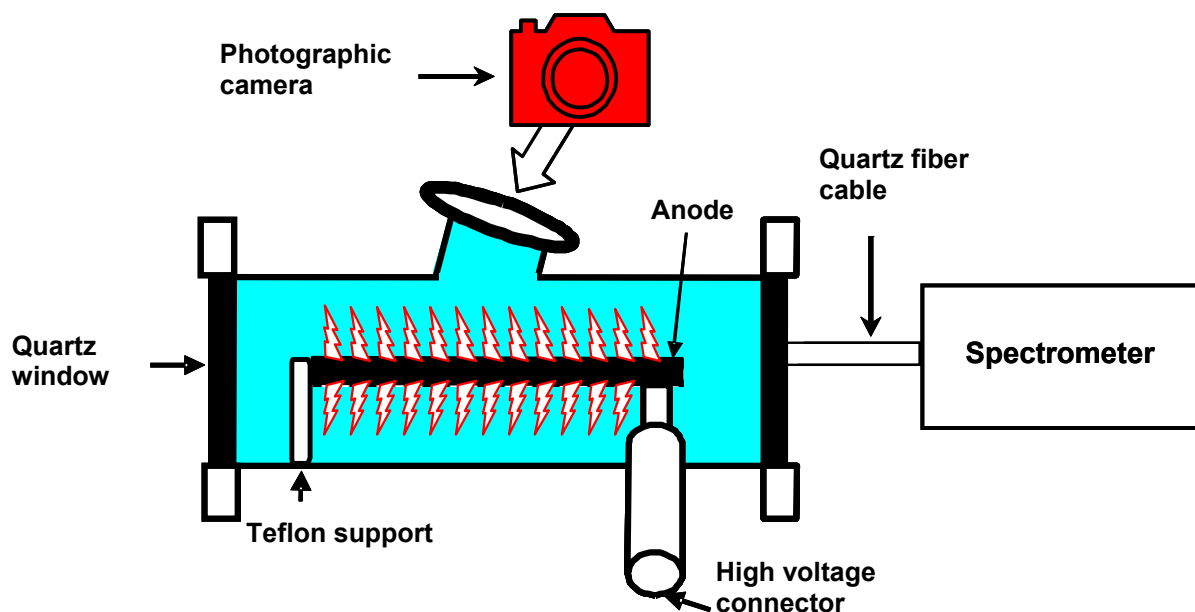


FIG. 3.2. Schematic of the reactor layout for the measurement of optical and electrical parameters.

As indicated in Fig. 3.2 the reactor was designed to perform photographic and spectroscopic studies simultaneously with electrical measurements. A side port was provided to study the numbers and lengths of streamers as a function of electrical parameters. Photographs of streamers in the test reactor were captured with a 35 mm digital camera (Canon EOS-20D) equipped with an objective of 18-125 mm focal length. All photographs were taken with an aperture of 2.8 and 1 s exposure time at a rate of 1 pulse/s. Optical spectra emitted from the streamer discharges were recorded with an Ocean Optics spectrometer (Model HR 2000). To collect and transmit the light from the reactor to the spectrometer a 600- μm diameter quartz fibre optic cable and a quartz diffuser prepared from sintered fused silica (M/s Gigahertz – optic GmbH) were used. The quartz fibre was positioned just behind the exit quartz window of the reactor. It was able to collect light from a large volume in the inter-electrode gap.

3.3 The corona reactor

The entire experimental setup for the pulsed underwater corona discharge studies is shown in Fig. 3.3. The reactor chamber must be designed sufficiently robust to withstand the pressure pulses created during the streamer discharges. In addition chemically inert materials should be selected since different chemical probes have to be applied to diagnose the oxidants produced during the discharges. For this purpose the reactor chamber was built from stainless steel and the insulation of the electrical feedthroughs was made from polytetrafluoroethylene, (PTFE or Teflon).

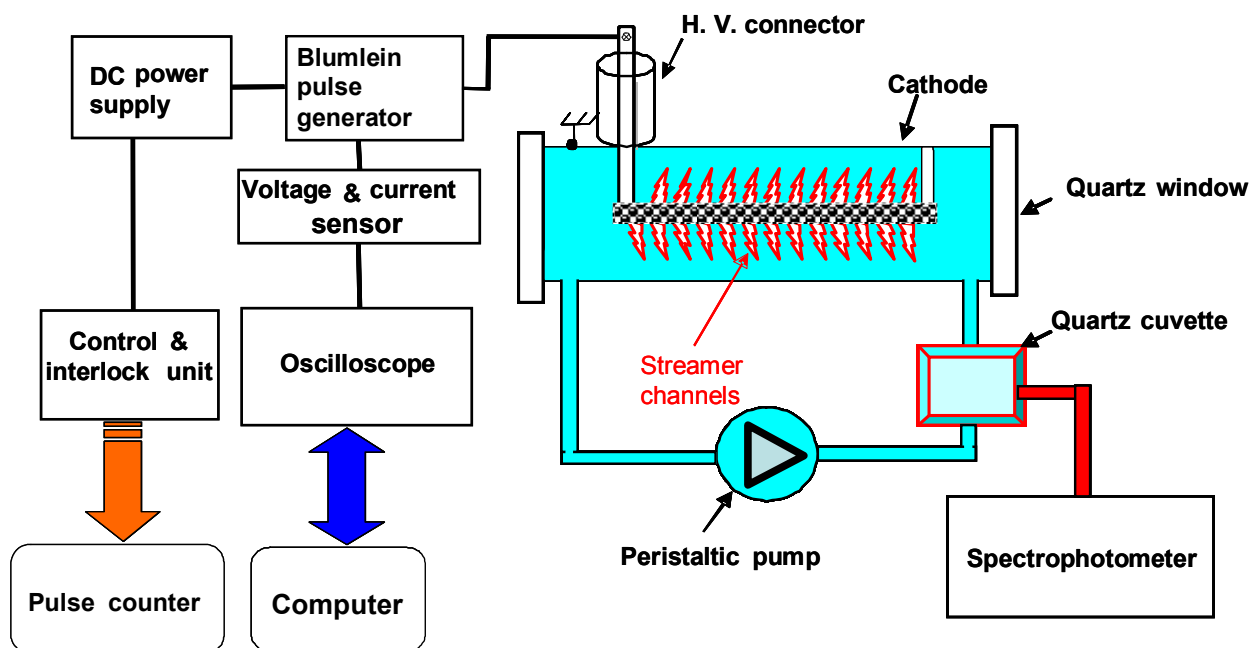
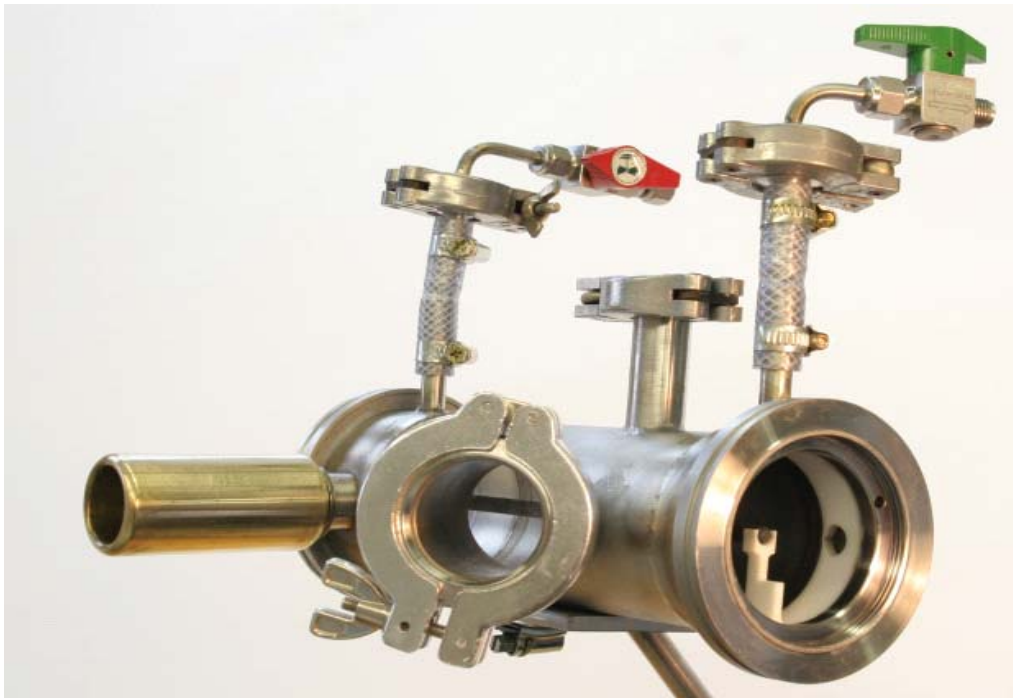
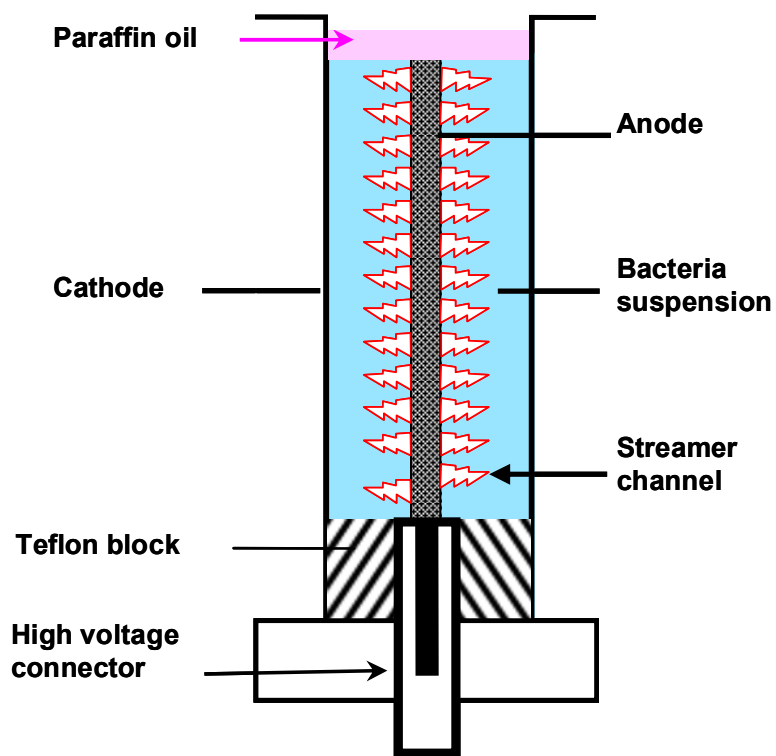


FIG. 3.3. Block diagram of the entire pulsed underwater corona treatment system.



[A]



[B]



[C]

FIG. 3.4. [A] Photograph showing the laboratory corona reactor chamber. [B] Schematic of the reactor modified for microbiological studies. Here the reactor was positioned vertically and the dead volume in the chamber was eliminated by a cylindrical Teflon block on the bottom and an oil paraffin layer on the top to avoid electrical breakdown in air. [C] Picture of the reactor used for disinfection experiments.

The laboratory reactor used in our experiments had an inner diameter of 70 mm and a length of 200 mm. including the additional side view port (for streamers) its volume was approximately 1 L. The end flanges of the cylindrical chamber could adopt quartz windows. Using a peristaltic pump the water could be circulated through an external cuvette, which was directly connected to a photo spectrometer. This Masterflex peristaltic pump was also applied to support sample collection from the active volume of the reactor and to maintain isothermal conditions in the reactor chamber. A 6 mm almandine coated titanium anode was mounted in the centre of the reactor. A specially designed high voltage connector was used to link the anode to the high voltage generator.

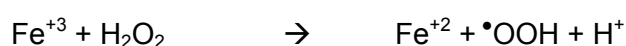
A photograph of the reactor chamber is shown in Fig. 3.4 [A]. Later it turned out that the dead volume of this chamber was too large for microbiological studies. Under dead volume we mean those volumes in the chamber that were unaffected by the streamer discharges. To eliminate the dead volume the chamber was modified as shown in Fig. 3.4 [B - C]. A Teflon block was used to fill the chamber around the high voltage connector which in this case was mounted coaxially. Also the entire reactor was placed vertically and the top water level was sealed by a thin layer of paraffin oil to avoid electrical breakdown at the water-air-interface. To prevent splashing of the bacterial suspension outside the reactor the top of the treatment chamber was additionally covered by a Teflon lid. Before and after each microbiological experiment the reactor was sterilized in an autoclave and after each experiment it was cleaned with a solution of 70 % ethanol.

3.4 Anode coatings

Almandine ($\text{Fe}_3\text{Al}_2(\text{SiO}_4)_3$) is an iron aluminium silicate mineral belonging to the garnet crystal group. As described in chapter 2, apart from its unceasing operation capability the release of Fe^{2+} ions from almandine coatings helps to decompose H_2O_2 (which is produced during the corona discharge) into OH radicals.



This process is self replicating since the reaction of ferric iron with hydrogen peroxide to regenerate the perhydroxyl radical occurs as well:



Titanium was used as the base material for the preparation of the anodes. Using the thermal plasma spraying technique an approximately 200-micron thick almandine layer was deposited on the anode surface [12, 58]. An advantage of titanium is that its thermal expansion coefficient is very close to that of almandine. Therefore during thermal cycling of the anode a better adhesion of the ceramic layer is expected.

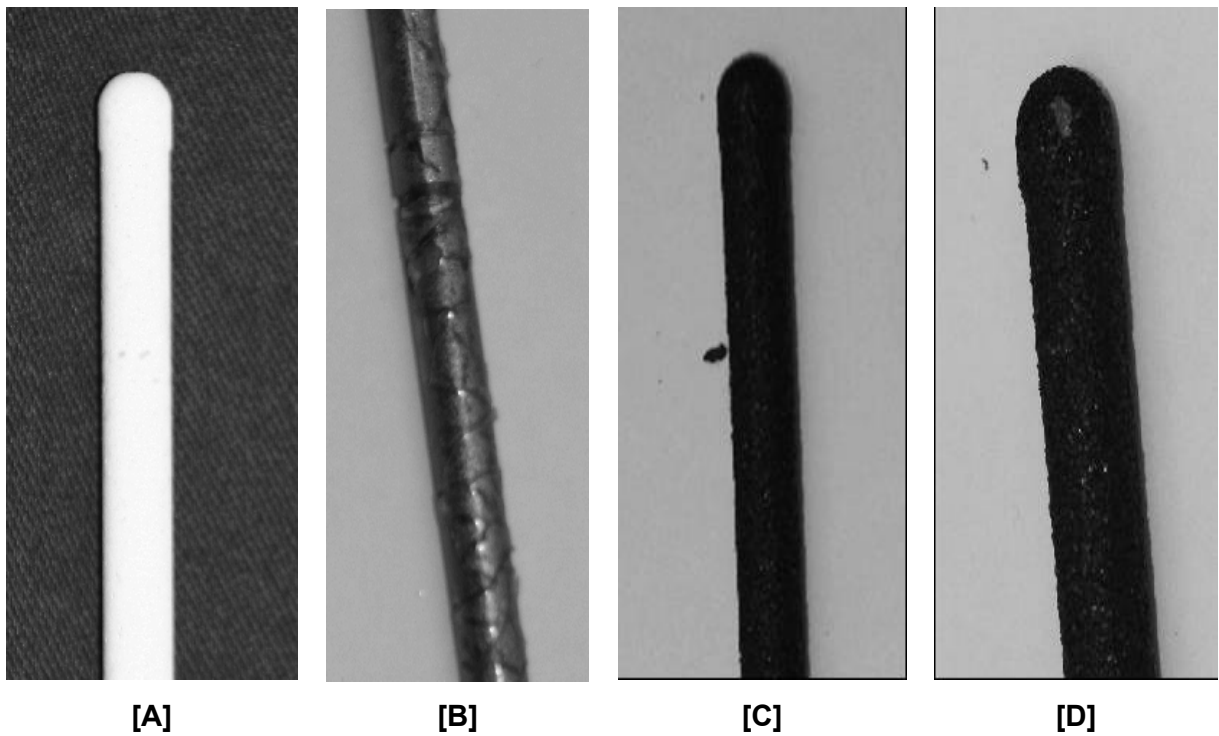


FIG. 3.5. Anodes coated with different ceramics and epoxy. [A] alumina [B] epoxy [C] almandine (fresh) [D] almandine (after 400,000 pulses).

Besides almandine other coatings were tried in the experiments. A selection is depicted in Fig. 3.5. After long operation some of the almandine coating was lost from the anode surface. As shown in Figure 3.6 the areas of erosion were mainly concentrated at the ends of the anode rod.

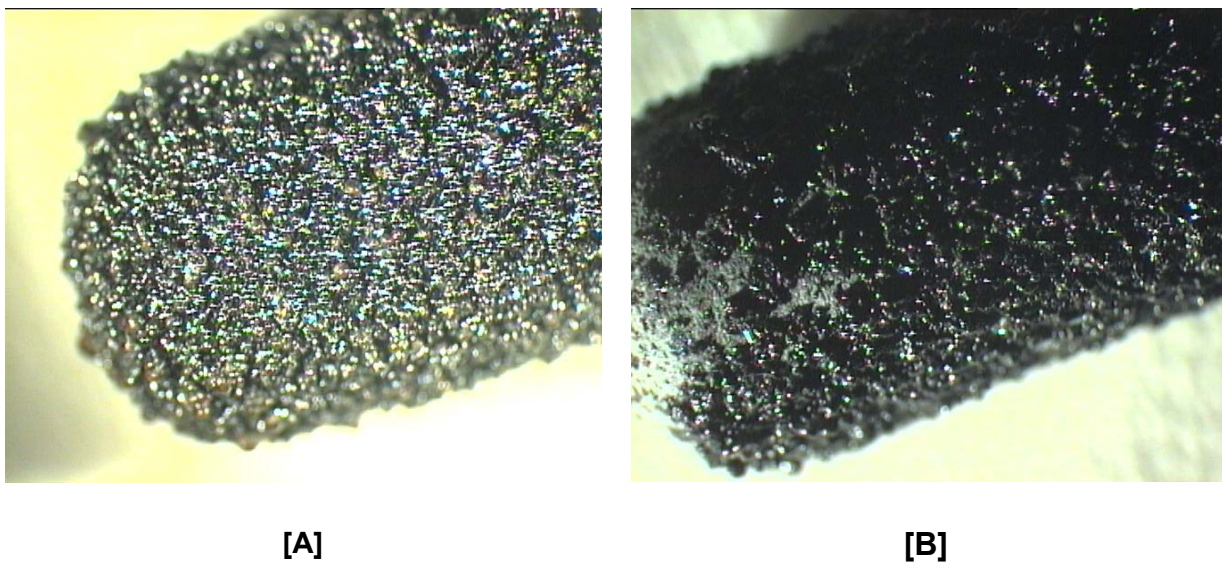


FIG. 3.6. Images of the rod ends of almandine coated anodes. [A] fresh anode; [B] after 400,000 pulses.

When the ceramic coating was replaced with an epoxy layer streamers were also observed after the layer had been broken down at some positions. In contrast to the ceramic layers the streamers always originated at the same positions and after longer operation burnt to become a larger hole. In some experiments we also studied the effect of different anode metals. For these experiments anodes were made from aluminium, copper, and steel.

3.5 Diagnostics of oxidants

3.5.1 Photometric diagnostics: The concentration of various chemical compounds produced in the underwater corona discharges was determined by absorption spectroscopy. The basic principal is to measure the attenuation of a beam of light transmitted through the sample.

According to Lambert Beer's law the ratio between incident light (I_0) and the transmitted light (I) is exponentially dependent on the concentration of absorbing molecules in the sample (C), the optical path length (l), and the absorption coefficient or molar absorptivity of the absorber (ϵ).

$$A = \epsilon / C$$

$$\text{where } A = \log_{10} \frac{I_0}{I}$$

$$\epsilon = \text{L mol}^{-1} \text{cm}^{-1}$$

$$C = \text{mol L}^{-1}$$

$$l = \text{cm}$$

$$L = \text{liter}$$

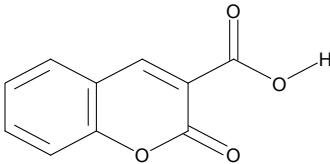
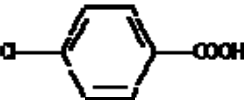
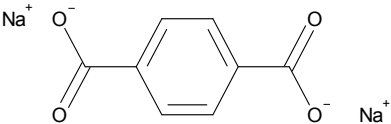
From A , measured at a fixed path length (l), the molecule concentration can be calculated. In this dissertation all absorbance measurements were performed with a Cary Scan 500 (Varian make) photo spectrometer. For all measurements a 1 cm path length cuvette was used.

3.5.2 Hydroxyl radicals: OH radicals are the most reactive oxidants produced in pulsed underwater streamer discharges. As described in chapter 2 they are mainly produced inside the streamer channel and become the source for the formation of other oxidants. Their lifetime inside the streamer channel is of the order of a few hundred ns.

A quantitative determination of the total yield of OH radicals inside the streamer channel from spectroscopic data is extremely difficult since it requires a reliable simulation of

the plasma physics inside the channel and an averaging over many streamers taking into account the view field of the spectrometer inside the reactor. Also using chemical probes is debatable. It is uncertain how many of the probe molecules will remain reactive in the extreme environment of the plasma channel. Also the OH radical concentration inside the channel may become much larger than the concentration of the probe molecules, thus consuming them rapidly. In addition there will always be competing reaction paths for the OH-radicals and a solution of the reaction kinetics would be required which needs to know the initial concentrations of all relevant species. Therefore chemical probes do mainly determine the OH radicals outside the streamer channel and their initial concentration inside the channel must be inferred from other secondary products like H₂O₂. Keeping in mind these restrictions we have applied different chemical probes for the detection of OH-radicals.

Table 3.4.1. Physical and chemical properties of different chemical probes used for \bullet OH detection.

Physical parameters	CCA	4-Chlorobenzoic acid (pCBA)	DNTA
Chemical formula	C ₁₀ H ₆ O ₄	C ₇ H ₅ ClO ₂	C ₈ H ₄ (COONa) ₂
Melting point	190.15524	240-243	-
Boiling point	-	274-276	-
Solubility	Poor	Poor	Very Good
Structure Formula			
Reaction rate constants with \bullet OH	$5 \times 10^9 \text{M}^{-1}\text{s}^{-1}$	$5 \times 10^9 \text{M}^{-1}\text{s}^{-1}$	$3.3 \times 10^9 \text{M}^{-1}\text{s}^{-1}$

Especially coumarin-3-carboxylic acid (CCA), para-chlorobenzoic acid (pCBA) and the disodium salt of terephthalic acid (DNTA) were considered. Some chemical and physical properties of these chemical compounds have been tabulated in Table 3.4.1. CCA and pCBA have a poor solubility in water which makes it impossible to prepare higher concentrations. DNTA has a higher solubility in water however it increases the conductivity of the solution, which can affect the streamer properties. It does not have a melting point because it disintegrates at higher temperatures. The experimental and calibration details of each method are described in the following sections.

Coumarin- 3-carboxylic acid (CCA): In an initial effort for OH radical measurement, coumarin-3-carboxylic acid (CCA) was used as a fluorescent chemical probe. CCA is a non-fluorescent compound. When it reacts with an OH radical, 7-hydroxycoumarin-3-carboxylic acid (7OH-CCA) is formed which is fluorescent (Fig. 3.7) [41, 77, 78]. Using a fluorescence spectrophotometer the area under the fluorescence line can be determined. The measured peak can be compared to a known calibrated concentration of 7-hydroxycoumarin-3-carboxylic acid [$C_{10}H_6O_5$]. Hoeben [41] has tried to quantify the yield of OH radicals by adding a small concentration of unstabilized H_2O_2 to an untreated CCA solution. [To minimize its self decomposition most commercially available H_2O_2 solutions contain stabilizers.] However he observed that low concentrations of H_2O_2 decayed rapidly which made the calibrations questionable.

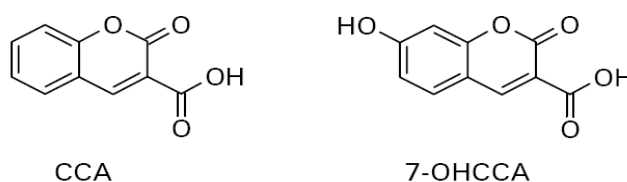


FIG. 3.7. Reaction path for the formation of 7-hydroxyCCA (7-OHCCA) from CCA

However, as 7-hydroxycoumarin-3-carboxylic acid (7OH-CCA) [$C_{10}H_6O_5$ F.W. =206.15., CAS No= 779-27-1] is commercially available it is unnecessary to use the H_2O_2 + CCA path for calibration. Instead one can use a known concentration of 7OH-CCA to calibrate the fluorescence spectrometer. Still the results are easy to interpret only if the reactions between OH and CCA prevail. Keeping in mind these limitations it was decided to try CCA as a chemical probe for OH radical detection.

Experimental method: For the pulsed corona experiments a 1.1 mM CCA solution was prepared using Millipore water. At fixed pulse intervals, samples of approximately 3 mL were drawn from the treated solution and its fluorescence yield was measured.

Para-chlorobenzoic acid (pCBA): In light of the limitations of CCA and because of the strong acidity of CCA solutions which influences the development of streamers, pCBA was considered as an alternative OH radical scavenger. pCBA is a highly selective probe for OH-radicals. It strongly reacts with OH radicals, but only weakly reacts with other oxidants created in the in the streamer discharge. [$k_{\bullet OH \text{ pCBA}} = 5 \times 10^9 \text{ M}^{-1} \text{ s}^{-1}$; $k_{O_3 \text{ pCBA}} < 0.5 \text{ M}^{-1} \text{ s}^{-1}$]. Based on the experience gained for OH radical detection in photochemically treated and ozonated media pCBA was expected to be a diagnostic for OH radical measurements in a

corona reactor. [77, 79-82]. A disadvantage of pCBA is its very low solubility. In addition the pH-value needs to be adjusted before treatment.

The usage of pCBA for OH radical determination is based on the disappearance of the probe compound.

$$\frac{-dC_{pCBA}}{dt} = k C_{pCBA} C_{OH}$$

The degradation of pCBA is a measure of the amount of OH radicals reaching the bulk water in the course of an experimental run. Its disappearance can be detected by using a reverse phase high performance liquid chromatography (HPLC). The chromatography is an analytical separation process, which is used to separate individual materials from material mixtures. The sample is injected into a stream of liquid (eluent, mobile phase) under high pressure which sweeps the sample components into a column (immobile phase) and then to a detector. Separation occurs in the immobile phase as different components have a different chemical affinity to it. To measure the pCBA concentration it is necessary to prepare standard solutions for calibration. The various solutions of known pCBA concentration have been prepared in the following way: First a stock solution of p-CBA is made with Millipore water (double distilled water) at pH=7. From this a set of dilutions is produced maintaining the water at pH =7.

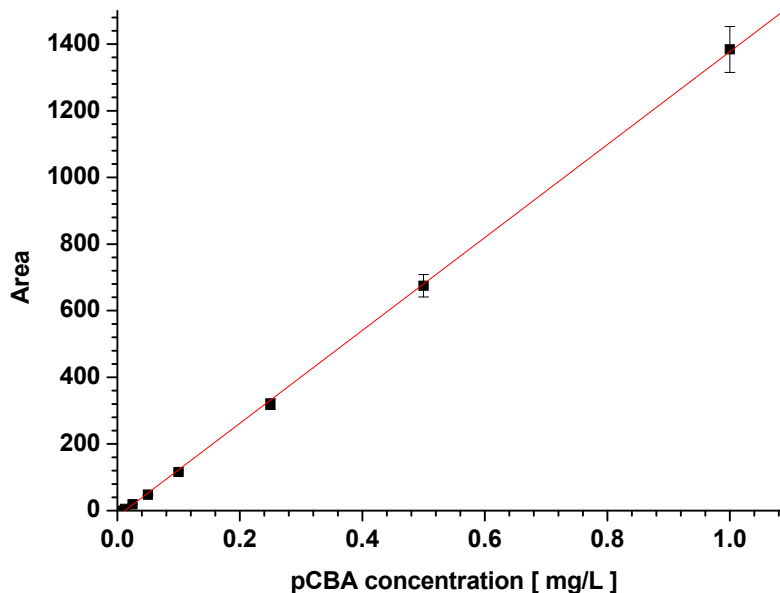


FIG. 3.8. Peak area counts of the HPLC UV-detector vs. pCBA concentration

To circulate pCBA under higher pressure through the detection column an eluent is required which has been prepared as follows. 1.94 g of $\text{NaH}_2\text{PO}_4 \cdot 2\text{H}_2\text{O}$ were dissolved in 225 mL of Millipore water and 275 mL of Methanol Lichrosolv (HPLC grade). In this solution H_3PO_4 was added till the pH had been reduced to 2.5. [83] This solution was double filtered. pCBA streaming through the HPLC column is detected through UV absorbance measurements at 234 nm. For retention times of 3.035 minutes the peak area counts from the UV-detector were determined for different known concentrations of pCBA. Fig. 3.8 shows the measured calibration curve of the HPLC for pCBA.

Experimental method For the corona experiments a solution of 200 μg pCBA in 1000mL of Millipore water was applied. This solution was exposed to the pulse corona discharges for different numbers of pulses. Samples were drawn at different pulse intervals.

Disodium salt of terephthalic acid (DNTA): The use of pCBA as a chemical probe for OH-detection requires a HPLC. Such an instrument was not available at our laboratory and therefore only few screening experiments could be conducted. The limitations connected with the other probes do not appear for terephthalic acid which finally was selected as the standard probe. DNTA is a well-known OH radical scavenger. It has been extensively applied in sono- and radiation chemistry experiments. Through the reaction with OH radicals DNTA is converted into the fluorescent compound hydroxyterephthalic acid (HTA) (Fig. 3.9) [70, 71, 84-89].

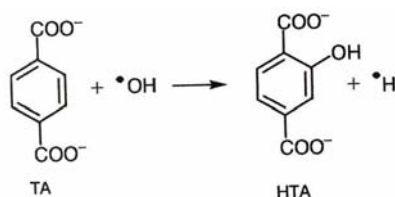


FIG. 3.9. Reaction path for the formation of hydroxyterephthalic acid (HTA)

The fluorescence yield is proportional to the number of hydroxy terephthalic acid molecules that are formed, which is proportional to the available $\cdot\text{OH}$ concentration if the initial DNTA concentration is much larger. The overall reaction path of a terephthalic dosimeter can be explained as:



The disodium salt of terephthalic acid (DNTA) is easily soluble in water and therefore can be used as an effective chemical probe for hydroxyl radical measurement. Because of its high solubility in water sufficiently high concentrations of DNTA can be

realized in the corona reactor. A large time independent concentration of DNTA at any location in the reactor ensures that the measured HTA yield becomes proportional to the $\cdot\text{OH}$ -production at least outside the streamer channel. This may also include the interface region. However, as said before it is unlikely to be true for the interior of the plasma channel. DNTA has a very high reaction rate constant with hydroxyl radicals [$k = 3.3 \times 10^9 \text{ M}^{-1}\text{s}^{-1}$]. Finally, it is non-toxic, which makes it suitable for some experiments involving microorganisms.

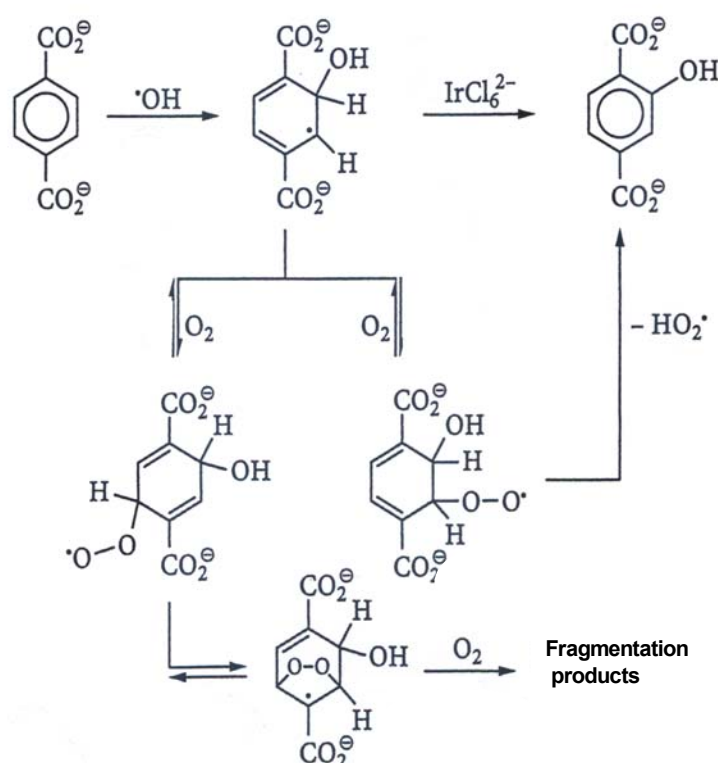


FIG. 3.10. Mechanism of HTA formation. The intermediate product, an $\cdot\text{OH}$ adduct, is oxidized into HTA by two pathways.[71]

This complete mechanism of $\text{OH} + \text{DNTA} \rightarrow \text{OH adduct} \rightarrow \text{HTA}$ is shown in Fig. 3.10. The transition from the $\cdot\text{OH}$ adduct to HTA has been studied by von Sonntag and co-workers [71] and based on their result it is estimated that in air saturated water only 35% of the $\cdot\text{OH}$ adduct will be converted into fluorescent HTA. In presence of a strong oxidant IrCl_6^{2-} (non-reactive towards OH radicals) the yield of HTA is 85 %. In this dissertation all experiments are performed very close to the possible natural conditions hence the measured OH radical yield is only 35 % of actual yield.

Experimental method: Initially for a few experiments a mixture of 2.0 mM terephthalic acid 5 mM NaOH was prepared [89]. To make the preparation simpler in later experiments we used solutions of the di-sodium salt of terephthalic acid (DNTA).

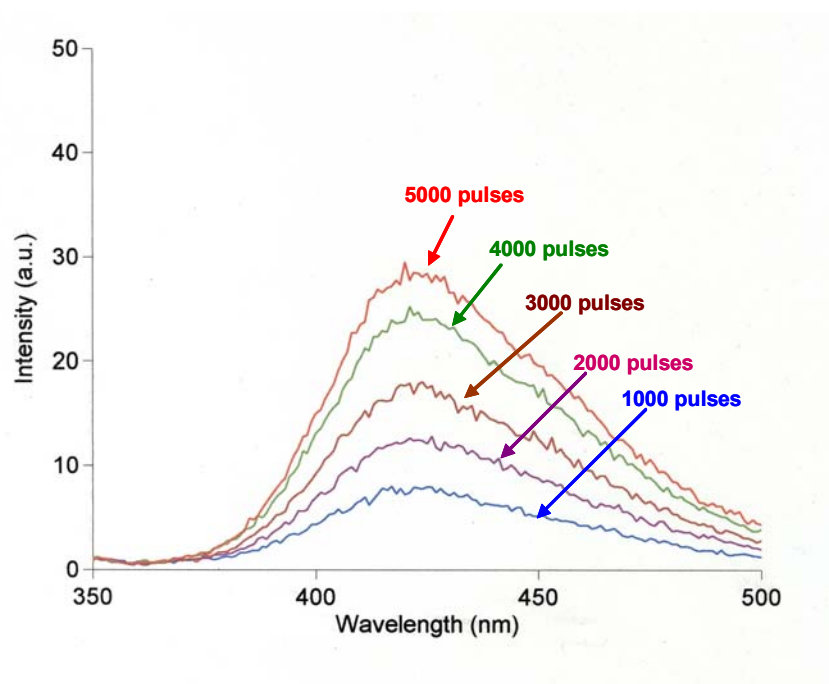


FIG. 3.11. Fluorescence spectra of HTA after different numbers of applied pulses

DNTA being an ionic salt increases the conductivity of the solution. Typically a 2 mM concentration of DNTA is sufficient to trap most of the OH radicals present in the bulk water of the corona reactor. By adding 2 mM DNTA in Millipore water the solution conductivity increases up to $380\mu\text{S}/\text{cm}$, which is very close to the conductivity of tap water. Using 2 mM DNTA solutions pulsed corona discharges with different electrical parameter variations were carried out. The HTA fluorescence yields from samples drawn from each run was detected with a Varian Cary Eclipse spectrophotometer using an excitation slit of $5\ \mu\text{m}$ and an emission slit of $2.5\ \mu\text{m}$ (excitation wavelength $\lambda_{\text{ex}} = 315\ \text{nm}$; emission wavelength $\lambda_{\text{em}} = 425\ \text{nm}$). A linear increase of fluorescence yield with increasing pulse numbers and pulse energies was observed. A set of fluorescence spectra obtained after different pulse numbers is shown in Fig. 3.11.

2-hydroxyterephthalic acid (HTA): To quantify the measurements a calibration curve for different known concentrations of HTA had to be prepared. Since HTA was not available commercially it had to be synthesized in our lab according to a procedure described in the literature by Mason [89]. A stock solution of synthesized HTA was prepared, which then could be used to make different dilutions of HTA to establish the calibration curve. The excitation wavelength was set at 315 nm and the fluorescence spectrum from the sample was recorded between 400 and 500nm. The fluorescence peak was quantified for various dilutions.

Preparation of HTA: The recipe for HTA preparation described by Mason [89] consists of the following steps: 2-bromoterephthalic acid (0.102 mol) and sodium hydroxide (0.204 mol) are dissolved in 470 cm³ of water; after addition of sodium acetate (0.224 mol), copper powder (0.13g) and a few drops of phenolphthalein, the aqueous mixture is stirred and heated at reflux for 10 hours; aqueous potassium hydroxide (5%) is added occasionally to keep the reaction mixture alkaline (pH=8); after cooling, the mixture is filtered, and the filtrate is acidified with HCl (2 mM). The white crystals are collected by filtration and dried in a vacuum oven. The final product was confirmed by measuring the melting point of HTA (325°C).

Calibration curve of HTA: A stock solution of 2-hydroxyterephthalic acid (HTA) was prepared as follows: 0.364 g of HTA, 0.200 g of NaOH, and a phosphate buffer (pH 7.39), made from KH₂PO₄ (0.588 g) and Na₂HPO₄·12H₂O (0.982 g) were dissolved in 1000 mL of Millipore water. The final concentration of HTA in this stock solution was 2 m mol/L. The stock solution was serially diluted down to a concentration of 0.2 μmol/L. As described before in this section the fluorescence yield from each solution was measured. All measurements were performed at room temperature. Fig. 3.12 presents a graph of fluorescence intensities versus HTA concentrations, which demonstrates the linear relationship in the plotted range of concentrations.

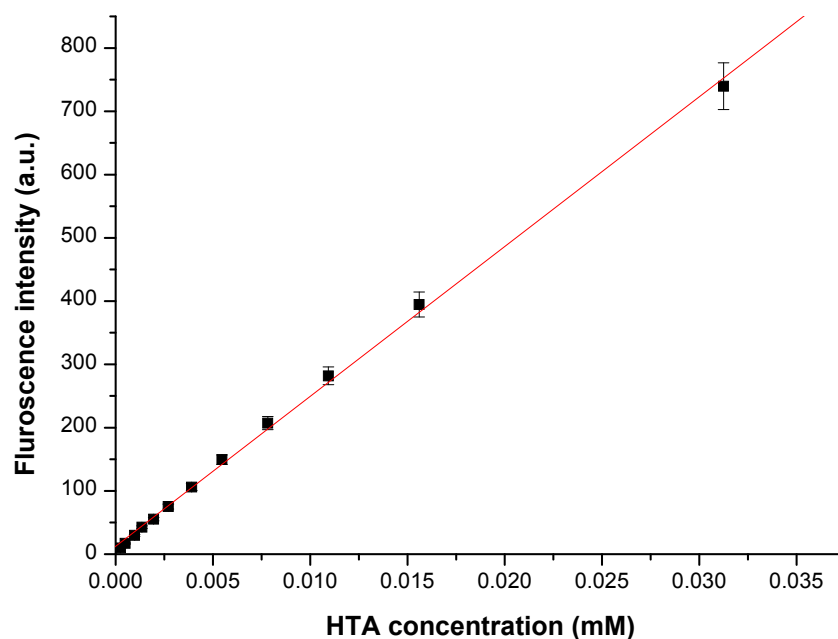
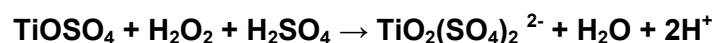


FIG. 3.12. Fluorescence intensity as a function of HTA concentration

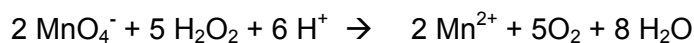
3.5.3 Hydrogen peroxide: The most stable and abundant oxidant appearing in the pulsed streamer discharges is hydrogen peroxide, (H_2O_2). Due to their short life time OH radicals have to be detected during the streamer discharges. In contrast the determination of H_2O_2 can be performed after termination of the discharges. H_2O_2 plays an important role in the disinfection of water. In the bulk solution it can react with other species and produce OH radicals. Two methods were used to determine the production of hydrogen peroxide in pulsed underwater corona discharges:

Eisenberg method: The well known colorimetric method proposed by Eisenberg [90] is based on the photometric analysis of the intense yellow-orange colour appearing in a solution containing hydrogen peroxide after the addition of titanyl sulphate. The yellow colour produced is due to peroxotitnylsulfonic acid. The reaction of H_2O_2 with the reagent takes place as follows:



The concentration of the yellow-coloured peroxotitanyl complex is determined by absorption spectroscopy at 410nm [91]. The absorbance at this wavelength is directly proportional to the initial hydrogen peroxide concentration.

Experimental method: 2.4 g titanylsulfate (hydrate) was mixed with 100 mL (20%) H_2SO_4 in a volumetric flask and the remaining volume of the flask was filled up to 500 mL with Millipore water. After pulse treatment a sample of 3 mL was drawn from the corona reactor and mixed with 0.3 mL of the prepared titanylsulphate solution in a cuvette. From the absorbance measured with a photo spectrometer the H_2O_2 concentration was derived. For a few samples this method was calibrated by determining the total number of H_2O_2 moles through titration with KMnO_4 .



Allen's method: In the underwater corona discharges the main pathway of H_2O_2 production is the self-reaction of OH radicals. Therefore it is desirable to measure the evolution of H_2O_2 and OH radical production simultaneously. As described earlier DNTA was used as an OH radical scavenger. However, in presence of DNTA titanyl sulphate precipitates and cannot be used for H_2O_2 detection. To overcome this problem, an alternative colorimetric method for the detection of hydrogen peroxide described by Allen was used. It is based on the reaction of H_2O_2 with iodide: [92].



The result of this reaction is iodide, an iodine complex of intense yellow colour. The absorption of the sample at 350 nm was measured with a UV-VIS photo absorption spectrometer. As described in section 3.5.1, the concentration of any compound is given as

$$C = \frac{A}{\epsilon l}$$

From this relation the H₂O₂ concentration was derived as follows.

$$\text{H}_2\text{O}_2 \text{ concentration} = \frac{D_A - D_B}{\epsilon l} \frac{V_T}{V_S} (\text{mol L}^{-1})$$

where,

- D_A = absorption of the mixture of H₂O₂ with Allen's reagent
- D_B = absorption of Allen's reagent alone
- V_T = total solution volume (Millipore water, iodide and H₂O₂)
- V_S = sample volume
- l = optical path length of cuvette (1 cm)
- ε = absorption coefficient of H₂O₂ (25000 L mol⁻¹ cm⁻¹)

Experimental method: As described by Allen [92] 1 g of NaOH, 33 g of KI, 0.1 g of ammoniumheptamolybdate tetra hydrate [(NH₄)₆M₀₇O₂₄·4H₂O], were mixed together in a volumetric flask and filled up with Millipore water to 500mL. A further solution was prepared by adding 10 g of potassium hydrogen phthalate [C₈H₅KO₄] in a volumetric flask, filled up with Millipore water to 500 mL. The alkaline solution of iodide is stable, but iodide is slowly oxidized by dissolved oxygen at the pH of the mixture of both solutions, where peroxide reacts rapidly with iodide in the presence of the molybdate catalyst. After pulsed corona treatment, a 1 mL sample of the treated water was added to 2.5 mL of freshly prepared iodide and ammonium molybdate solution (by mixing both solutions) in a 5mL volumetric flask. The excess flask volume was filled up with Millipore water. A yellow iodine complex was formed. Its absorbance counts were measured at 350 nm.

3.5.4 Ozone: As mentioned previously, small quantities of ozone have also been detected in underwater streamer discharges. Its bactericidal effects are well known and it reacts with pollutants as well. Ozone also reacts with H₂O₂ and generates OH radicals. Therefore it is important to determine the formation of ozone in underwater streamer discharges quantitatively. Again this will only access the ozone that finally reaches the bulk water or is collected in a gas plenum.

Detection in the gas phase: It is expected that the production of ozone can be increased if a stream of oxygen micro bubbles flows through the reactor. As sketched in Fig. 3.13, this was achieved with a special micro bubble generating apparatus at the bottom of the vertical reactor.

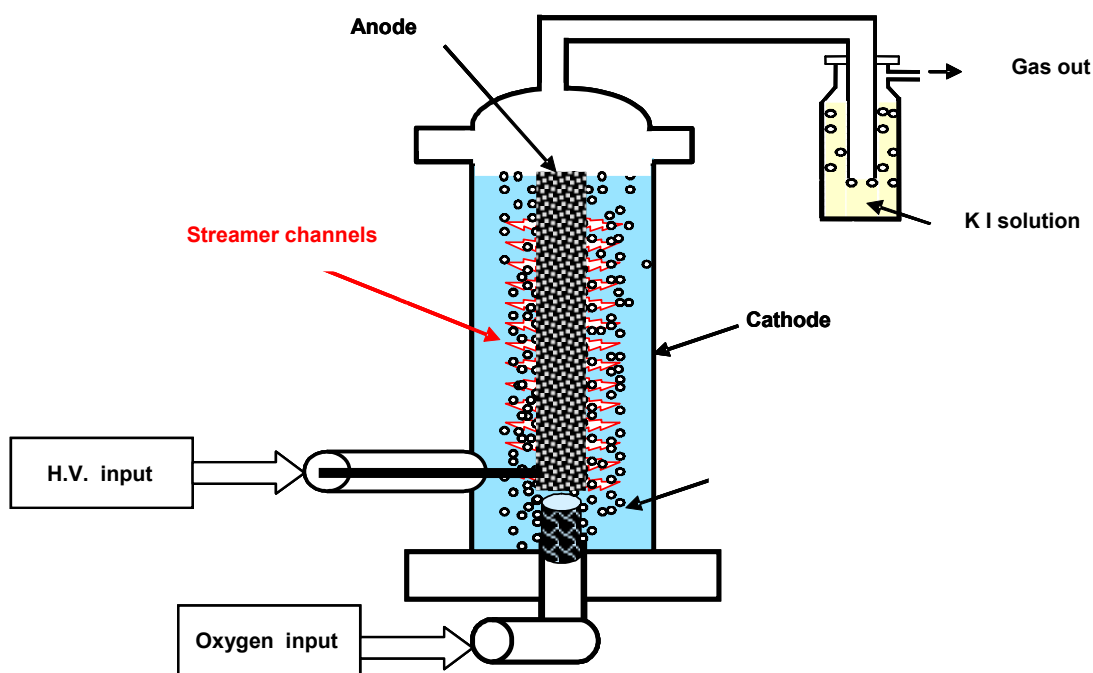


FIG. 3.13. Setup for the determination of ozone out gassing from the corona reactor while a stream of oxygen micro-bubbles flows through the active volume.

To assess the total amount of ozone produced during the streamer discharges in this case the ozone was collected in a gas plenum above the reactor and ventilated through a bottle filled with an iodide solution. The ozone reacts in the bottle with the potassium iodide solution and forms a yellow iodine complex.



Preparation of KI solution: 13.12 g $\text{Na}_2\text{HPO}_4 \cdot 12\text{H}_2\text{O}$, 3.52 g KH_2PO_4 and 20 g KI were mixed in 1L of Millipore water, stirred and kept in dark.

Experimental method: The formation of the iodine complex is determined by again measuring the absorbance of a sample filled into a cuvette with a photo spectrometer. Using the extinction coefficient of iodine ($2.4 \times 10^4 \text{ L mol}^{-1} \text{ cm}^{-1}$) [93] the ozone concentration trapped in a 10 mL volume of the KI solution was determined. This measurement can only

give a rough estimate of the ozone leaving from the reactor, since the gas retention time is too short to lead to a complete reaction between the percolating ozone and KI.

Detection in the liquid phase: Part of the ozone produced in underwater streamer discharges will remain dissolved in the water. As described by Bader and Hoigne [94] this ozone can be detected with the help of the indigo method. Indigo has a strong absorbance at 600 nm ($\epsilon = 20000 \text{ L mol}^{-1} \text{ cm}^{-1}$). One molecule of ozone can decolourise one molecule of the indigo. The decolorized products scarcely consume further ozone. The amount of ozone that has been scavenged can be determined from the decolourisation of the reagent measured at 600 nm. As this measurement is performed after pulsing of the reactor no interference with OH radicals is expected. It has been observed that the presence of hydrogen peroxide does not interfere with the measurement. A similar result has been reported in earlier studies [94, 95]. The reaction mechanism of ozone with indigo is shown in Fig. 3.14.

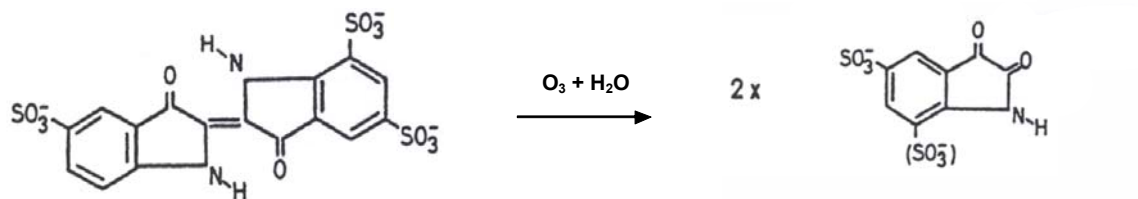


FIG. 3.14. Reaction of ozone with indigo trisulfonic acid and formation of isatin sulfonic acid

Preparation of Indigo reagent: As described by Hoigne [94-95] for ozone detection two different solutions were prepared.

Solution-A: About 0.5 mL phosphoric acid and 310 mg indigo trisulfonate, were mixed together in a volumetric flask and filled up with Millipore water to 500mL.

Solution-B: 14 g of sodium dihydrogen phosphate and 17.5 g H_3PO_4 were mixed together in a volumetric flask and filled up with Millipore water to 500 mL.

Ozone measurement: 2 mL of each reagent solution were mixed together in a volumetric flask and filled up with Millipore water to 25 mL. The absorbance of this solution was measured and recorded as a reference [**blank** absorbance count]. To determine the ozone concentration dissolved in the water again 2 mL volumes of each reagent were mixed together in a 25 mL volumetric flask and rest of the volume was filled up with treated water. Then the absorbance of the solution was measured and recorded as the **sample** absorbance.

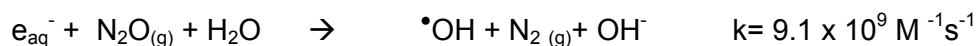
Calculation of dissolved Ozone: As described before (page 40) the O_3 concentration was calculated from the differences of absorbance between the initial Indigo solution and the one exposed to ozone. The absorption coefficient of indigo ($\epsilon = 20000 \text{ L mol}^{-1} \text{ cm}^{-1}$) has been taken from Ref. [94-95].

Experiment method: Na_2SO_4 salt was added to Millipore water until a conductivity of $400 \mu\text{S/cm}$ was obtained. Before pulsed corona treatment this solution was saturated with oxygen gas, by bubbling oxygen through the reactor with a flow rate of approximately 500 mL/min for 20 minutes. During this experiment the top flange was removed from the reactor and prior to the application of corona discharges the oxygen flow was stopped. After fixed pulse intervals samples were drawn from the reactor and the dissolved ozone concentration was determined by the method described above. The results will be discussed in section 4.4.

3.6 Diagnostic of reductive species

In addition to primary oxidative species some reactive reductive species are also produced in the streamer discharges. Among these are H^\bullet , energetic electrons, and the super oxide radical anion ($O_2^{\bullet-}$). These reactive reductive species also take part in many chemical as well as disinfection reactions. Here the experimental method used to confirm the appearance of solvated electrons (e_{aq}^-) and super oxide radical anions ($O_2^{\bullet-}$) are presented.

3.6.1 Solvated electrons: In an aqueous solution saturated with N_2O solvated electrons will be converted into OH radicals by the following reaction [96]:



Experimental method: A 2 mM DNTA solution in water ($400 \mu\text{S/cm}$, at neutral pH) is saturated with N_2O by continuously (for 2 hours) bubbling the gas through it. The maximum solubility of N_2O in water at 25°C and standard pressure is equal to $56.7 \text{ mL}/100 \text{ mL}$. The saturated solution was treated with pulsed underwater corona discharges for different numbers of pulses. A stream of N_2O bubbles continued to flow through the reactor chamber also during the experiment. Results will be discussed in chapter 4.

3.6.2 Super oxide ions ($O_2^{\bullet-}$): Nitro blue tetrazolium chloride (NBT) was used to detect the super oxide anion ($O_2^{\bullet-}$). NBT reacts with super oxide ions by forming purple formazan (Fig. 3.15). The presence of super oxide anions is detected by measuring the reduction in absorbance of NBT (at 280 nm) and the increase in absorbance by formazan (at 530 nm) [70, 97-100]. The presence of H_2O_2 does not disturb the measurement.

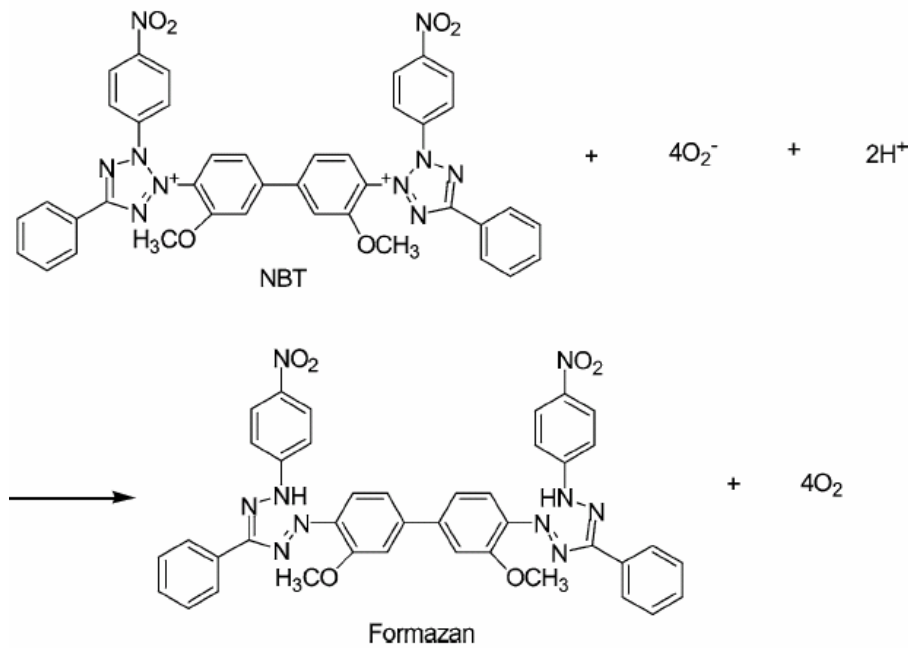


FIG. 3.15. Reaction mechanism of NBT with super oxide anions and the formation of formazan [100].

Experimental Method: A NBT solution was prepared as described in the literature by Kovache [97] by dissolving 408.82 mg of NBT in Millipore water using a volumetric flask. The 1000 mL flask was filled with Millipore water containing 10% of ethanol. A 0.1 mM concentration of n- butanol was added to scavenge the produced OH radicals. The total number of n- butanol molecules added was 100 times higher than the number of OH radicals reaching the bulk solution during an experimental run with 5000 pulses. As previously the solution conductivity was adjusted to $400 \mu\text{S}/\text{cm}$ by adding the necessary amount of Na_2SO_4 salt. All experiments were performed at neutral pH. After fixed pulse intervals 2 mL samples were drawn from the reactor. Since the formazan produced during the experiment is insoluble in the aqueous solution an equal amount of 2 mL methanol was added to the sample. A light purple colour was obtained. Using this sample the absorbance spectra of NBT and formazan were recorded.

3.7 UV diagnostics

Nowadays disinfection of water by UV irradiation is a commonly applied technique. Short wavelength ($<220 \text{ nm}$) UV radiation can directly dissociate water molecules into OH radicals. UV-radiation can also react with H_2O_2 or ozone producing OH radicals. UV radiation can directly kill micro organisms. Hence UV reacts with micro organisms through various path ways. To detect the UV radiation emitted from the streamer channels spectroscopic and chemical diagnostics were applied in our experiments.

3.7.1 Spectroscopy: To determine the UV-spectrum emitted from the streamer channels a calibration of the complete set-up is required. This includes the spectrometer, the fibre optic cable, the diffuser and the quartz window of the reaction chamber. The measured spectrum is an average over many streamers and a large volume. However not all volume elements in the viewfield of the spectrometer contribute with the same weight to the spectrum since the radiation paths in water and therefore the attenuations are much different. The calibration which is done with a calibrated UV lamp does not take into account these factors. The calibration was carried out at the Institute of Lighting Technology (LTI) at the University of Karlsruhe.

UV calibration lamp: A standard deuterium lamp (OL UV-40 serial number 731) emitting a line-free continuum radiation in the wavelength range between 200 and 400 nm was used for the calibration of the spectrometer. The lamp emission is strongest at 200nm, where most instrument sensitivities are low and weakest in the visible and infrared region (which reduces stray-light problems). The OL UV-40 consists of a stable, 30-watt deuterium lamp with an ultraviolet transmitting suprasil window. Its absolute spectral irradiance values (for a distance of 30 cm) are known at 10 nm steps between 200 and 400 nm. These irradiance values have been reproduced in Fig. 3.16. Using this lamp the spectral intensity distribution plotted in Fig 3.17 was obtained with the complete experimental spectrometer setup (for the same distance of 30 cm). At the position of the diffuser the measured spectral intensity was compared with the known spectral irradiance values of the reference source. From both curves the absolute efficiency of our spectrometer setup was derived.

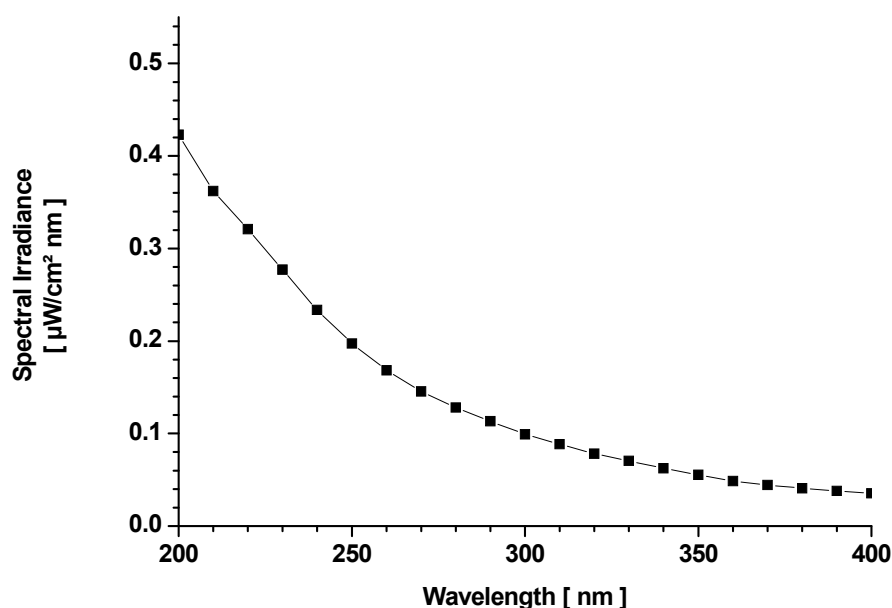


FIG. 3.16. Calibrated spectral irradiance values of the deuterium UV source at a distance of 30 cm.

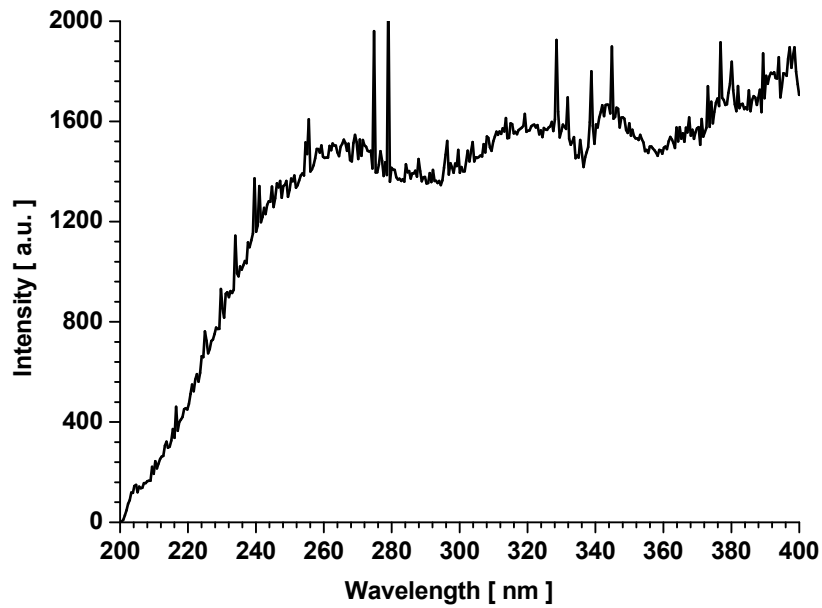


FIG. 3.17. Spectral intensity distribution from the UV calibration source as measured with the experimental setup. Distance from the lamp: 30 cm.

Calibration of the experimental set up: The set up used to calibrate the UV spectrometer is sketched in Fig.3.18. The set up used in the pulsed corona experiments includes a spectrometer, an optical fibre cable and a quartz diffuser. The quartz diffuser was obtained from the Institute of Lighting Technology (LTI), Karlsruhe Technical University.

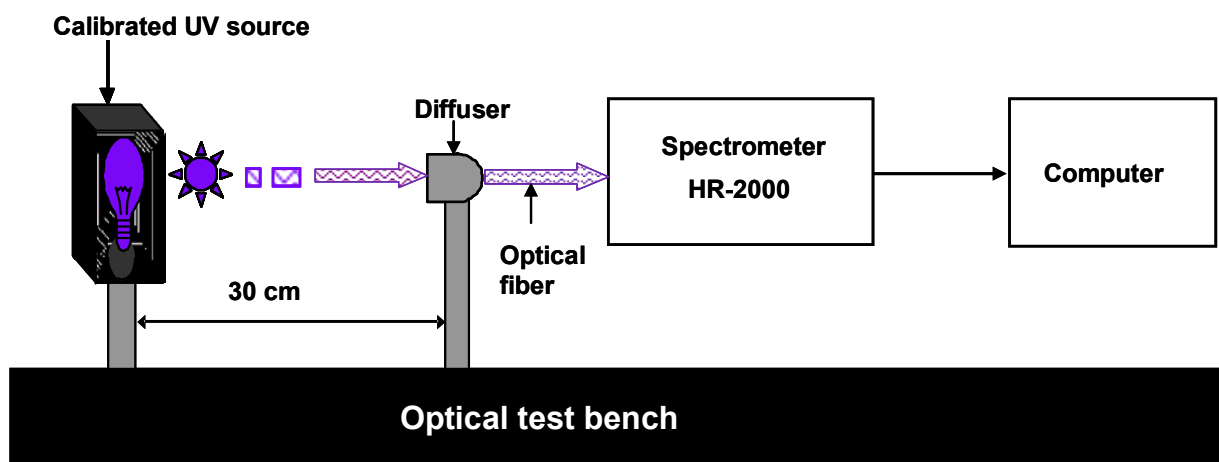


FIG. 3.18. Set up for the calibration of the UV spectrometer used in the pulsed underwater corona experiments.

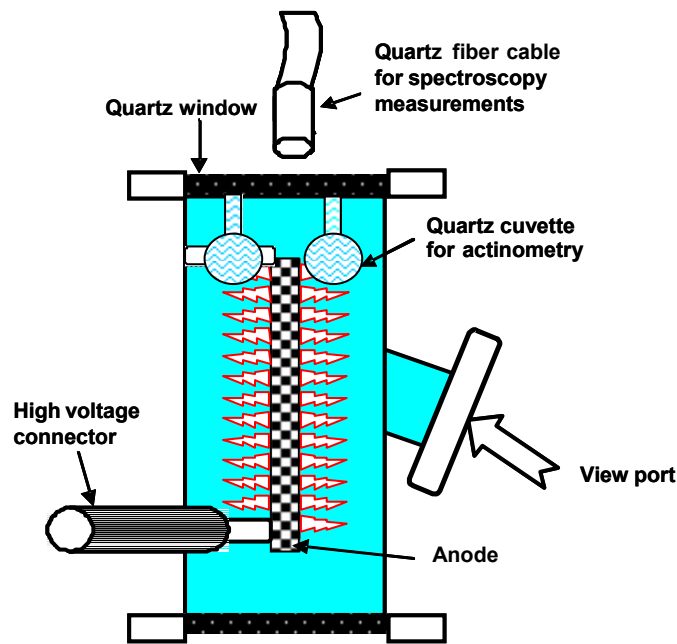


FIG. 3.19. Arrangement for the measurement of UV-radiation from the corona reactor. The sketch indicates the light pick-up for the spectroscopic measurements and the set-up for the actinometry as well.

Experimental method: The position of the quartz diffuser was chosen to receive a high UV irradiance from the streamer channels. The quartz diffuser accepts a large range of entrance angles and couples the UV radiation into the optical fibre. This experimental set up is sketched in Fig. 3.19. Using the following expression, for the spectral irradiance ($\mu\text{W}/\text{cm}^2\text{nm}$) from the plasma channels was calculated.

$$\frac{\text{Spectral irradiance of reference source}}{\text{measured reading from reference source}} \times (\text{measured reading from pulsed corona source})$$

3.7.2 Chemical actinometry: UV radiation from an unknown source can also be measured, on the basis of chemical changes induced by the light; which is known as 'chemical actinometry'. In this case a chemical compound, whose photochemical reaction mechanism is known, is exposed to the UV irradiation. Depending on the kind of chemical compound either the build-up of a product or the destruction of the compound is measured. Knowing the quantum yield (Φ_{λ}) of this reaction the UV irradiance can be calculated. Existing actinometric methods are calibrated by using a calibration lamp or by measuring the irradiance quantitatively e.g. with a calibrated photo diode. For our experiments uridine has been selected as the chemical compound [101-105].

Uridine actinometry: The utilization of uridine is one of the most accepted and well-proven methods in UV dosimetry. The uridine molecule contains uracil a naturally occurring nucleobase. Its UV absorption characteristics are very similar to those of DNA (Fig. 3.20 [A – B]).

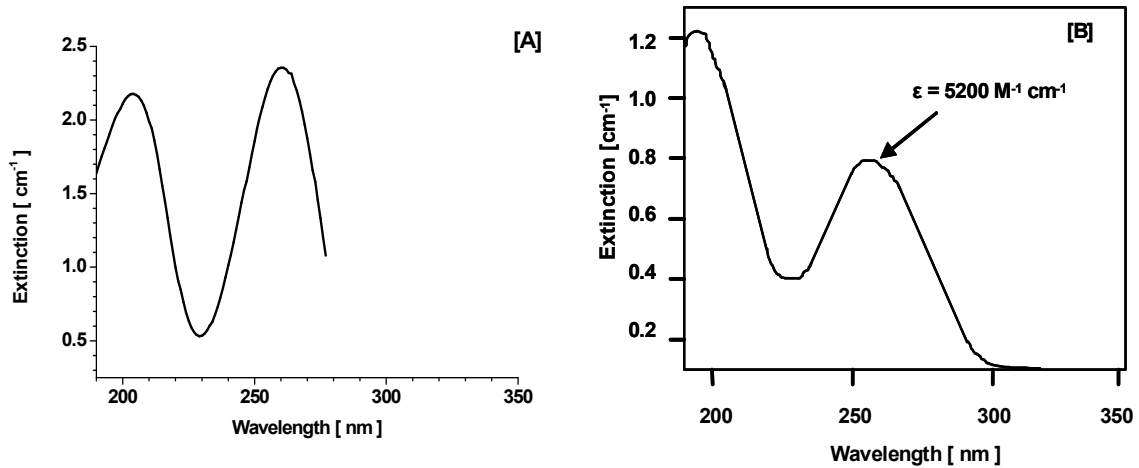


FIG. 3.20. UV absorption characteristics of uridine [A] and DNA in aqueous solutions [B].

The maximum absorption of uridine occurs at $\lambda = 262 \text{ nm}$. If the uridine molecule interacts with UV-radiation it gets converted into its photohydrate (i.e. one molecule of H_2O is added to uridine) version. Absorption at 262 nm is absent for the photohydrate molecule of uridine [104, 105]. Therefore with increasing UV dose the absorption of the uridine probe in the wavelength range between 216 and 280 nm decreases. The quantum efficiency of uridine destruction through hydrate formation is almost wavelength independent in the range 220 nm to 280 nm. For this range the calculated quantum yield varies between 0.016 and 0.019. This means that the chemical response of the uridine actinometer is largely independent of the UV source spectrum and its similarity to DNA absorbance mirrors the bactericidal effect of UV-radiation quite well.

In uridine actinometry the incident photon flux ($P_{0,\lambda}$) can be derived from the following expression [104, 105].

$$\ln\left(\frac{[C]}{[C_0]}\right) = -\frac{\epsilon I \Phi_{\lambda}}{V} P_{0,\lambda} t$$

where $\ln\left(\frac{[C]}{[C_0]}\right)$ = ratio of final and initial concentration of uridine.

ϵ = extinction coefficient of uridine ($8410 \text{ L mol}^{-1} \text{ cm}^{-1}$)

l	=	optical path length (1cm)
Φ_{λ}	=	quantum yield of uridine (0.019) (ratio of reacting and incident photons)
V	=	volume
$P_{0,\lambda}$	=	incident photon flux (mol/s)
t	=	time (s)

The total incident photon flux $P_{0,\lambda}$, [mol/s] is related to the incident photon energy flux by:

$$E \text{ [W/m}^2\text{]} = P_{0,\lambda} \frac{\hbar c}{\lambda}$$

Experiment method: It was tried to apply uridine actinometry to determine the average UV dose occurring in the corona reactor. For this purpose a small concentration (7 μM) of uridine was dissolved in the Millipore water used in the reactor. After pulse treatment the change of uridine absorbance in the wavelength range 200 to 300 nm was measured with the Cary scan-500 (make: Varian) UV spectrophotometer. Especially the peak absorbance at 262 nm was evaluated. However the measurements led to contradictory results. It is believed that the oxidants from the streamers were mainly responsible for these findings.

Therefore indirect measurements were performed too. As shown in Fig 3.19, a cuvette of Suprasil quartz (transparent for 200 – 400 nm) filled with a uridine solution was located at a position inside the reactor where it could collect a large fraction of the UV radiation from plasma channels. After exposure the absorbance of the cuvette solution was measured and compared to its absorbance before treatment.

3.8 Diagnostics of bactericidal effectiveness

The ultimate goal of the investigation of pulsed underwater corona discharges is to optimize the disinfection efficiency of the system. For that purpose a strain of bacteria (*Pseudomonas putida*) that can be handled without safety regulations was exposed to the streamer discharges and its inactivation rate was determined after increasing pulse numbers. To detect the killing rates two methods were applied: epifluorescence microscopy and heterotrophic plate counting (HPC). The difference between both methods is that epifluorescence microscopy counts all bacteria which show metabolic activity, while plating

counts make only those bacteria visible that are able to reproduce themselves. These plate counts measurements were performed with the support of the microbiology laboratory at the Institute of Technical Chemistry (ITC-WGT) at Forschungszentrum Karlsruhe (FZK) [106].

3.8.1 Epifluorescence microscopy: For the epifluorescence microscopy the bacterial cells were stained with 4', 6-diamidino-2-phenylindole (DAPI), and 5-cyano-2, 3-ditolyl tetrazolium chloride (CTC) dyes which are commonly used in cell biology [106, 107].

The CTC is a monotetrazolium redox dye, which produces a fluorescent formazan (CTF) when it is chemically or biologically reduced. CTF crystals are not soluble in water and they remain inside the cell. This compound can be easily detected because of its bright red fluorescence when illuminated by long-wavelength UV light (>350nm). The unreduced CTC does not emit light above 400 nm. While the excitation maximum of the formazan is at 450 nm, the emission maximum of formazan is at 630 nm.

DAPI is a fluorescent dye that binds unspecifically to DNA molecules and induces a blue fluorescence. The excitation wavelength of DAPI is at 358 nm and its emission maximum is at 461 nm (Fig. 3.21). DAPI staining allows the determination of the total number of bacteria in the sample.

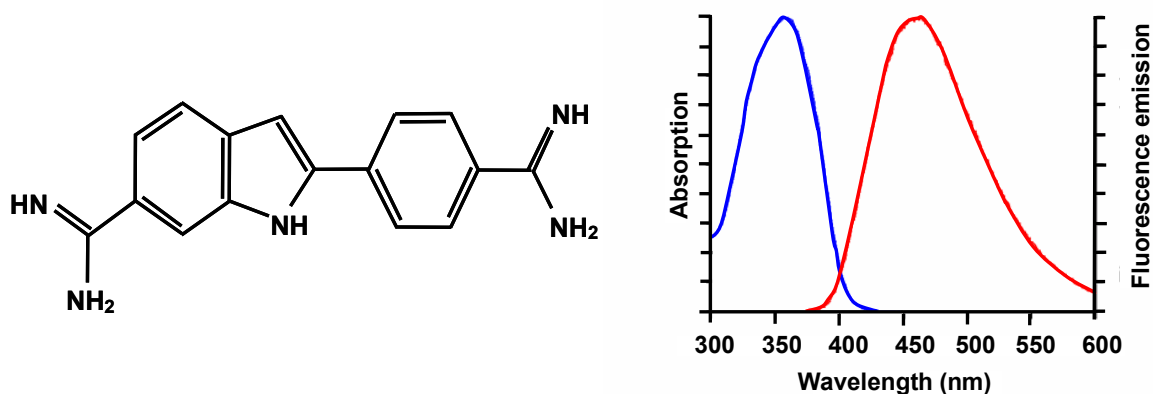


FIG. 3.21. The DAPI (4', 6-diamidino-2-phenylindole) molecule and its absorption and fluorescence spectra

Experiment methods: The reactor was filled with water containing a known concentration of *Pseudomonas putida* bacteria. A control sample was kept as a reference. After exposure to different numbers of pulses samples were taken from the reactor for evaluation. To stain the bacteria with CTC first a stock solution of CTC (Polyscience, Eppelheim, Germany) was prepared by dissolving one vial of 100 mg CTC compound in 6.6 ml double distilled water to get a final concentration of 50 mM. 200 μ L of this stock solution was added to the test tubes containing 2 mL water samples either from the reactor or from the control. In this solution the resulting concentration of CTC was 4 mM. The filled test tubes

were incubated for 60-90 minutes at 30 °C. After that, the samples were dispensed into filter towers over 25 mm (diameter) black Nucleopore polycarbonate membrane filters (filter pore size 0.2 µm) and 100 µL aliquot was filtered by using a vacuum pump. The filter was covered for about 15 minutes with a 0.5 mL solution of DAPI. The DAPI solution had been prepared by adding 2 µL of stock solution (2 mg DAPI from Merck, Germany, in 1 mL distilled water) in 1 mL of distilled water. The filter was removed, air-dried and mounted on a glass microscope slide. To prevent bleaching of the dye by UV light or other oxidants during fluorescence microscopy a drop of anti-fading reagent (Citifluor, London, UK) was added to the filter. All bacterial cells in the grid field of the microscope were counted at a magnification of 10 x 63. Generally 4–6 images per slide were captured with a digital camera. The cells were counted on the monitor screen using inbuilt software. Zeiss filter sets FS05 and FS09 were used for counting. For statistical evaluation, the number of cells observed in 5 microscopic grid fields per sample was calculated. In epifluorescence microscopy we can discriminate between active and inactive bacteria. The killing rate is calculated from the ratio of active bacteria in the treated and control samples.

3.8.2 Heterotrophic plate counting (HPC): The heterotrophic plate count method, formally known as the standard plate count, is a procedure to determine the number of living heterotrophic bacteria in water. Bacterial colonies may arise from pairs, chains or single cells, all of which are summarized in terms of a “colony forming unit” (CFU). The final count also depends upon the interaction among the developing colonies. For our experiments the pour plate method with R2A agar (Merck Darmstadt) as a broth medium has been used.

Pour plate method: The pour plate method can accommodate sample volumes ranging from 0.1 to 2.0 mL. The colonies produced are relatively small and compact, showing less tendency to encroach on each. On the other hand, submerged colonies often are slower growing and are difficult to transfer for bacterial characterization. R2A agar which has been used as the medium for bacterial growth leads to higher counts than any other medium. To prepare the agar broth it was heated and sterilized at 121 °C for 15 minutes. After this it was allowed to cool down. To keep it melted it was kept in a water bath at around 48 °C.

Experimental method: The treated as well as the control samples were serially diluted by powers of ten in PBS buffer (1350 µL Phosphate Buffer Solution (PBS buffer) + 150 µL water sample). Up to 6 dilution steps were applied. A 400 µL portion of the dilution was dropped onto petri dishes (in triplicate). Then R2A agar (16 ml/dish) was added. The neck of the agar bottle was flamed before pouring it onto the petri dishes. Each dish was numbered and all samples were thoroughly distributed by rotating the plates. Once the agar

solution gets solidified the plates were turned round so that moisture could not leave the plates. To get the maximum count the dishes were incubated at 30° C for 5 days. During this incubation period the humidity was controlled. After this all colonies, which were formed, were counted. To avoid errors colony counts below 20 or above 300 were discarded from further evaluation. Bacterial count was performed using following expression:

$$\text{CFU/mL} = [\text{Colonies counted}] / \text{actual volume of sample in dish, mL.}$$

Suspension preparation: A 30 mL Brain Heart Broth was inoculated with 50 μL bacterial suspension of *Pseudomonas putida* reference strain (10^5 - 10^6 bacteria) and incubated at 37° C for 24 hours. To prepare the experimental suspensions a sample from this culture was taken out and then centrifuged at 5000 *g* for 6 minutes. The pellet (settled bacteria) was diluted with a sterilized electroporation buffer (diluted PBS buffer) up to 1000 mL. To achieve the desired conductivity a diluted PBS buffer of pH = 7 was used. The bacterial concentration was estimated spectrophotometrically by determining the absorption at 600 nm wavelength of a 1cm broad cuvette filled with the suspension. In our set-up an absorption value of 0.05 corresponded to 10^5 cells/mL. It is clear that this method can only give rough estimates of the bacterial concentration in the applied solution and the accurate has to be determined by the plate count method of the reference probe that was kept for each experiment.

4. RESULTS

In this chapter we describe the results from electrical, chemical and optical diagnostics obtained with the pulsed underwater corona reactor. In addition measurements of the efficiency of bacterial decontamination are presented.

4.1 Electrical and optical observations

The most important electrical parameters that determine the development of streamer discharges in water are the rise time, the amplitude and the duration of the voltage pulses. The rise time affects the number of streamers that are launched simultaneously while the voltage amplitude and the pulse widths regulate the streamer length.

In order to obtain a large number of streamers in every pulse the voltage rise time should be less than a few tens of ns. For our experiments we have chosen a Blumlein line pulse generator based on lumped inductive (L) and capacitive (C) components. The corona reactor impedance depends upon the reactor geometry, the water conductivity and the thickness and conductivity of the ceramic layer covering the anode. In the course of our experiments four different corona discharge reactors were used. The outer diameters of the cylindrical reactor chambers were 30mm, 36mm, 70mm, and 110mm respectively. The anode lengths and diameters were 200 mm and 6 mm respectively in all cases. The calculated water and ceramic layer resistances and capacitances are presented in Table 4.1. To calculate the ceramic layer resistance it was assumed that it is merely determined by the pores filled with water resulting in a conductivity that is given by the water conductivity multiplied with the porosity. The capacitance of the ceramic layer was the same for all reactor geometries.

Table 4.1. Calculated resistances and capacitances of different corona reactors used for the experimental investigations.

Reactor	Reactor diameter ($l = 200$ mm)	Resistance of water layer (between electrodes) ($\sigma = 400$ μ S/cm)	Resistance of ceramic layer (200 μ m thick with 5% porosity)	C_{water}	C_{ceramic}
	mm	Ω	Ω	pF	nF
A	30	32	25.6	553	2.0
B	36	36	25.6	496	2.0
C	70	49	25.6	361	2.0
D	110	58	25.6	305	2.0

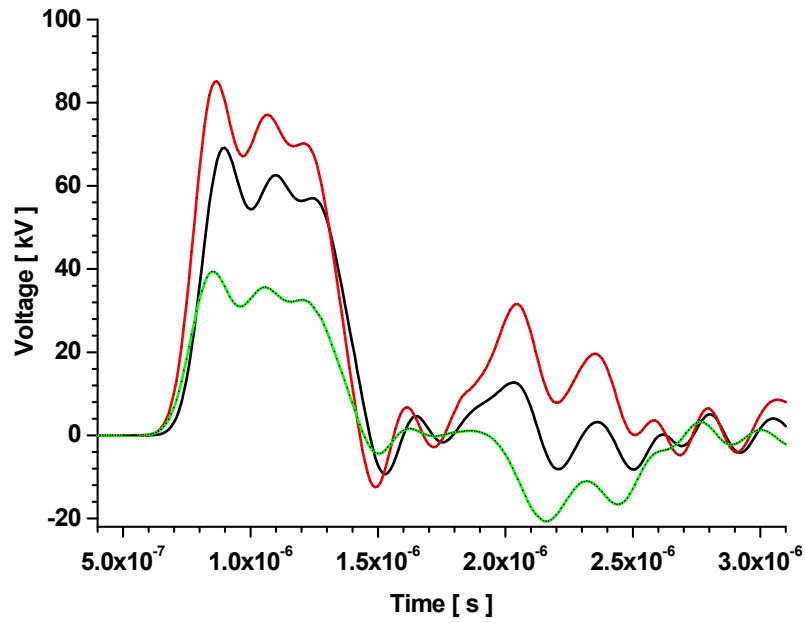


FIG. 4.1. PSpice calculations of voltage pulse shapes for different reactor impedances connected to the $50\ \Omega$ Blumlein LC generator ($L = 1.3\ \mu\text{H}$; $C = 2\ \text{nF}$; 6 LC sections; charging voltage: 60 kV).
 — $Z_{\text{Load}} = 50\ \Omega$; — $Z_{\text{Load}} = 80\ \Omega$; — $Z_{\text{Load}} = 20\ \Omega$

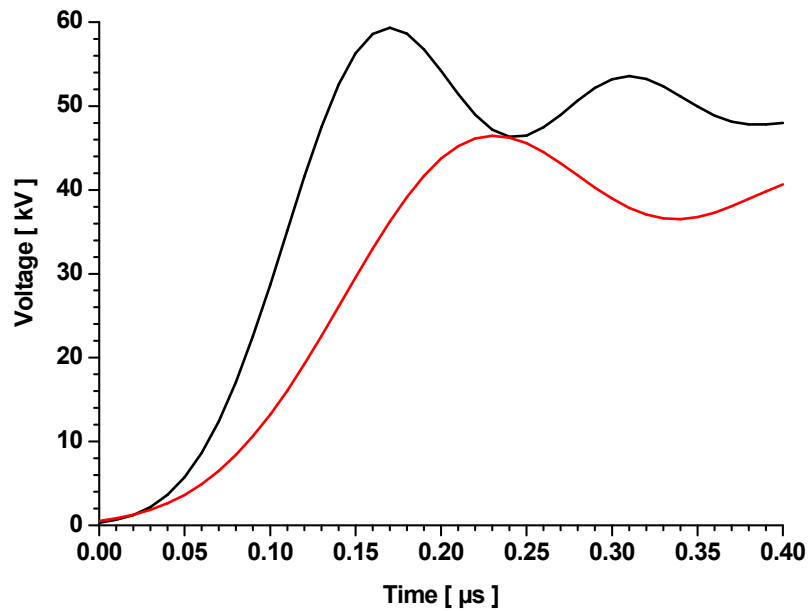


FIG. 4.2. Voltage pulse rise time for two different inductance values (— $0.6\ \mu\text{H}$ and — $1.3\ \mu\text{H}$) in the Blumlein pulse generator circuitry ($C = 2\ \text{nF}$; 6 LC stages; charging voltage: 60 kV)

The water conductivity was assumed to range from $175\ \mu\text{S}/\text{cm}$ to $1200\ \mu\text{S}/\text{cm}$; the typical conductivity of tap water lies around $500\ \mu\text{S}/\text{cm}$. The reactor impedances (for reactor B) were then expected to vary between 20 and $80\ \Omega$. Obviously, it is impossible to match this

impedance range with one generator. To predict the resulting pulse shape variations at the reactor terminals Pspice simulations were carried out assuming a six stage 50Ω Blumlein generator. The results are presented in Fig. 4.1.

Changing the inductance values while keeping the capacitances of the LC-chain elements constant does not only alter the generator impedance and the pulse width but also influences the rise time of the voltage pulse. This effect is shown in Fig. 4.2 for two different values of L . Since both the impedance and the pulse width vary just with the square root of L it was finally decided to use $L=0.6\mu\text{H}$ for the sake of a faster rise time. This Blumlein line consisted of 6 LC elements ($L = 0.6 \mu\text{H}$, $C= 2\text{nF}$) leading to an effective pulse width of 350 ns and a pulse rise time of 60 ns.

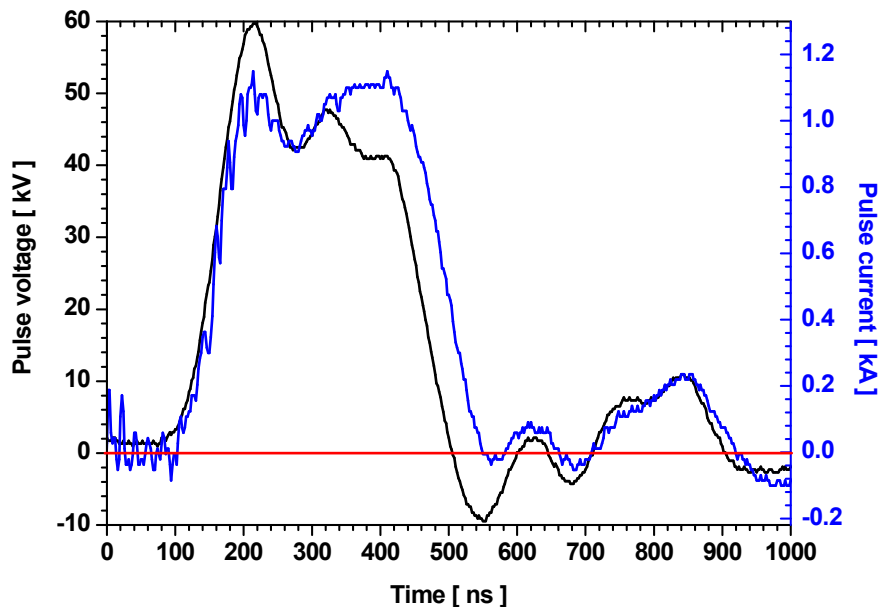


FIG. 4.3. Voltage and current waveforms obtained during an underwater corona discharge (charging voltage: 40 kV; 6 LC sections; $L = 0.6 \mu\text{H}$; $C= 2\text{nF}$; $Z_0 = 35 \Omega$; reactor volume 1L).

Using these values the nominal driver impedance $Z_0 = 2 \sqrt{L/C} = 35 \Omega$ was close to the load impedances of the corona reactor used for the disinfection studies [reactor B]. Using a dummy load the generator was tested for an output voltage of up to 65 kV and a load current of up to 1500 A at a repetition rate of 10 Hz. Typical voltage and current waveforms measured during an underwater corona discharge are shown in Fig.4.3. Using the generator set-up described and a charging voltage of 35 kV experimentally observed pulse shapes for three different corona reactors are shown in Fig. 4.4. Little change in the pulse rise time is observed as the reactor impedance varies.

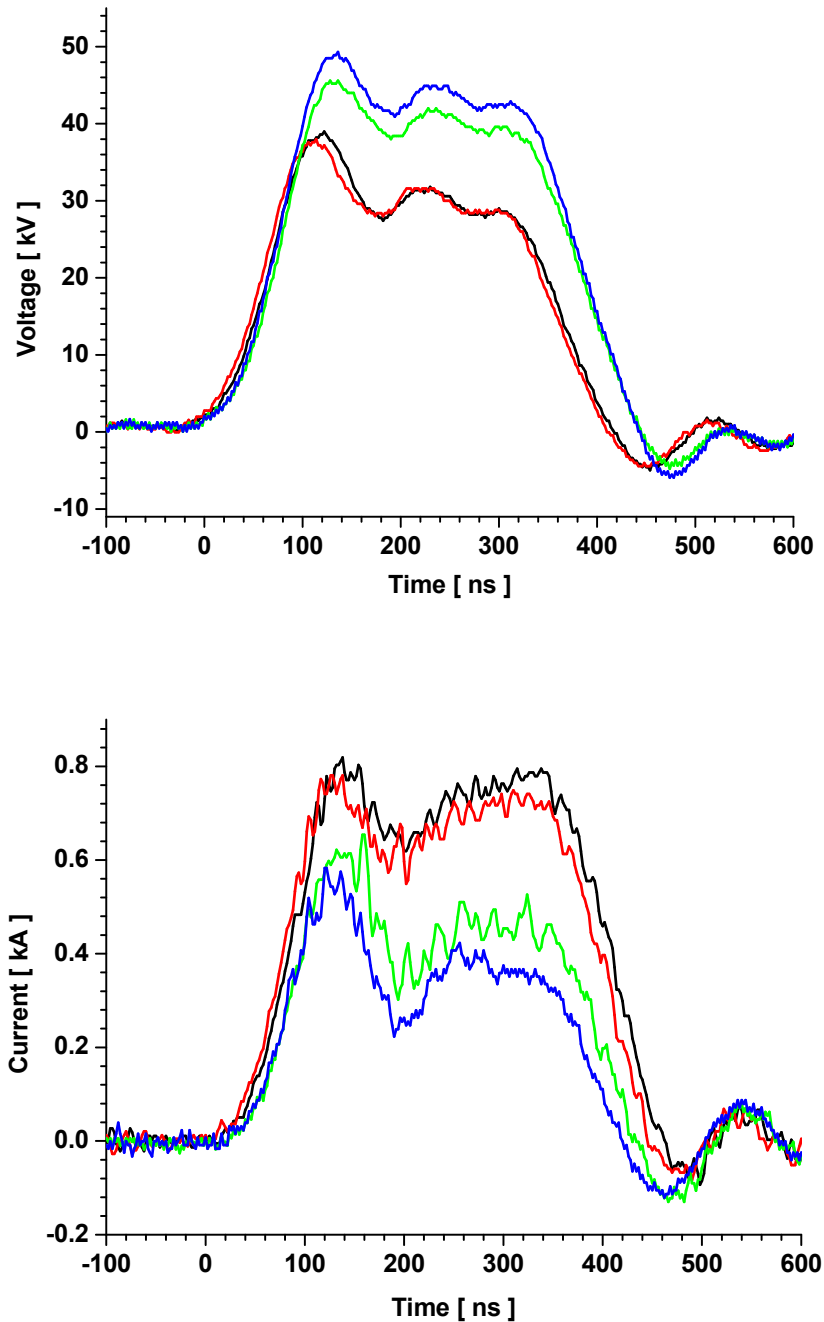


FIG. 4.4. Experimentally observed voltage (top) and current (bottom) waveforms for three different reactors (—, — reactor A= 30 mm (Φ); — reactor C= 70 mm (Φ); — reactor D= 110 mm (Φ)). Here the $35\ \Omega$ Blumlein generator had always been charged to around 35 kV.

The electrical current flowing in the corona discharge reactor consists of two components: an electrolytic current due to the ionic conductivity of the water and a capacitive current due to the propagation of streamers. The magnitude of the latter depends on the number of streamers and their propagation velocity while its duration corresponds to the streamer propagation time, which is limited by the onset of arcing.

Influence of reactor geometry: The main parameters which influence the corona onset voltage are the reactor geometry, the water conductivity, the material composition, and the thickness and porosity of the ceramic coating on the anode surface. In addition the observed corona onset may depend on the pulse width if the delay for streamer appearance is larger than the pulse duration.

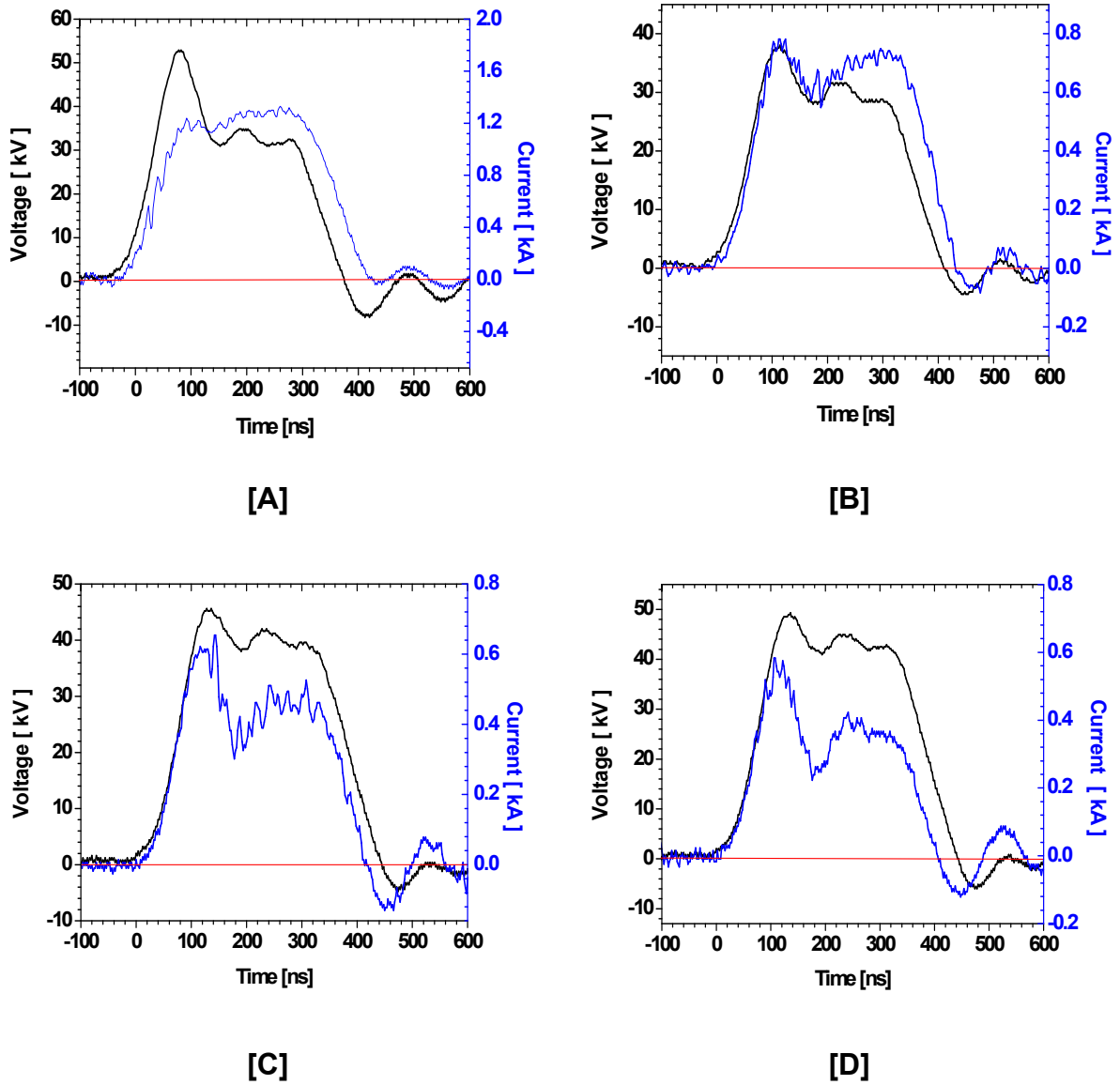


FIG. 4.5. Experimentally observed voltage and current waveforms for different reactor geometries (Pulse generator $Z_0 = 35 \Omega$). **[A]** Reactor A; $V_{\text{charging}} = 37 \text{ kV}$; $\sigma = 1200 \mu\text{S/cm}$ **[B]** Reactor B; $V_{\text{charging}} = 35 \text{ kV}$; $\sigma = 400 \mu\text{S/cm}$ **[C]** Reactor C; $V_{\text{charging}} = 35 \text{ kV}$; $\sigma = 400 \mu\text{S/cm}$ **[D]** Reactor D; $V_{\text{charging}} = 36 \text{ kV}$; $\sigma = 400 \mu\text{S/cm}$.

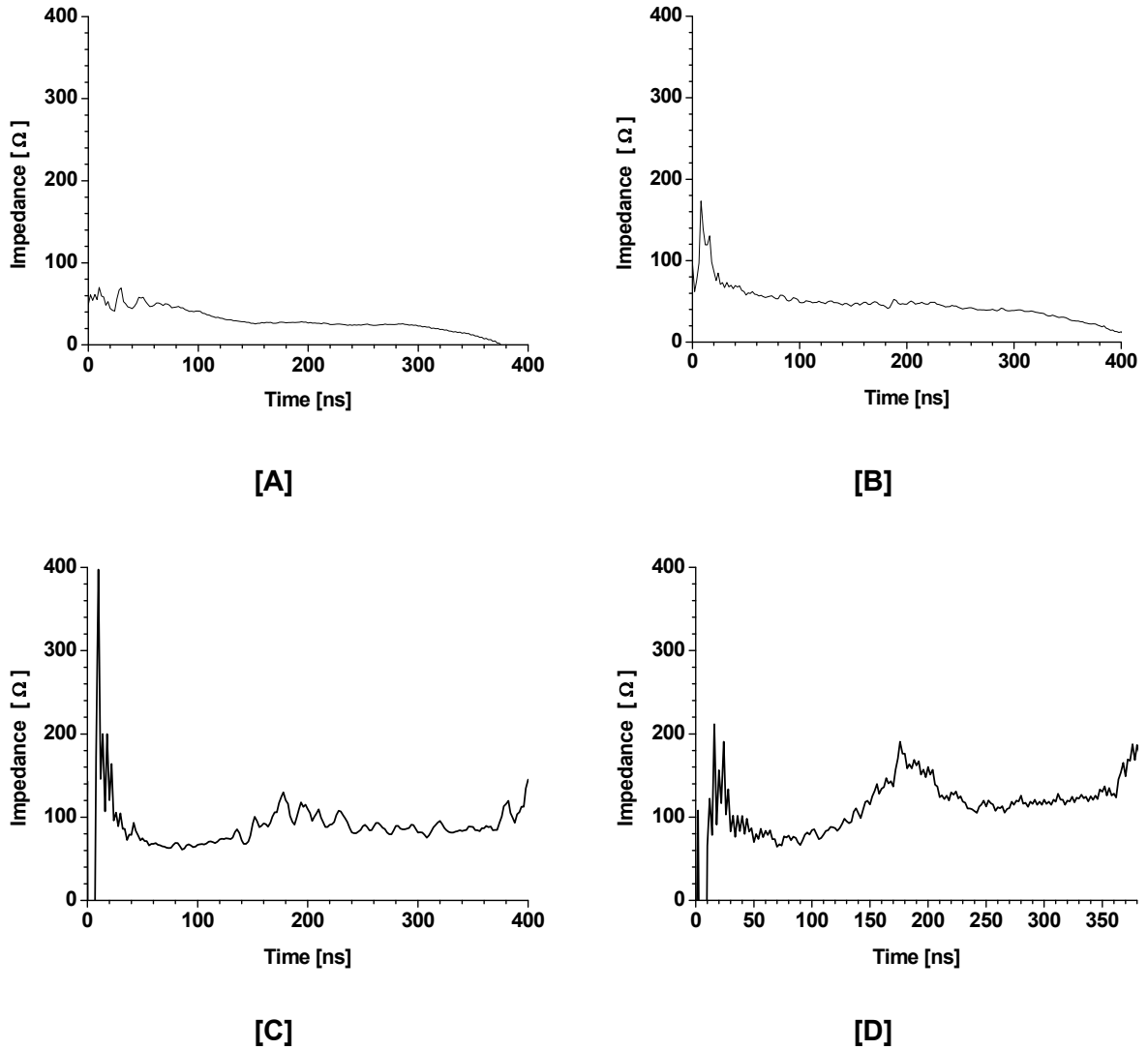


FIG. 4.6. Temporal evolution of the corona reactor impedance for different reactor geometries and water conductivities. (Pulse generator $Z_0 = 35 \Omega$) **[A]** Reactor A, $V_{\text{charging}} = 37 \text{ kV}$; $\sigma = 1200 \mu\text{S/cm}$; **[B]** Reactor B, $V_{\text{charging}} = 35 \text{ kV}$; $\sigma = 400 \mu\text{S/cm}$; **[C]** Reactor C, $V_{\text{charging}} = 35 \text{ kV}$; $\sigma = 400 \mu\text{S/cm}$; **[D]** Reactor D, $V_{\text{charging}} = 36 \text{ kV}$; $\sigma = 400 \mu\text{S/cm}$.

Using a 350 ns pulse and filling the reactors with water of $\sigma = 400 \mu\text{S/cm}$ the corona onset voltage has been determined for the relevant reactor geometries. For the small reactor having an inter-electrode gap of 12 mm and an almandine coated 6 mm anode the corona onset occurred at a peak anode voltage of $\sim 15 \text{ kV}$. When the peak voltage reached 45 kV spark over started between the anode and the reactor wall. For the larger reactor with an inter-electrode gap of 32 mm and a 6 mm anode, the corona onset voltage increased to $\sim 30 \text{ kV}$. A larger inter-electrode gap leads to an increased water layer resistance. Thus the electric field across the ceramic layer becomes smaller and the anode voltage for corona onset increases. Calculating the electric field at the ceramic surface for a constant peak anode voltage of 40 kV reveals that the field is reduced from 87 MV/m to 60.2 MV/m if the

electrode separation increases from 12 to 32 mm. To compensate this, a higher anode voltage or a smaller porosity is required.

For reactor C up to a maximum possible peak anode voltage of 65 kV no spark over was observed. However if the pulse width was increased to $\sim 1.3 \mu\text{s}$ spark over developed at 38 kV. Thus as expected the operating range of the system increased with electrode gap distance but decreased with growing pulse width. The voltage and current pulses obtained for different reactor geometries are shown in Fig. 4.5.

Calculating the impedance from the ratio of voltage and current for the cases presented in Fig. 4.5 reveals that it does not remain constant for the complete pulse duration, which indicates that the impedance of the corona reactor is not purely resistive. Fig 4.6 shows the temporal variation of this impedance. Around 200 ns after voltage rise the reactor impedance increases (Fig 4.6 [C] [D]). At the higher conductivity (1.2 mS/cm) of waste water (Fig 4.6 [A]) or for the smaller electrode gap (Fig 4.6 [B]) this effect was not observed. It is expected.

Influence of anode voltage on reactor impedance: To investigate the dependence of reactor impedance on anode voltage at constant water conductivity ($\sigma = 550 \mu\text{S/cm}$) the anode voltage was varied between 6.4 and 47 kV. Two extreme cases (i.e. 6.4 kV and 47 kV) are depicted in Fig. 4.7 and Fig. 4.8. Little changes of the reactor impedance are observed in this range.

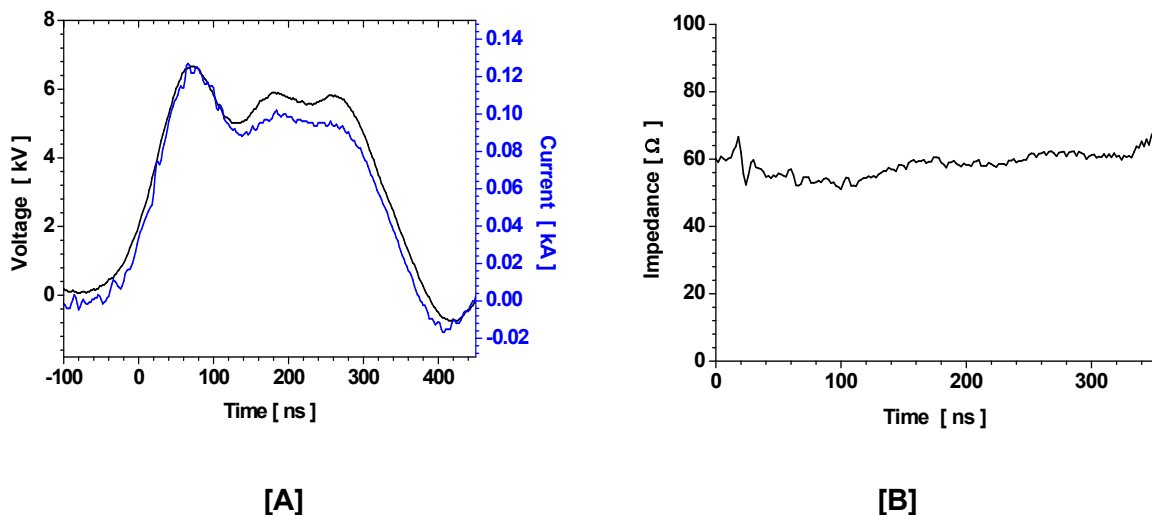


FIG. 4.7. Voltage and current waveforms at 6.4 kV [A]. Corresponding impedance [B]. (water conductivity = $550 \mu\text{S/cm}$)

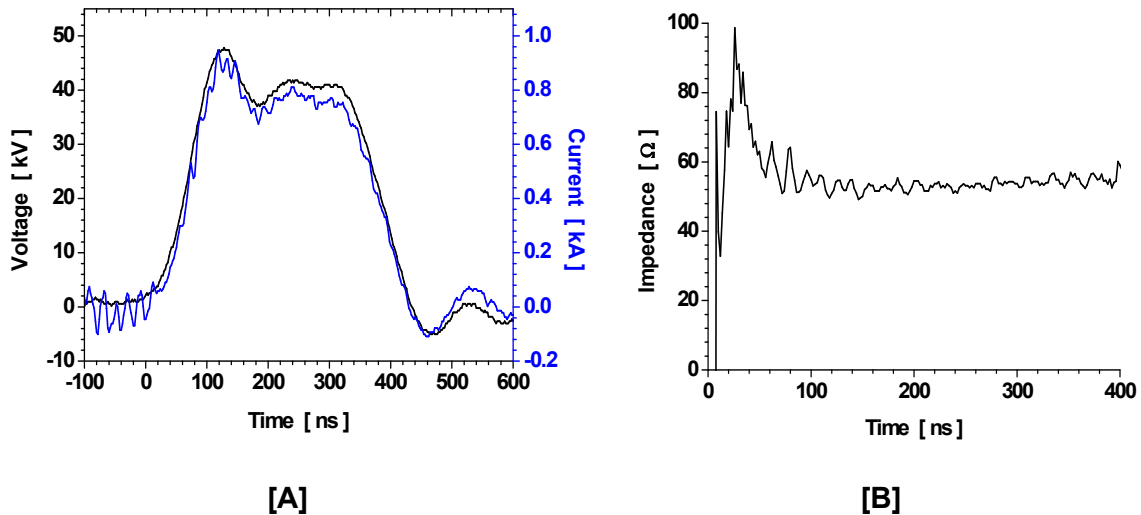


FIG. 4.8. [A] Voltage and current waveforms at 47 kV. [B] Corresponding impedance. (water conductivity = 550 $\mu\text{S}/\text{cm}$)

Influence of water conductivity: The water conductivity plays an important role in oxidant production. As described in section 2 the propagation length of streamers in water depends upon the water conductivity. It was noticed that the streamer brightness became poorer with higher conductivity. In addition their propagation length became shorter. Raising the water conductivity enhances the bypass current outside the streamer channel and causes a reduction of the streamer current and the potential at the tip. Once the potential at the tip of the streamer falls below the threshold value the streamers stop propagating.

Using reactor C, the water conductivity has been varied from 100 $\mu\text{S}/\text{cm}$ to 1.5 mS/cm . The measured voltage and current signals show that the influence of the reactor capacitance on the signal shape increases with decreasing water conductivity. This becomes especially apparent in the current signal. Generally speaking the signal shape is determined by the parallel connections of resistances and capacitances in the water and ceramic layers. The situation may be complicated by the fact that their values change as a function of time due to polarisation effects and streamer formation. To see the effects of streamer formation on the signal shape the reactor has been pulsed at two different voltage levels below and above streamer initiation. Some voltage and current waveforms are presented in Fig. 4.9.

Fig. 4.10 shows the differentiated voltage signal from experiment A of Fig. 4.9 together with the measured current signal demonstrating that for this low conductivity case capacitive terms of the reactor impedance prevail. In contrast the high conductivity case E of Fig. 4.9 clearly shows the dominance of resistive terms in the impedance. In all cases only minor effects can be identified from the appearance of streamers in the reactor.

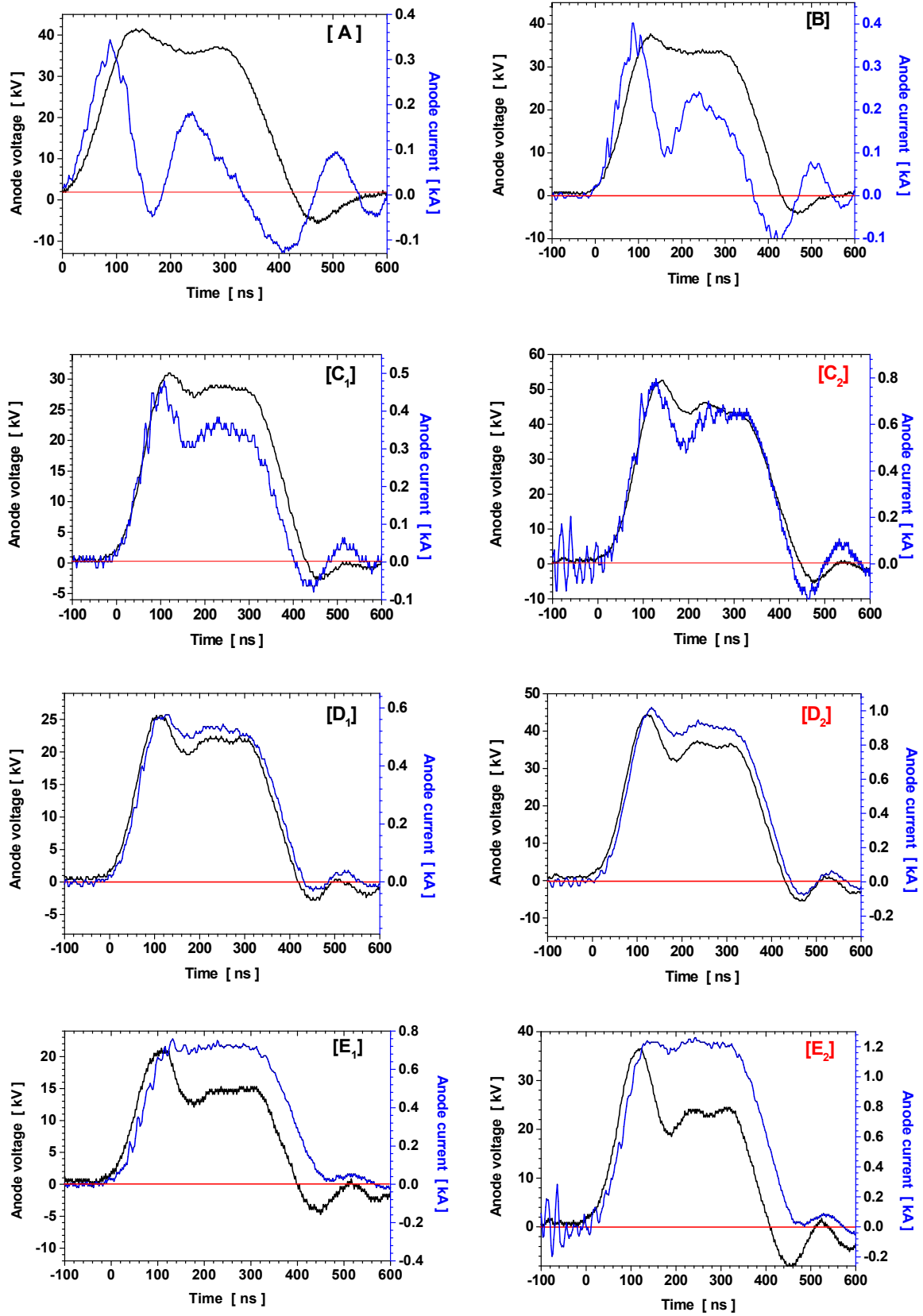


FIG. 4.9. Measured voltage and current waveforms at different water conductivities (Pulse generator $Z_0 = 35 \Omega$; Reactor C). [A] $\sigma = 100 \mu\text{S/cm}$ [B] $\sigma = 200 \mu\text{S/cm}$ [C₁₋₂]; $\sigma = 400 \mu\text{S/cm}$ [D₁₋₂] $\sigma = 800 \mu\text{S/cm}$ [E₁₋₂] $\sigma = 1500 \mu\text{S/cm}$. — Voltage below corona onset; — Voltage above corona onset.

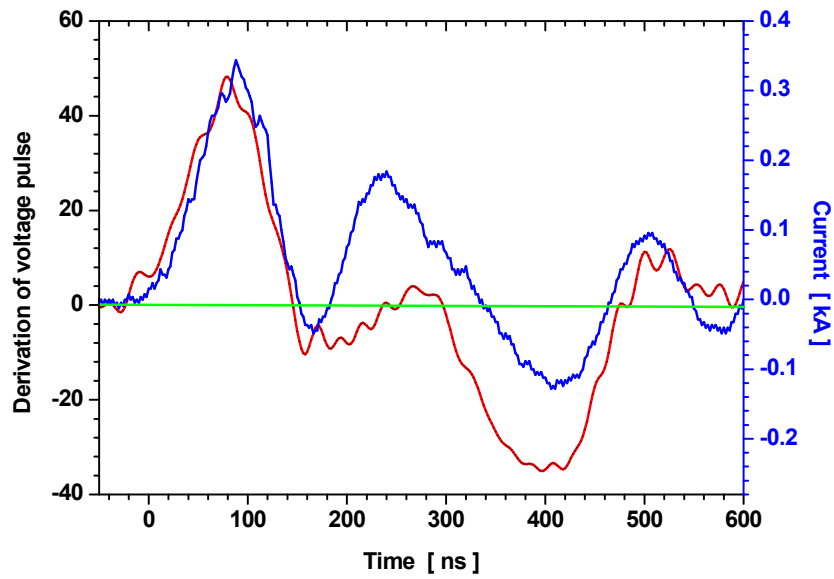


FIG. 4.10. Comparison between the measured current signal (—) and the differentiated voltage signal (—). (Experiment A from Fig. 4.9; $\sigma = 100 \mu\text{S}/\text{cm}$).

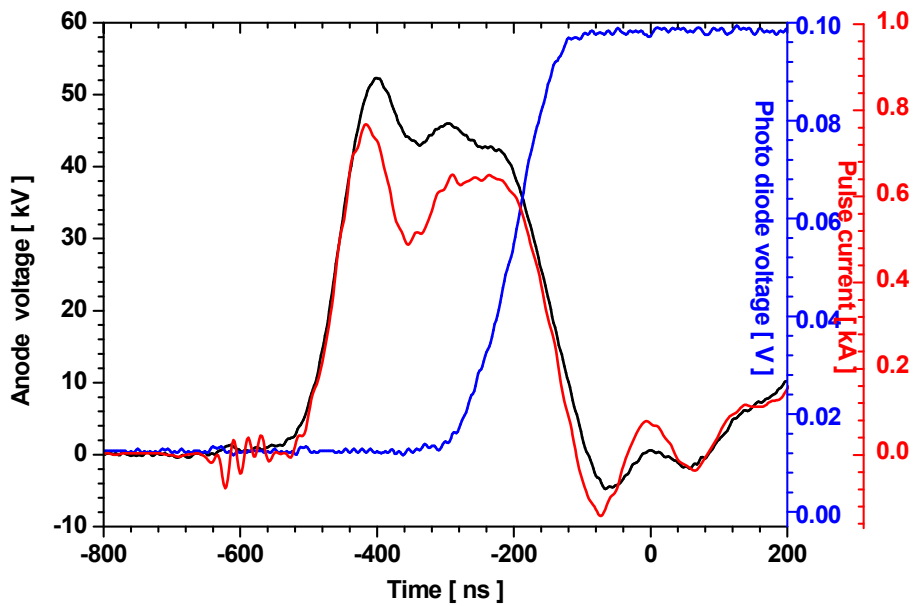


FIG. 4.11. Time correlation between pulse voltage and current rise and appearance of intense light emission from streamers. {Reactor- C; water conductivity $\sigma = 400 \mu\text{S}/\text{cm}$; pulse generator impedance = 35 Ohm}.

The inception of intense light emission connected with streamer propagation has been determined with a PIN photodiode. When reversely biased to 40 V the Si photodiode (FND-100) achieved a signal rise time of 1.5 ns. To avoid EM interference a quartz fibre

optic cable was used to guide the light to the photodiode located in a screen room. The fibre length was kept nearly equal to the length of the cables transmitting the electrical signals. Reactor C filled with water of 400 $\mu\text{S}/\text{cm}$ conductivity powered by the 35 Ω generator has been used for these measurements. The result is plotted in Fig. 4.11.

As shown in Fig 4.11 a time delay of 200 ns appears between current rise and intense light emission from the streamers.

Influence of anode voltage on streamer length: To study the effect of anode voltage on streamer length pulses of 240 ns duration generated by a single stage *LC* Blumlein set-up ($L = 2.0 \mu\text{H}$, $C = 9 \text{ nF}$) have been applied. The growth of streamer length was determined by increasing the pulse voltage stepwise above the corona onset voltage. For that purpose time integrated images of streamers were evaluated. Such streamer images are represented in Fig. 4.12 and Fig. 4.13. Mean streamer lengths were estimated from many of these photographs by analysing entirely visible streamers oriented parallel to the image plane. Although corona onset occurred at 15 kV their length could not be measured before they had reached ~ 1 mm, which happened at ~ 20 kV. At ~ 44 kV a streamer length of up to 8 mm was reached. In Fig. 4.14 the measured average length of streamers has been plotted as a function of peak anode voltage. From this figure we can derive an average voltage drop of 4 kV/mm along the streamer. Streamer propagation stops if the potential at the streamer tip falls below the streamer onset voltage. As the applied anode voltage increases the streamer length advances towards the cathode. However due to statistical variations of the streamer properties safe operation below arcing requires a sufficiently large margin of the streamer tips from the cathode.

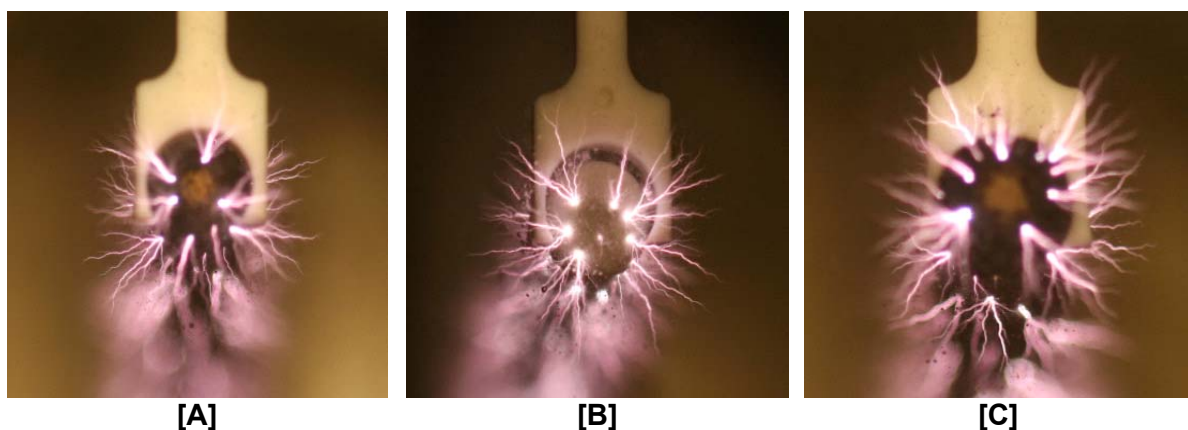


FIG. 4.12. Effect of anode voltage on streamer formation. Radially distributed streamers at different anode voltages [A= 31 kV] [B= 38 kV] [C= 43.8kV]. (pulse width 240 ns; water conductivity: 400 $\mu\text{S}/\text{cm}$; neutral pH)

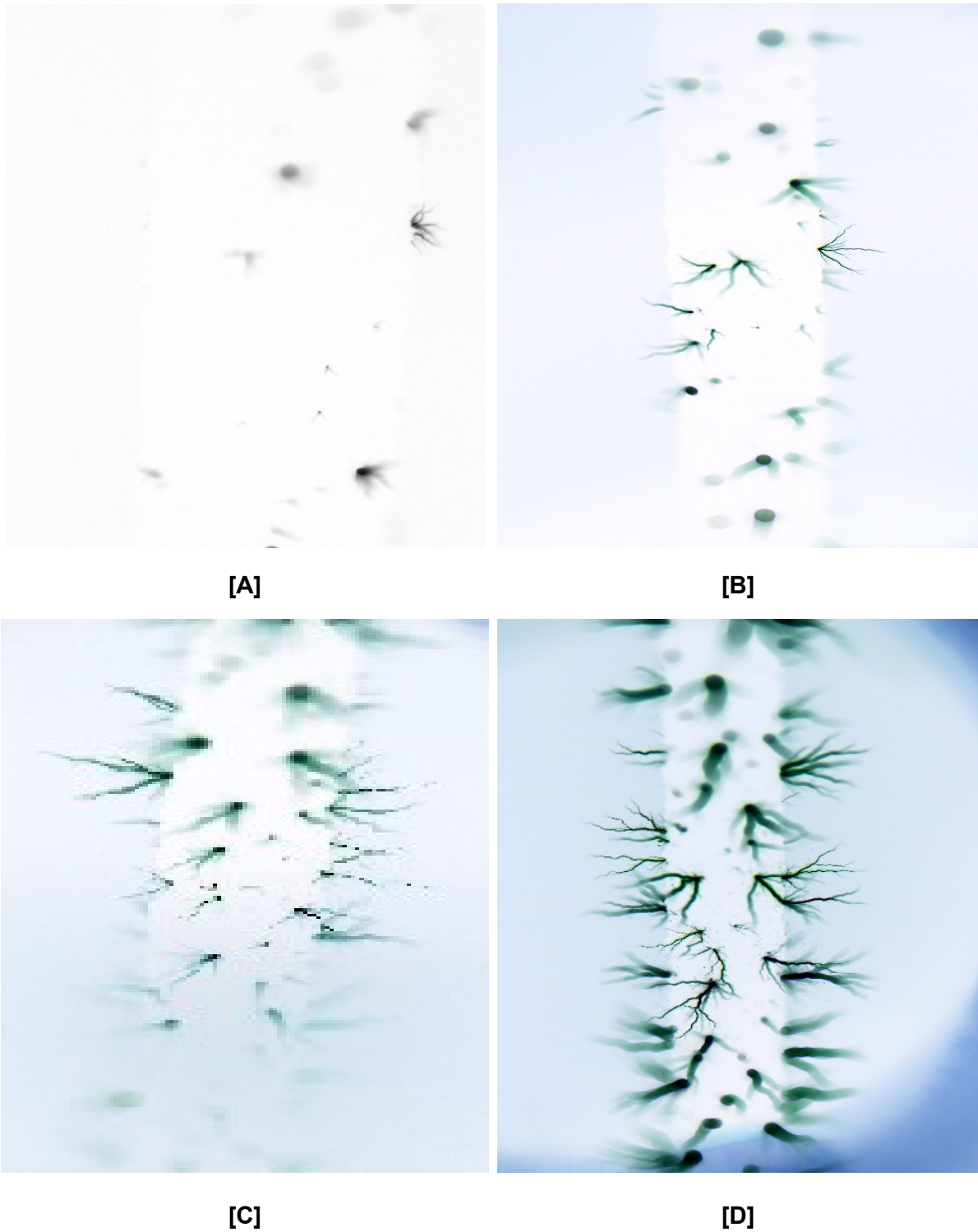


FIG. 4.13. Inverted photographs of axially distributed underwater corona discharge channels for different anode voltages [A= 19.8 kV], [B= 31 kV] [C= 38 kV] [D= 43.8kV]. All images were obtained for a solution conductivity of $400 \mu\text{S}/\text{cm}$ and at neutral pH.

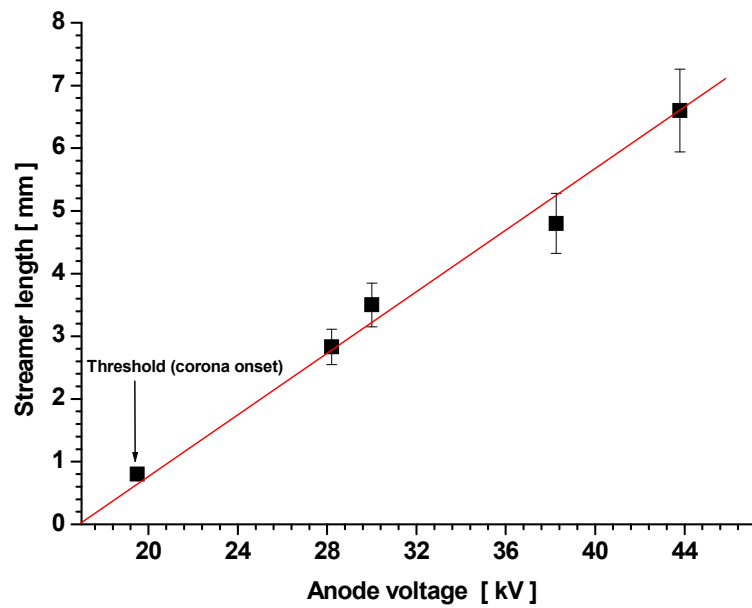


FIG. 4.14. Dependence of streamer length on anode voltage for a fixed pulse width of 240 ns, a water conductivity of 400 $\mu\text{S}/\text{cm}$ and neutral pH.

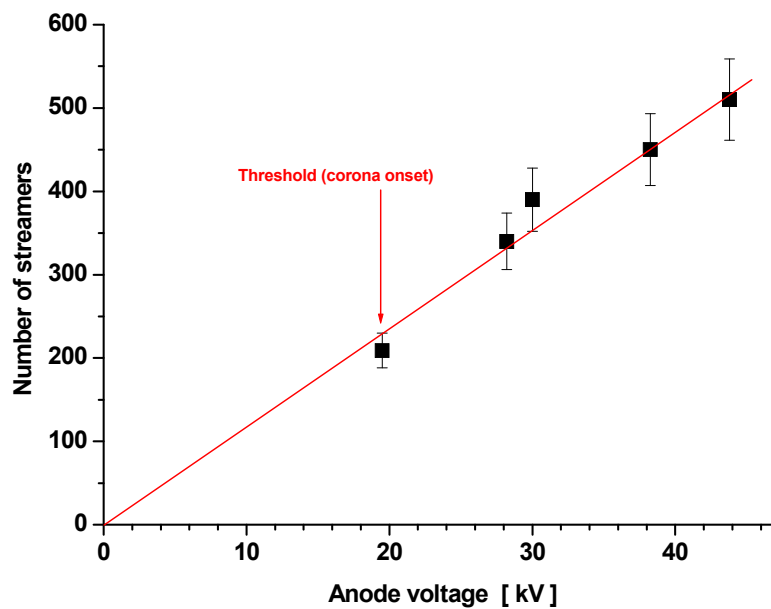


FIG. 4.15. Dependence of streamer numbers on anode voltage (pulse width: 240 ns; water conductivity: 400 $\mu\text{S}/\text{cm}$; and neutral pH)

Influence of anode voltage on streamer numbers: Apart from the streamer length the number of streamers launched from the anode increases too as the anode voltage becomes greater than the streamer onset voltage. For each reactor system one obtains a

different corona onset voltage. As explained above this results mainly from the differences in voltage division between the water and the ceramic layer. Partly it may also be caused by relatively large variations in porosity and thickness of the ceramic layers on the anode. As the anode voltage increases the conditions for streamer initiation become satisfied at more and more locations. Therefore with higher anode voltages larger numbers of streamer channels are produced.

To understand this further, the total numbers of visible streamer channels per axial length have been determined as a function of anode voltage. Similarly to the dependence of streamer lengths a linear co-relation was observed between the peak anode voltage and the number of produced streamers. For this aim, a small section of 20 mm length with 50% streamer visibility has been taken as a reference for streamer counting. The counts were then extrapolated to the entire anode length (i.e. 200 mm). A graph showing the dependence of the number of streamers on peak anode voltage is plotted in Fig. 4.15.

Influence of pulse width: If the pulse duration becomes shorter than the time required to reduce the potential at the streamer tip below the corona onset voltage, the streamer will stop before the maximum length of the streamer has been reached. Correspondingly the streamer length at a fixed anode voltage should increase with pulse duration up to a maximum value.

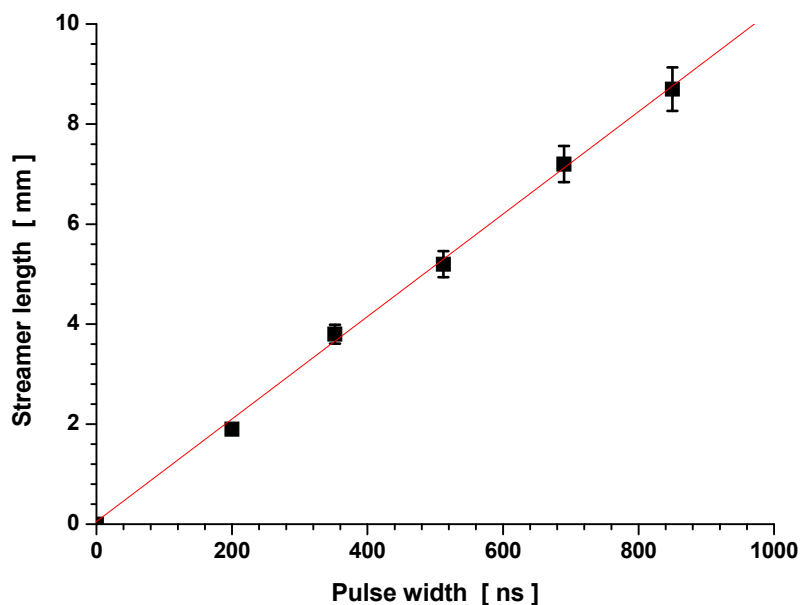


FIG. 4.16. Dependence of the streamer length on pulse width (anode voltage: 24 kV; solution conductivity: 400 $\mu\text{S}/\text{cm}$; neutral pH).

Fig. 4.16 presents the results of streamer length measurements where the anode voltage was kept constant while the pulse width was increased from 350 to 850 ns. Reactor C ($\Phi=70$ mm and $l = 200$ mm) was used for these measurements. To generate pulses of 350 ns, 512 ns, 690 ns, and 850 ns duration, 4, 6, 8, and 10 LC sections ($L = 1 \mu\text{H}$; $C= 2\text{nF}$) were used in the Blumlein. Despite the relatively low anode voltage of 24 kV an upper limit for the streamer length was not observed in the range of pulse widths. Therefore, it is suggested that other effects which reduce the voltage drop along the streamer come into play. e.g. it is conceivable that channel expansion reduces the resistivity of the plasma channel. From the data in Fig. 4.16 we derive a propagation velocity of 8 km/s. An increment in the number of streamers with increasing pulse width was not observed. This shows that above the corona onset threshold, the initiation of streamers, which is a statistical phenomenon, is mainly governed by the pulse amplitude.

Energy released per streamer: Since the electron temperature in the streamer channel and correspondingly the oxidant yields and the emitted UV-intensity depend on the electrical energy deposited in the streamer it is important to determine the parametric dependence of this quantity. The average energy expended per streamer has been calculated from the total electrical energy supplied to the reactor divided by the number of visible streamers.

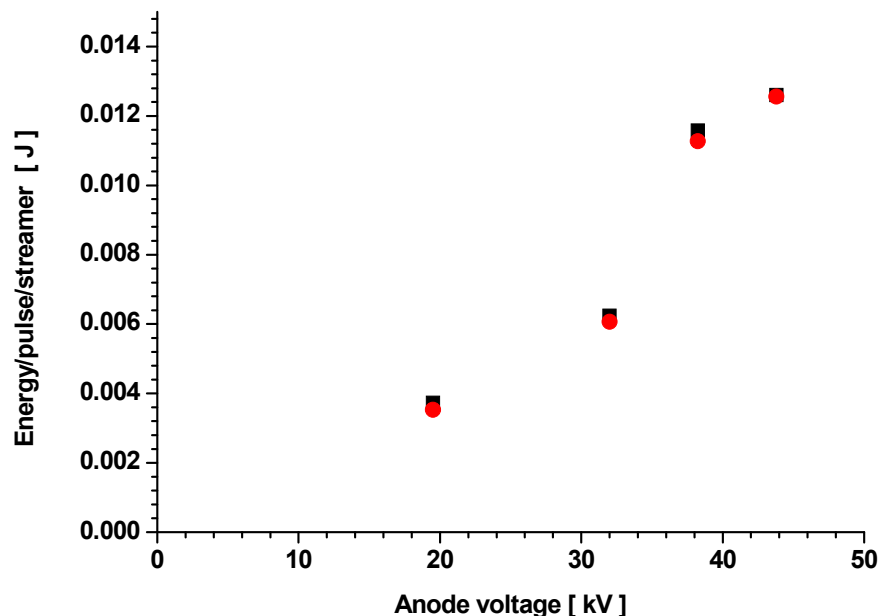


FIG. 4.17. Energy expended per streamer (calculated by dividing the total energy by the number of visible streamers) as a function of peak anode voltage (pulse width: 240 ns) ■ = Total pulse energy delivered to the anode ● = energy consumed in joule heating.

In Fig. 4.17 this energy has been plotted as a function of peak anode voltage for a pulse width of 240ns. It is important to notice that this energy is not the energy deposited in the streamer channel since it contains a Joule heating term from the electrolytic current flow in the water. In Fig. 4.17 the total energy has been represented by black squares. At corona onset-voltage, the energy delivered to the system was 3.73 mJ and at the maximum applied anode voltage of 43. kV it reached 12.6 mJ per streamer channel. From the experimentally measured current flowing through the reactor, and using the known reactor resistance, the energy consumed in joule heating was calculated (shown by the red circles Fig. 4.17). By subtracting this joule heating term from the total electrical energy delivered to the reactor, the energy deposited into the streamer channels was determined. It was found that approximately 99% of the supplied energy was dissipated in reactor as thermal energy and only a very small part was deposited into the streamer channels. Therefore the appearance of streamer channels has only little influence on the reactor impedance. Consequently it was also observed that for different anode voltages reactor the impedance remained constant.

Anode temperature: It has been suspected that the anode temperature rise during operation affected the lifetime of the anode coating. Due to the different thermal expansion of the metallic anode and the ceramic coating the bonding between the metal and the ceramic might suffer and the coating might partially flake off. Therefore a set-up was realized to measure this temperature rise during operation.

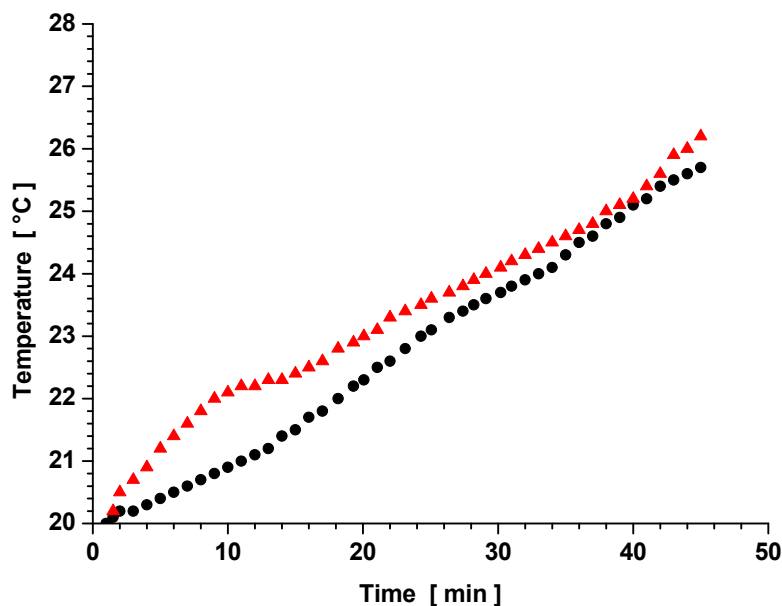


FIG. 4.18. Temperature evolution in a ceramic coated anode and in the surrounding bulk water during pulse operation with 2 Hz. The energy input into the reactor corresponded to 6 Joule per pulse (reactor volume 1L). (▲ = anode surface temperature; ● = water temperature)

This required a thermocouple floating at the high voltage of the anode. The thermocouple was entered into a central bore of the anode. The result of this measurement is shown in Fig. 4.18. With a pulse repetition rate of 2 Hz, and for a treatment time of 45 minutes with 6 joule/pulse, the observed temperature rise at the anode surface remained below 6 °C. A simultaneous measurement of the temperature rise in the bulk water gave 5°C. The small temperature difference is easily explained by heat losses through the reactor wall into the environment. We can conclude that the difference in temperature rise between the ceramic and the metal are probably not the cause for the destruction of the coatings. It seems more likely that localized pressure pulses due to the streamer discharges in the pores of the ceramic are responsible for the peeling off of the layer.

Emission spectra: The optical emission from the pulsed corona discharges in the wavelength range between 350 nm to 1000 nm is shown in Fig. 4.19. This spectrum has been time-integrated over 10 pulses of 240 ns pulse width and 35 kV, voltage amplitude. It proves the appearance of H_{α} , H_{β} , and oxygen lines corresponding to the dissociation of the water molecule and the formation of hydrogen and oxygen in the discharge channel. The quantification of these chemical species will be discussed from section 4.2 onwards.

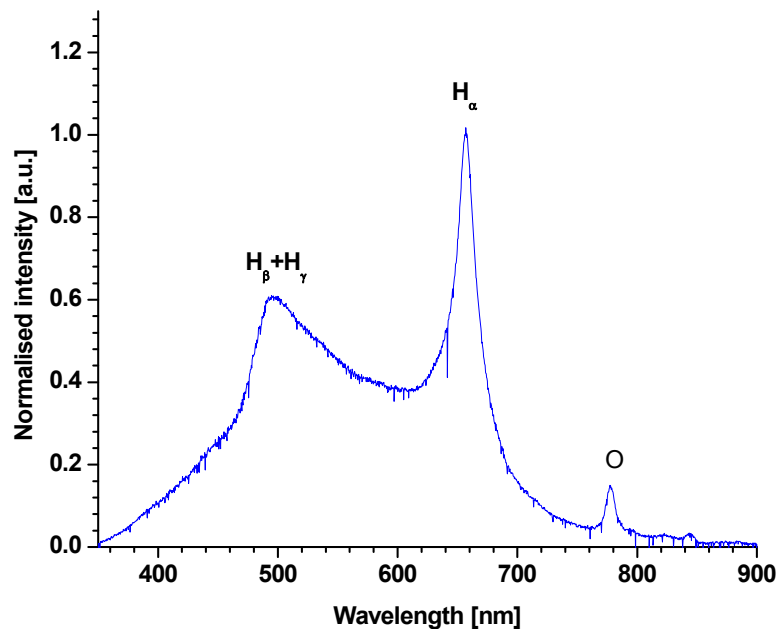


FIG. 4.19. Spatially and temporally integrated emission spectra from a pulsed underwater corona discharge (energy per pulse: 6.5 Joule; reactor diameter: 30 mm; water conductivity $\sigma = 500 \mu\text{S}/\text{cm}$)

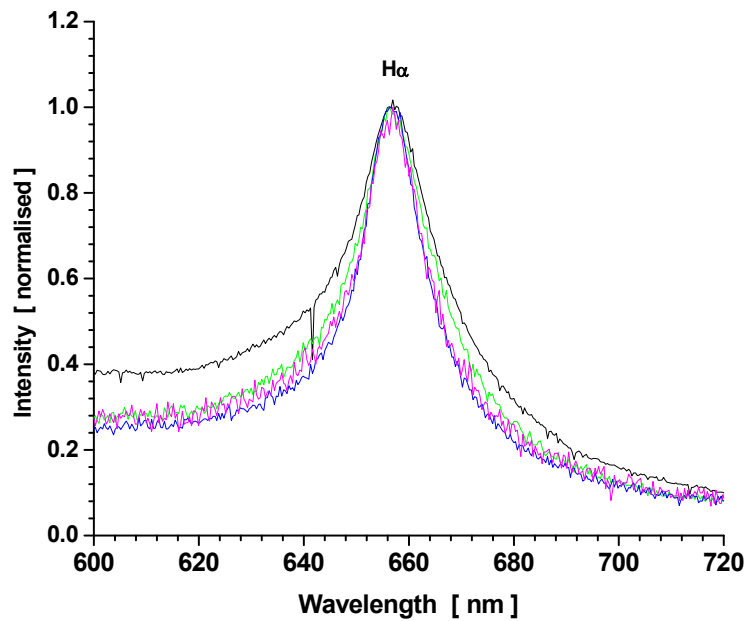


FIG. 4.20. H_{α} line broadening at different water conductivities. — 533 $\mu\text{S/cm}$, — 280 $\mu\text{S/cm}$, — 104 $\mu\text{S/cm}$, — 52 $\mu\text{S/cm}$ (energy/pulse = 6.5 Joule)

As shown in Fig. 4.20 a broadening of the H_{α} line profile is observed when the water conductivity increases. A detailed analysis of the H_{α} line profiles shows that this broadening is due to the electron Stark effect. Fitting the lines measured at different locations along the streamer with a Voigt function, An et al. were able to determine the electron densities along the streamer [37]. They obtained a value around $10^{18}/\text{cm}^3$ at the foot and more than $10^{19}/\text{cm}^3$ at the tip of the streamer.

4.2 Oxidant production

4.2.1. OH radicals: The chemical probes described in chapter 3 have been applied to quantify the production of OH radicals in pulsed underwater corona discharges.

C.C.A.: The experimental results obtained after exposing a 1.1 mM CCA solution to pulsed corona discharges are shown in Fig. 4.21. A 1.1 mM CCA concentration in water reduces the pH of the solution to 3.5. In such a strongly acidic medium the streamer generation from the almandine surface starts to become weaker after 2000 pulses. After 3000 pulses it drops sharply and after 4000 pulses very few visible streamers remain (section 2.1). These discoveries obviously explain the observed saturation effect. Because of these findings it was decided to discard CCA from further OH radical measurements.

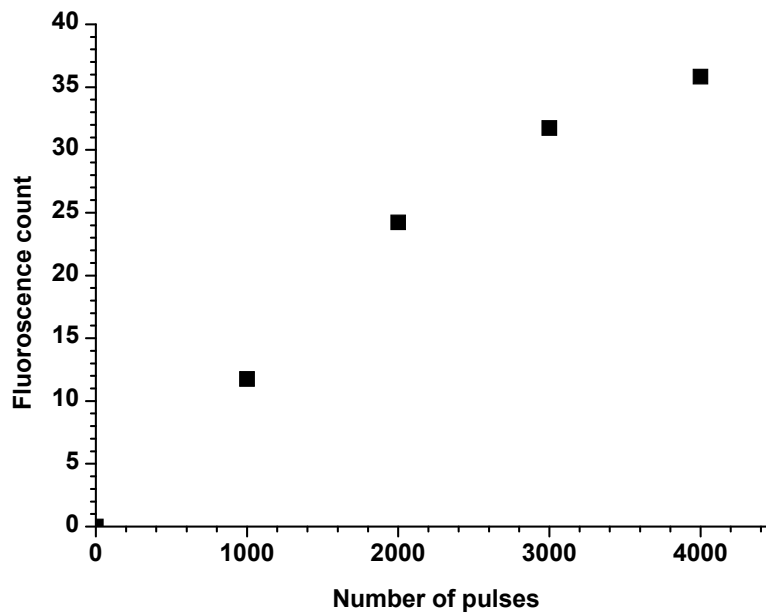


FIG. 4.21. Fluorescence yield of 1.1 mM CCA after exposure to different number of pulses ($\sigma = 380 \mu\text{S}/\text{cm}$, $\text{pH} = 3.5$)

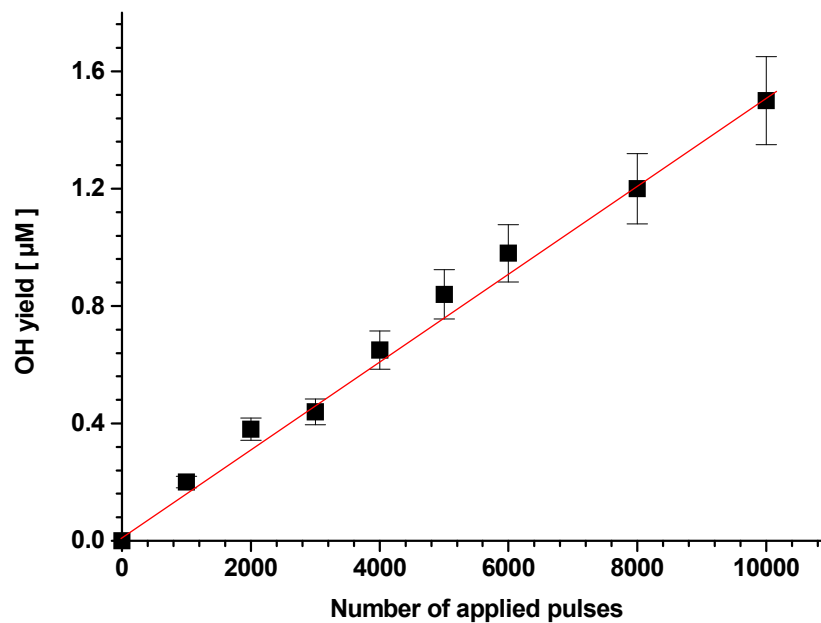


FIG. 4.22. Yield of OH radicals as a function of applied pulses determined from the consumption of the $\bullet\text{OH}$ scavenger pCBA. (pCBA concentration = $200\mu\text{g}/\text{L}$).

pCBA: As shown in Fig. 4.22 for a treatment cycle of up to 10,000 pulses a linear increment of the OH radical production was observed using pCBA as a diagnostic probe. This kind of measurement has been performed for the first time in connection with pulsed corona discharges. Although this probe worked rather satisfactory there were some

deficiencies connected with it. Especially the limited solubility of pCBA in water and the restricted range of pH-values for its applicability hinder the general use. In addition the required high performance liquid chromatography (HPLC) equipment was not available in house which made it difficult to conduct large series of experiments.

DNTA: As described previously DNTA is selectively sensitive to OH radicals. Therefore it can be used in presence of other radicals such as H^\bullet and HO_2^\bullet . The efficiency of this probe does not vary over a range of pH values from 6-11. Moreover compared to the other probes discussed earlier this diagnostic is relatively simple. Unless otherwise specified all experiments were performed in air saturated water. As shown in Fig. 4.23 a rather linear increase of the integral OH radical formation with the number of applied pulses has been found for a large range of pulse numbers. This confirms and extends the results obtained with pCBA.

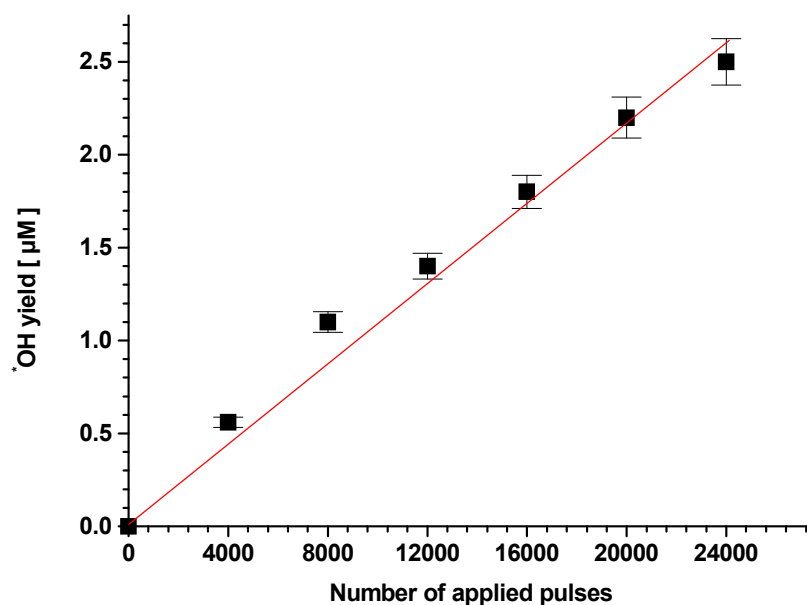


FIG. 4.23. $\bullet OH$ yield as a function of the number of applied pulses using DNTA as the probe compound. (DNTA concentration: 2×10^{-3} M)

4.2.2. Influence of reagent concentration: Increasing the concentration of DNTA in the reactor from 0.5 mM to 8 mM led to an increased yield of HTA by a factor of ~ 5 . However, raising the concentration from 2 to 8 mM caused only an addition of less than 10% and remained within the error bar limits (Fig. 4.24). It is assumed that this result is due to competition between reactions of OH with the reagent and with other species, including the recombination of two OH radicals forming H_2O_2 .

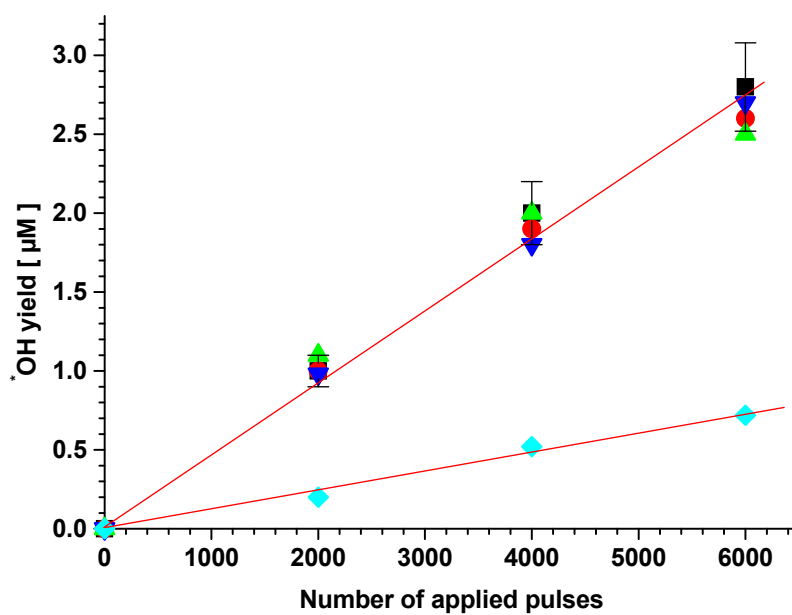


FIG. 4.24. OH radical yield as a function of pulse numbers for different concentrations of DNTA (■ = 8 mM DNTA, ● = 6mM DNTA, ▲ = 4mM DNTA, ▼ = 2mM DNTA ◆ = 0.5mM DNTA)

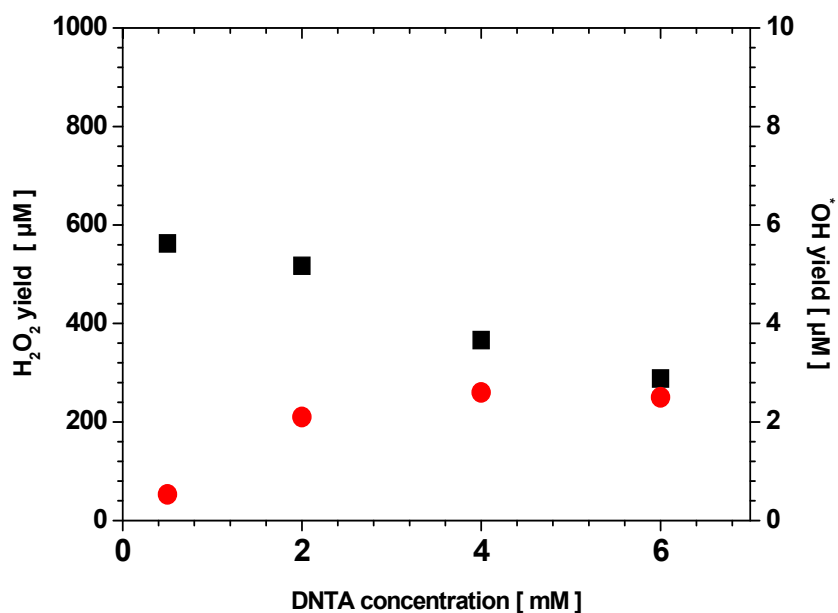


FIG. 4.25. Simultaneous determination of $^{\bullet}\text{OH}$ and H_2O_2 with increasing concentrations of DNTA (■ = H_2O_2 yield ● = $^{\bullet}\text{OH}$ yield)

As the concentration of DNTA increases OH radicals diffusing to the streamer interfacial region and into the bulk water react quantitatively with DNTA. However since DNTA does not exist in the hotter zones of the streamer channel this does not mean that the formation of H_2O_2 , as well as the recombination of $\cdot\text{H}$ and $\cdot\text{OH}$ to water, etc. are prevented. As OH radicals are the prime path for H_2O_2 production we conducted a simultaneous measurement of OH radical and H_2O_2 yields. The determination of the H_2O_2 yield was performed by using the Allen reagent described previously [92].

As shown in Fig. 4.25 it was observed that with increasing DNTA concentration the OH radical detection rate increases but at the same time the H_2O_2 formation decreases. Increasing the DNTA concentration causes an increase of the solution conductivity from $100 \mu\text{S}/\text{cm}$ (0.5 mM DNTA) to $1.6 \text{ mS}/\text{cm}$ (8 mM DNTA). Due to the higher solution conductivity the streamer lengths get shorter, which effectively results in a lower oxidant production. Therefore with increasing DNTA concentration a lower H_2O_2 yield was observed accompanied by a minute increment of the OH radical yield. Also it is important to note that the recorded H_2O_2 yields are 100 times higher than the detected OH radical yields. Based on these findings, unless otherwise specified, in this thesis a concentration of 2 mM DNTA has always been applied for OH radical detection. This concentration is selected because with 2 mM DNTA concentration the solution conditions are very close to tap water conditions (i.e. $\sigma = 400 \mu\text{S}/\text{cm}$ and neutral pH).

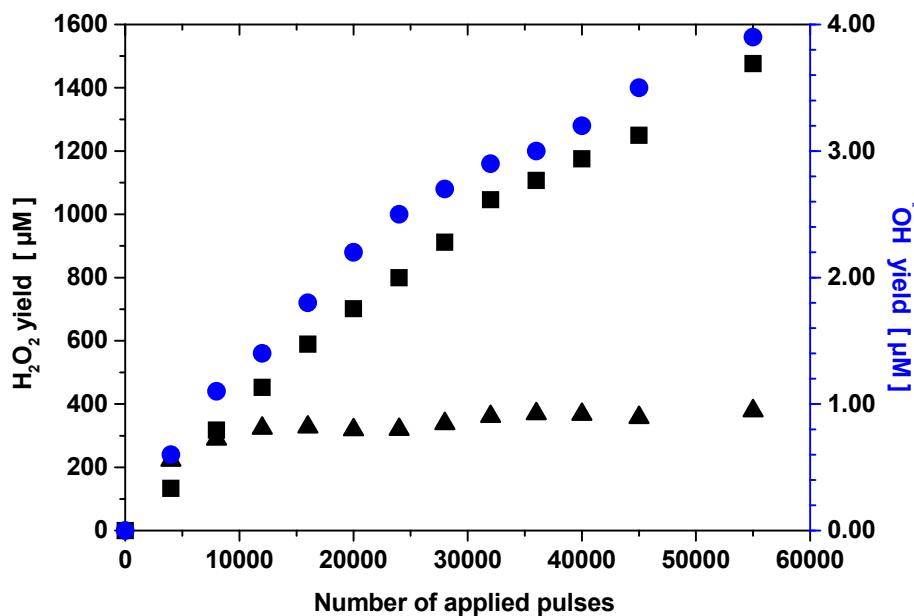


FIG. 4.26. Measured yields of OH radicals and H_2O_2 vs. number of pulses. (■ = H_2O_2 ; ● = $\cdot\text{OH}$; ▲ = ratio $\text{H}_2\text{O}_2/\cdot\text{OH}$; solution conductivity: $400 \mu\text{S}/\text{cm}$; neutral pH; energy per pulse: 4.68 J)

Fig. 4.26 shows the increase of the detected $\cdot\text{OH}$ and H_2O_2 yields as a function of the number of pulsed discharges in the reactor. A parallel increase has been observed for both species. The ratio of H_2O_2 and OH radical yields remains constant for a treatment cycle of up to 55,000 pulses. This again demonstrates the inter-relationship between the formation of hydrogen peroxide and the production of $\cdot\text{OH}$.

Fig. 4.26 also reveals a deviation from linearity at large pulse numbers. It has been supposed that this might have been caused by an increasing concentration of H_2O_2 accumulating in the bulk water.

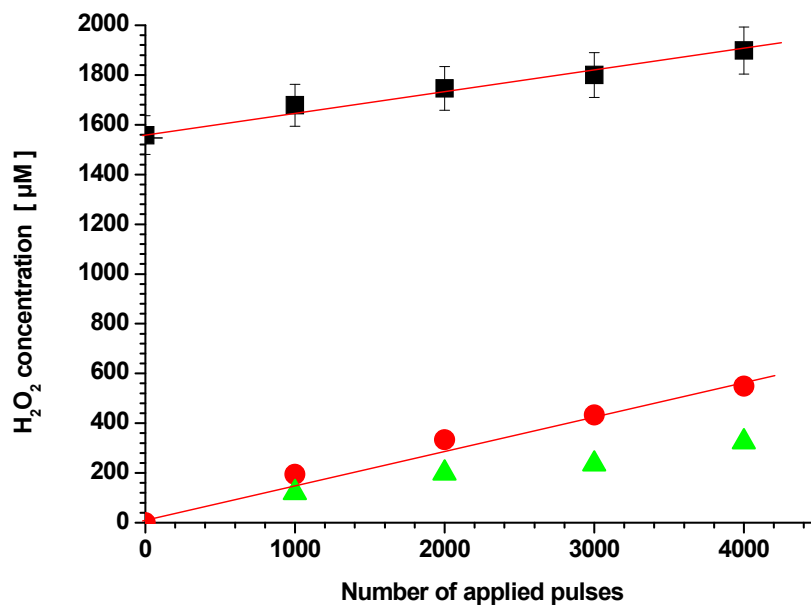
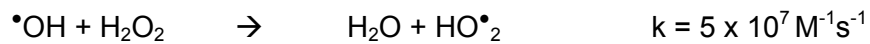


FIG. 4.27. Influence of an initial H_2O_2 addition on the production of H_2O_2 (■ = initial H_2O_2 concentration of 1.5 mM; $V_{\text{charging}} = 36$ kV; ● = without H_2O_2 addition, $V_{\text{charging}} = 37$ kV; ▲ = initial H_2O_2 concentration subtracted; water conductivity: 400 $\mu\text{S}/\text{cm}$; neutral pH)

To verify this assumption an initial concentration of 1.5 mM of H_2O_2 was added to the water before pulsing. However, exposing this solution to 4000 pulses did not lead to any departure from linearity (Fig. 4.27). Also the $\cdot\text{OH}$ yield measured simultaneously grew linearly in this experiment (Fig. 4.28).

More likely the non-linear growth of H_2O_2 and $\cdot\text{OH}$ yields indicates a lower productivity of the source due to some erosion of the ceramic coating on the anode. One reason for this was the higher repetition frequency applied in the present experiment which resulted in a faster destruction of the ceramic layer, especially at the ends of the anode rod.

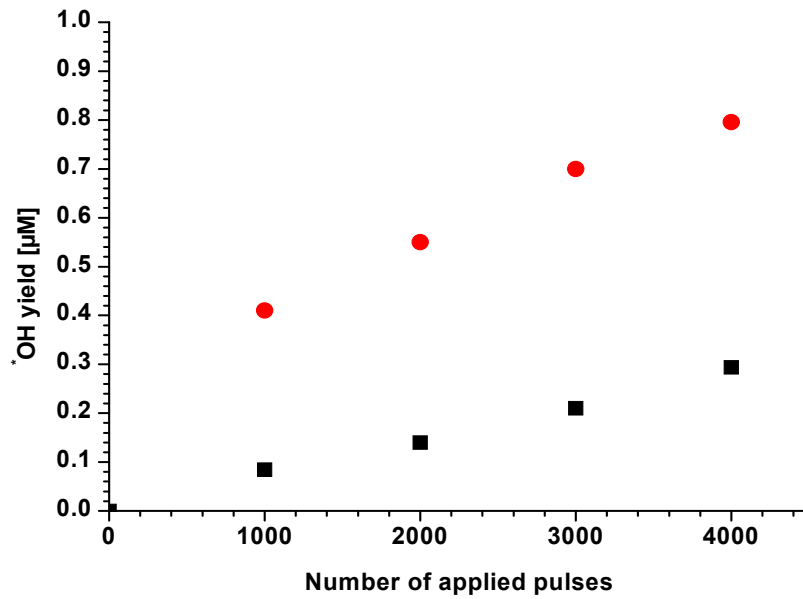
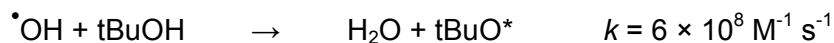
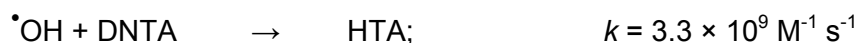
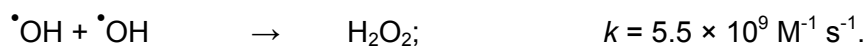


FIG. 4.28. Influence of an initial H₂O₂ addition on the measured OH radical yield (● = initial H₂O₂ concentration: 1.5 mM; V_{charging} = 36 kV; ■ = without H₂O₂ addition, V_{charging} = 37 kV; solution conductivity: 400 μS/cm; neutral pH)

To get an estimate of the OH radical concentration at the streamer-water-interface the standard probe of 2 mM DNTA was combined with another OH radical scavenger of varying concentration. Tertiary Butanol (tBuOH) was selected for this purpose because it did not change the water conductivity. Solving the relevant kinetic equations, assuming different initial OH radical concentrations, and comparing the calculated decrease of HTA-yields at increasing tBuOH-concentrations with the measured reduction of HTA-yields leads to a reasonable assessment of the initial OH radical concentration at the streamer surface. tBuOH concentrations of 0, 10, 100, and 500 μM have been used for that aim. Besides the HTA-yields the H₂O₂ concentrations were determined simultaneously.

For the kinetic simulations only the following three major reactions were considered:



$$\frac{d[OH]}{dt} = -2k_1[{}^{\bullet}OH][{}^{\bullet}OH] - k_2[{}^{\bullet}OH][TA] - k_3[{}^{\bullet}OH][tBuOH] \quad [{}^{\bullet}OH](0) = [{}^{\bullet}OH]_0$$

$$\frac{d[HTA]}{dt} = k_2[{}^{\bullet}OH][TA] \quad [HTA](0) = 0$$

$$\frac{d[TA]}{dt} = -k_2[{}^{\bullet}OH][TA] \quad [TA](0) = [TA]_0$$

$$\frac{d[tBuOH]}{dt} = -k_3[{}^{\bullet}OH][tBuOH] \quad [tBuOH](0) = [tBuOH]_0$$

$$\frac{d[H_2O_2]}{dt} = 2k_1[{}^{\bullet}OH][{}^{\bullet}OH] \quad [H_2O_2](0) = 0$$

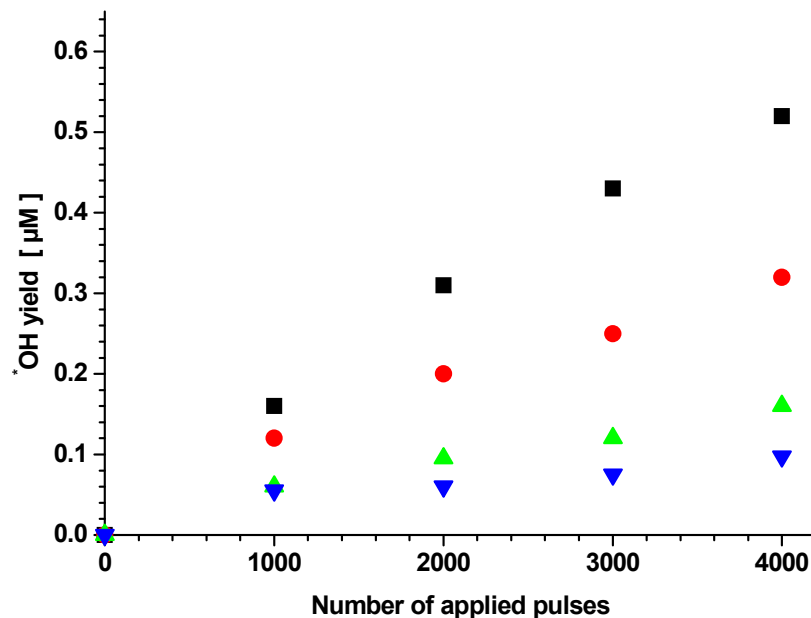


FIG. 4.29. Measured yield of HTA as a function of the applied number of pulses at a DNTA probe concentration of 2mM and for various tBuOH concentrations. (■ = 2 mM DNTA only; ● = DNTA + 10 mM tBuOH; ▲ = DNTA + 100 mM tBuOH; ▼ = DNTA + 0.5 M tBuOH);

As shown in Fig. 4.29 and Fig. 4.30, increasing the tBuOH concentration reduces both the yield of OH radicals and the H_2O_2 yield simultaneously. DNTA can react only in bulk zone therefore a very small amount of produced OH radical could be detected. Comparing the experimental and calculated results summarized in Table 4.2 we observe that the relative reductions of HTA-yields and H_2O_2 yields agree best for an assumed initial ${}^{\bullet}OH$ concentration of 30 mM. However the calculated HTA/ H_2O_2 yield ratio is roughly a factor of 10 larger than the measured one.

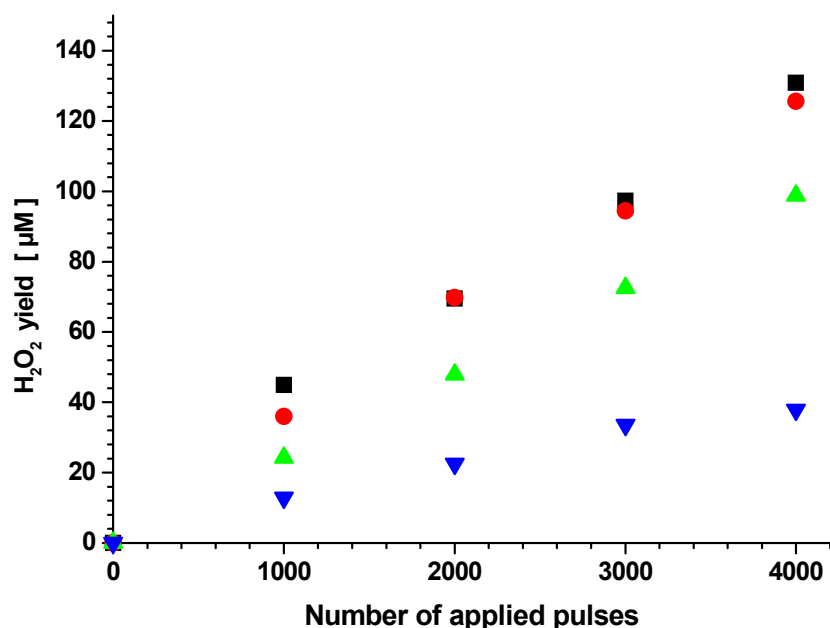


FIG. 4.30. H_2O_2 yield as a function of the number of applied pulses at a DNTA probe concentration of 2 mM and for various concentrations of tBuOH (■ = 2 mM DNTA only; ● = DNTA + 10 mM tBuOH; ▲ = DNTA + 100 mM tBuOH; ▼ = DNTA + 0.5 M tBuOH)

Table 4.2. Effect of increasing tBuOH scavenger concentration on HTA and H_2O_2 yields

tBuOH + 2mM DNTA	Experimental HTA-yield [µM]		Calculated HTA-yield (for 30 mM initial $\cdot\text{OH}$ - concentration)		Experimental H_2O_2 -yield [µM]		Calculated H_2O_2 -yield (for 30 mM initial $\cdot\text{OH}$ - concentration) [µM]	
0	0,52	100%	0.00165	100 %	136	100%	0.0141	100%
10 mM	0,32	61%	0.00146	88%	123	90%	0.0133	94%
100 mM	0,16	30%	0.000963	58%	100	73%	0.00971	69%
500 mM	0,097	18.75%	0.00046	28%	40	29%	0.00485	34%

Nevertheless the common decrease of HTA- and H_2O_2 -yields with increasing tBuOH scavenger concentration observed in both the experiment and in the simulation, suggests that most of the H_2O_2 production occurs when the $\cdot\text{OH}$ radicals reach the interface region. Otherwise there would only be a small effect of the tBuOH concentration on the H_2O_2 -yield. We therefore must conclude that the further oxidation of the $\cdot\text{OH}$ -adduct to TA required for creating the fluorescent hydroxyphthalate ion is not quantitative in the environment of the corona reactor. In addition other reactions can compete which may reduce the yield further [88].

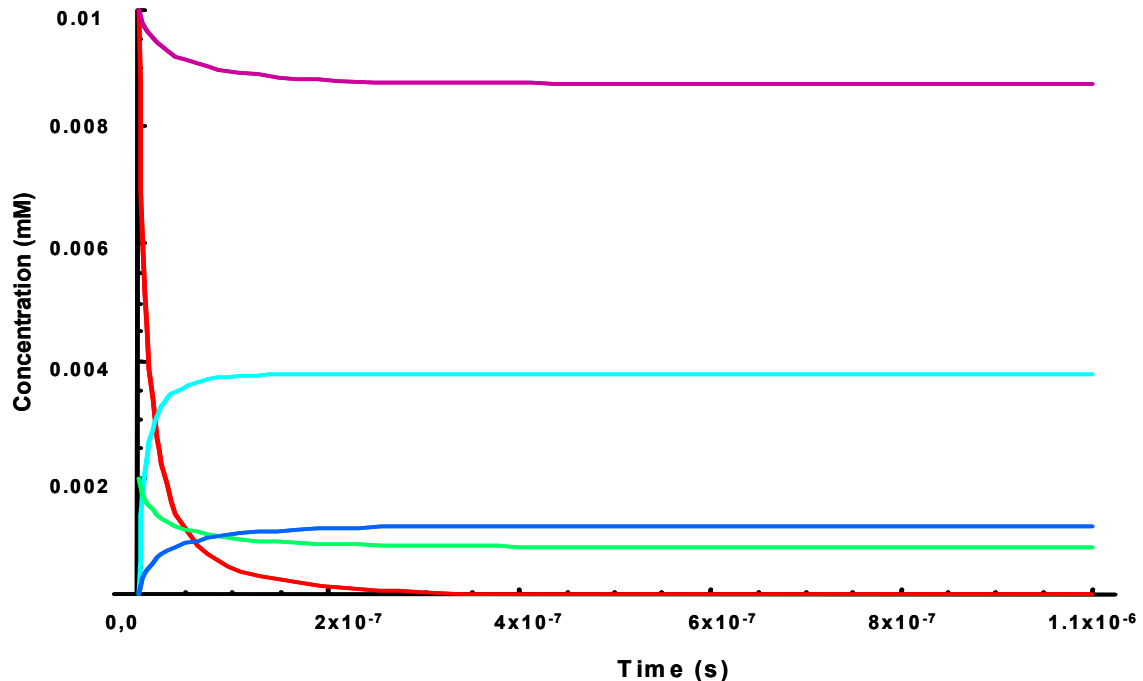


FIG. 4.31. Calculated time dependent consumption and formation of molecular species in an $\bullet\text{OH}$ + DNTA + tBuOH system, assuming an initial OH radical concentration of 10 mM. (— Consumption of tBuOH, — Formation of H_2O_2 , — Consumption of DNTA, — Formation of HTA, — Consumption of OH radicals.

Also the strong radial gradients of species concentrations around the streamer channel may influence the result. Fig. 4.31 shows the calculated consumption and formation of different molecular species in a solution containing initial concentrations of 2 mM of DNTA, 10 mM of tBuOH and 10 mM of OH radicals. At the conditions assumed here the half life of OH radicals is of the order of a few hundred ns, and therefore much higher than the values generally reported in the literature [41].

4.2.3. Relation between oxidant yield and streamer volume: The oxidant production increases proportional to both, the streamer length and the number of streamer channels. It is therefore obvious that the production of $\bullet\text{OH}$ and H_2O_2 must linearly depend on the product of l and N (l = length, N = number of streamers). This product is apparently proportional to the total surface area (or streamer volume) in the corona reactor. On the other hand $l \times N$ is a function of the pulse voltage. The OH radical and H_2O_2 yields have therefore been re-plotted in Fig. 4.32 and Fig. 4.33 as a function of this basic parameter.

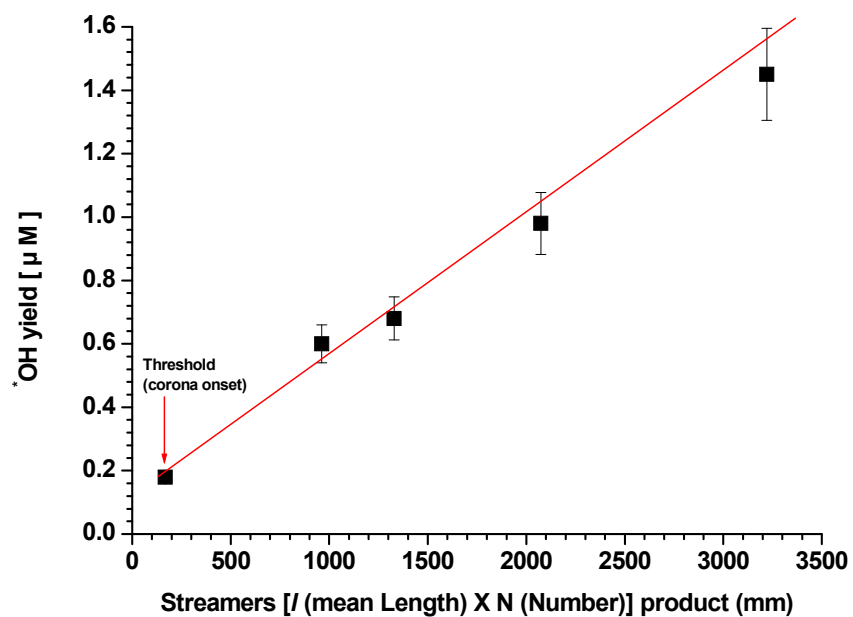


FIG. 4.32. Dependence of the OH radical yield on the length number product of streamers. $l \times N$ increases with anode voltage. (pulse width: 200 ns; solution conductivity 400 $\mu\text{S}/\text{cm}$; neutral pH; 4 Hz pulse repetition rate)

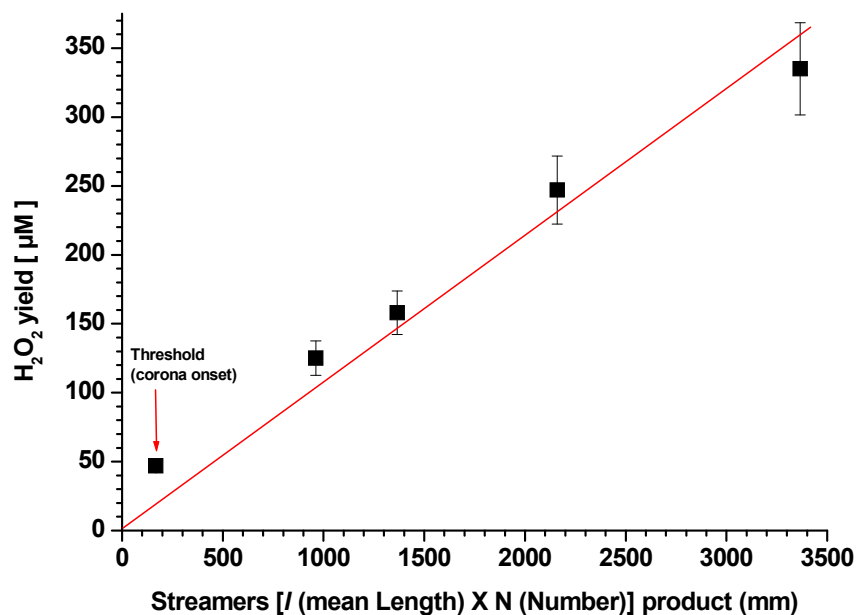
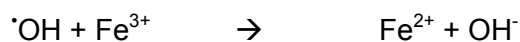


FIG. 4.33. Dependence of the H_2O_2 yield on the length number product of streamers. $l \times N$ increases with anode voltage. (pulse width: 200 ns; solution conductivity 400 $\mu\text{S}/\text{cm}$; neutral pH; 4 Hz pulse repetition rate)

4.2.4. Effect of anode material: From studies with biological cells it is known that the simultaneous presence of H₂O₂ and Cu or Fe ions causes damage to the bases of the DNA. Under these conditions OH radicals are created due to the reaction of these metal ions with H₂O₂ [108]. It is expected that metal ions can be liberated from the anode as well as from the ceramic layer. To separate these sources various metallic anodes (titanium, copper, aluminium and stainless steel) have been studied. Their surfaces were coated with a thin porous layer of Al₂O₃ which is considered to be chemically more inert than almandine. In the pulsed underwater corona discharges the released metal ions can react with hydrogen peroxide accumulated in the water. The anodes were exposed to the streamer discharges under equal water conditions (400 μS/cm, neutral pH) and the electrical operating parameters were kept constant in all experiments. Samples of approximately 3 mL. were drawn every 1000 pulses, and the OH radical and H₂O₂ yields were determined simultaneously from the collected samples.

It has been described in chapter 2 that active streamer channels contain a hot plasma in contact with the anode. At the foot point a potential drop exists between the plasma column and the metallic anode in which electrons and negative ions can be accelerated towards the anode sputtering ions off from the metallic surface. The released metal ions can then react with H₂O₂ accumulated in the bulk water and produce OH-radicals. As shown in Fig. 4.34 the [•]OH radical production was highest for copper anodes and lowest for titanium anodes. Copper and iron ions have been studied extensively in natural waters because of their importance for biological systems. Depending upon the presence of other reactive species and solution pH hydrogen peroxide can act as an oxidant or a reductant in its reactions with Fe ions and Cu ions. A mechanism for Cu⁺ and Fe²⁺ oxidation can be described as follows: [108, 113]



The OH-radicals released in these reactions interact with the added DNTA probe leading to an additional HTA concentration representative for a higher yield of OH radicals. Based on these results for OH radicals it is anticipated that the opposite trend should occur for the H₂O₂ yield. However since the H₂O₂ concentration is a factor of 100 larger than the detectable OH yield only small effects in the H₂O₂ balance are expected. Nevertheless the results presented in Fig. 4.35 confirm the supposed trend.

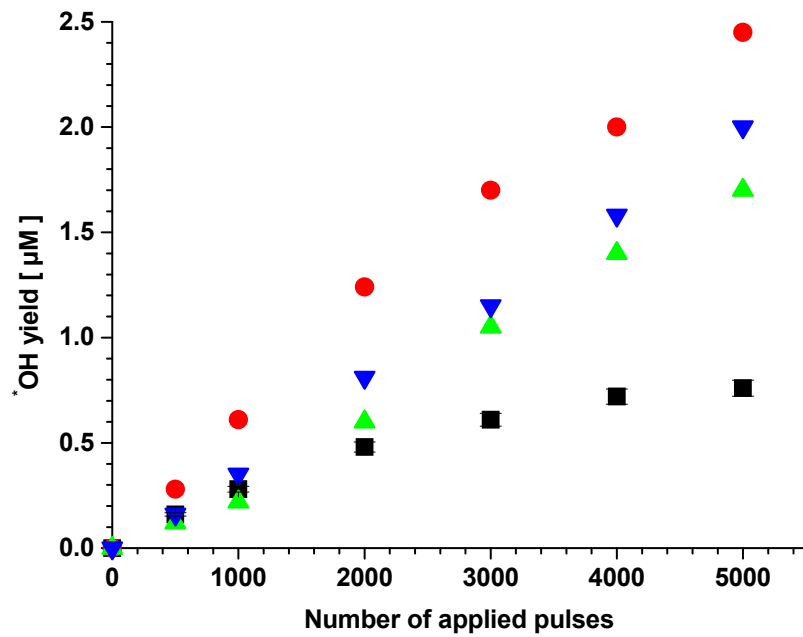


FIG. 4.34. Effect of anode material (Cu, steel, Al. and Ti) on OH radical yield. In these experiments porous Al_2O_3 has been used as the ceramic coating material [■ =Titanium 6 mm, ● = Copper ▲ = Aluminium ▼ = Steel]

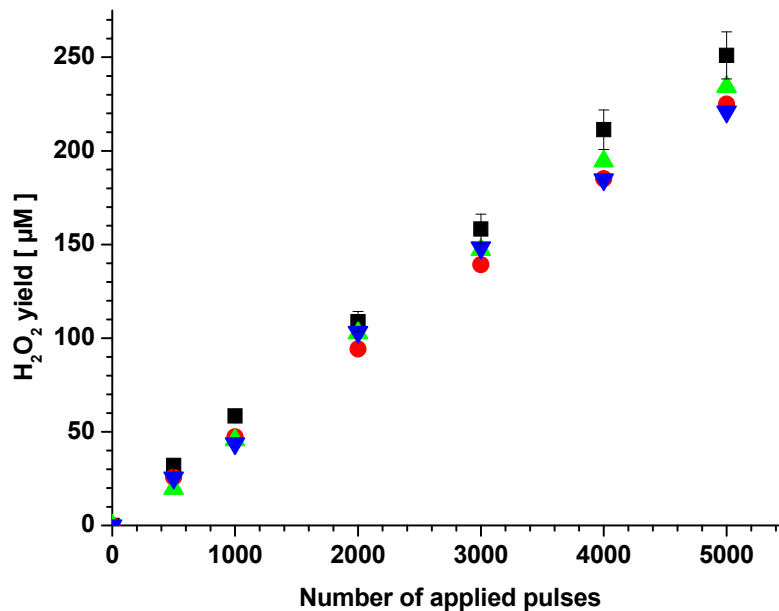


FIG. 4.35. Effect of anode material (Cu, steel, Al. and Ti) on H_2O_2 yield. The same porous Al_2O_3 as in Fig. 4.34 has been used as the ceramic coating material. (■ =Titanium 6 mm, ● = Copper ▲ = Aluminium ▼ = Steel ; water conductivity: $400 \mu\text{S}/\text{cm}$, $\text{pH} = 6.8$)

Since the $\cdot\text{OH}\cdot\text{OH}$ and the $\cdot\text{OH}\text{-DNTA}$ reaction rate constants are of the same order we must conclude that most of the H_2O_2 production takes place where DNTA is absent or the OH radical concentration is much higher.

This is certainly not the case in the bulk water. However it is most likely to happen at the interface of the streamer plasma channel.

The concentration of released Fe metal ions has been determined separately. It turned out to be of the order of a few μM after 5000 pulses, which is very close to the measured increase of the OH radical yield. A summary showing the most abundant metal ions released from different anode configurations is presented in Table 4.3. The chemical analysis was performed with the support of the Institute of Technical Chemistry (ITC-WGT) at Forschungszentrum Karlsruhe (FZK).

Table 4.3. Release of metal ions from different anode materials (after 5000 pulses)

Anode	Element	Measurement	Measurement	Measurement	Mean	Standard deviation
		I	II	III		
		mg/L	mg/ L	mg/ L	mg/ L	mg/ L
Ti (6mm) + Al_2O_3	Ti	0,16	0,14	0,16	0,15	0,01
	Al	0,35	0,38	0,34	0,36	0,02
Cu (6mm) + Al_2O_3	Cu	1,08	1,13	1,08	1,10	0,03
	Al	0,33	0,18	0,22	0,25	0,06
Al (6mm) + Al_2O_3	Al	1,75	1,87	1,53	1,72	0,14
Steel (6mm) + Al_2O_3	Fe	0,28	0,22	0,27	0,26	0,03
	Al	0,66	0,39	0,55	0,53	0,11
Ti (10mm) + Al_2O_3	Ti	0,11	0,10	0,15	0,12	0,02
	Al	0,20	0,24	0,34	0,26	0,06
Cu(6mm) without coating	Cu	0,92	0,93	0,81	0,88	0,05
Ti (6mm) + Almandine	Fe	0,43	0,34	0,36	0,38	0,04
	Mg	0,06	0,04	0,03	0,04	0,01
	Ti	0,17	0,16	0,31	0,21	0,07
	Al	0,12	0,08	0,05	0,08	0,03
Ti (6mm) + Almandine	Fe	0,29	0,25	0,31	0,28	0,03
	Mg	0,04	0,03	0,02	0,03	0,01
	Ti	0,12	0,12	0,22	0,16	0,05
	Al	0,11	0,08	0,05	0,08	0,03

4.2.5. Influence of ceramic coatings: The effect of different ceramic coating materials (almandine, alumina and epoxy) on the production of OH radicals and H₂O₂ has been studied using titanium as the anode substrate in all cases. It was observed that the yield of OH radicals and H₂O₂ is highest in case of almandine. The results of these experiments are presented in Fig. 4.36 and Fig. 4.37.

Initially the yield of OH radicals increases linearly for both almandine and alumina coated anodes. However after a few thousand pulses the yield of [•]OH levels off in case of Al₂O₃ coated anodes, i.e. the further production of [•]OH stops. As discussed in chapter 2 this results from a change of the electrical properties of alumina. A similar trend is observed for the production of H₂O₂. In these experiments apparently saturation in the H₂O₂ production seemed to occur too at larger pulse numbers. This could be attributed to a growing destruction of the almandine coating in these experiments. Even larger destruction appeared to the epoxy coating. In addition the length and numbers of streamer were not identical for all coatings.

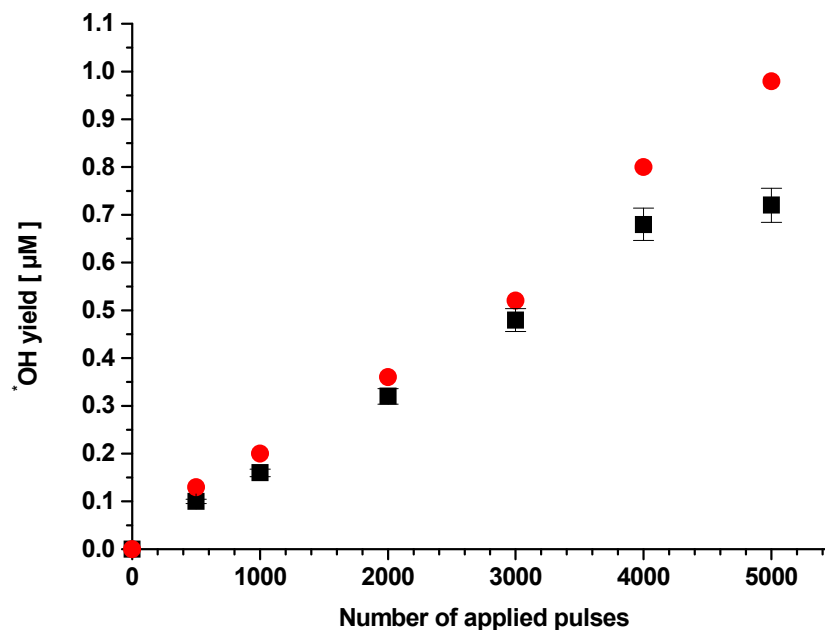


FIG. 4.36. Influence of the ceramic coating material (alumina and almandine) on the OH radical yield. The anode substrate was Ti in all cases. (■ =titanium + alumina, ● = titanium + almandine; water conductivity: 400 $\mu\text{S}/\text{cm}$, pH= 6.8.)

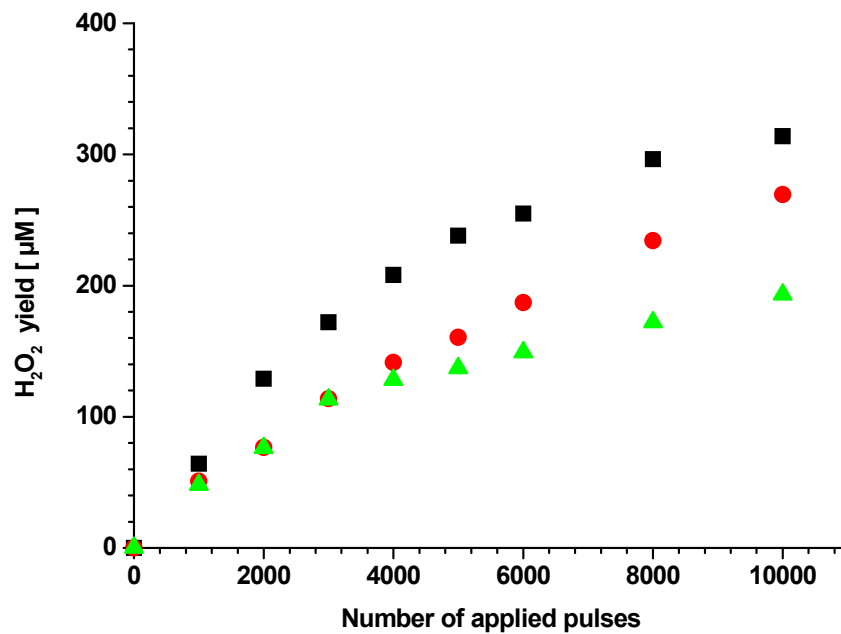


FIG. 4.37. Influence of the ceramic coating material (alumina, epoxy, and almandine) on the H₂O₂ production. The anode substrate was Ti in all cases. (■ = almandine + titanium, ● = epoxy + titanium ▲ = ceramic + titanium; water conductivity: 400 µS/cm, pH= 6.8)

4.2.6. Anode aging: Industrial applications for water disinfection and decontamination require stable long lifetime operation of anodes. To achieve this goal an improved understanding of the causes for anode degradation and its effects on oxidant production is necessary.

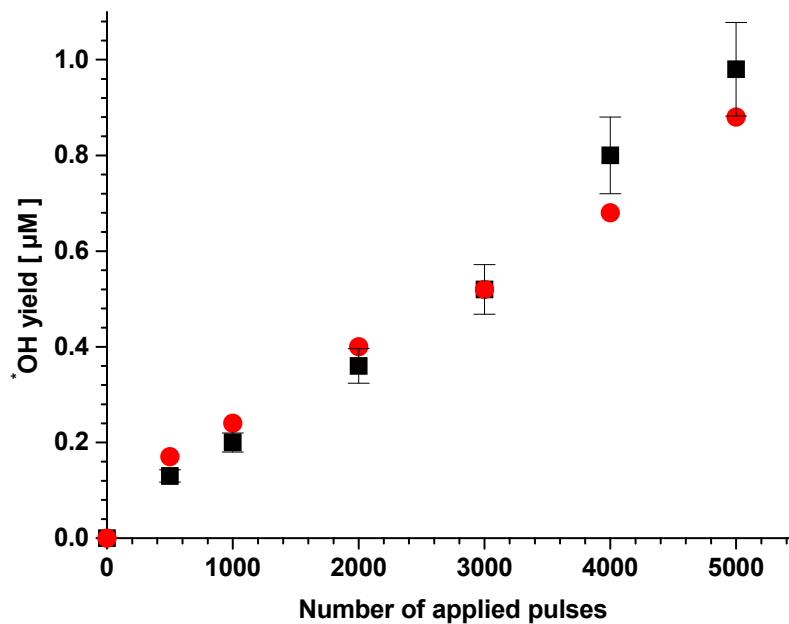


FIG. 4.38. Comparison of OH radical yields from fresh and abraded almandine coated titanium anodes. (■ = fresh anode, ● = anode after 400,000 pulses; $\sigma = 400 \mu\text{S/cm}$, pH= 6.8)

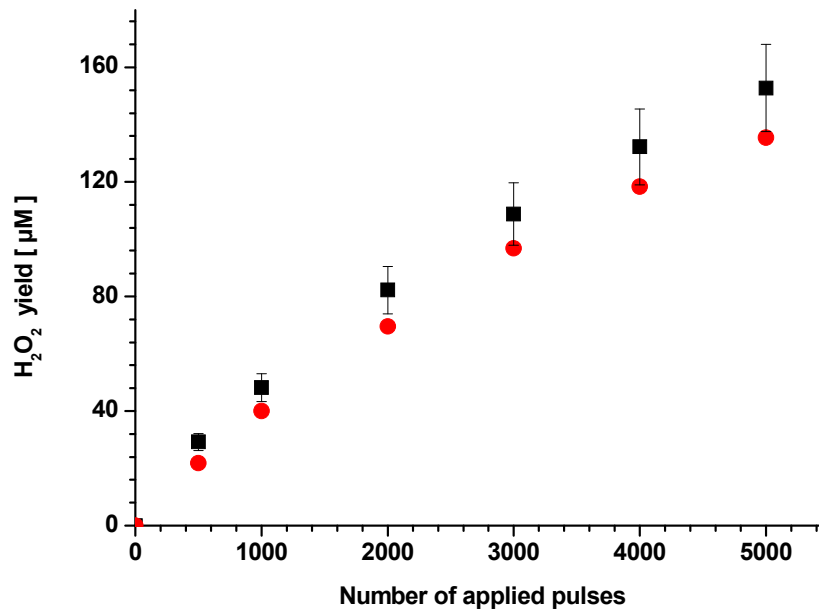


FIG. 4.39. Comparison of H₂O₂ yields from fresh and abraded almandine coated titanium anodes. (■ = fresh anode; ● = after 400,000 pulses; water conductivity: 400 µS/cm, pH= 6.8)

For these investigations the anodes were operated for up to 400 000 pulses and the oxidant productivity of fresh and used anodes were compared. Here only almandine coated titanium anodes were considered since they promised the largest lifetime and the highest oxidant yields. The results of these preliminary studies are depicted in Fig. 4.38 and in Fig. 4.39.

The data show a reduction in the yield of OH radicals and H₂O₂ of up to 10%. Most of this reduction in oxidant yield can be attributed to the blistering of some coating material from the anode. This primarily reduces the number of streamers. More detailed material studies are required to improve the bonding between the ceramic coating and the metallic anode.

4.2.7. Effect of electrode surface area: To increase the throughput in a water disinfection system based on underwater corona discharges one can either enlarge the free cross section of the reactor or augment the flow velocity of the water. To keep the oxidant reactions with the contaminants at the required level an extension of the electrode area seems the most appropriate choice for both cases. Other possibilities are to increase the pulse repetition rate and the interelectrode gap. The consequences of extending the distance between electrodes have already been discussed in section 4.1. Increasing the pulse repetition rate seems limited to a few times 10 Hz because of electrode heating and the streamer decay time. Here we shall discuss the issue of electrode area enlargement

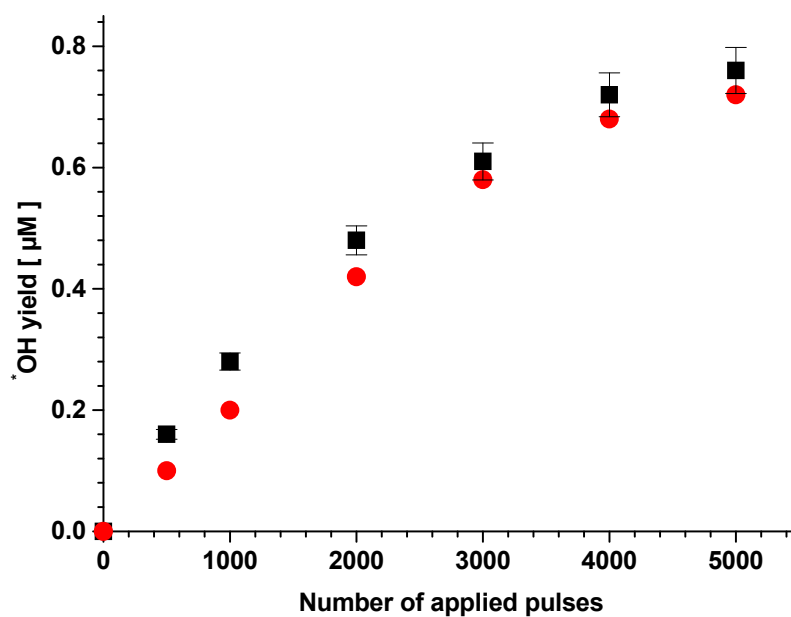


FIG. 4.40. Effect of anode surface area on OH radical production (■ = 6mm titanium + alumina, ● = 10 mm titanium + alumina). Water conductivity: 400 $\mu\text{S}/\text{cm}$, pH= 6.8.

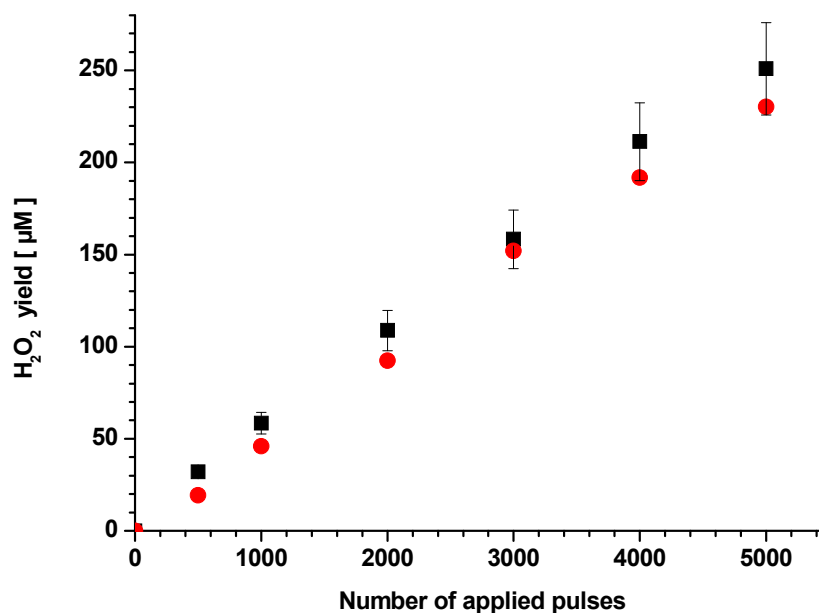


FIG. 4.41. Effect of anode surface area on H₂O₂ production. (■ = 6 mm alumina + titanium, ● = 10 mm alumina + titanium). Water conductivity: 400 $\mu\text{S}/\text{cm}$, pH= 6.8.

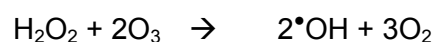
Maximum system efficiency can only be obtained if the pulse generator impedance is matched to the reactor impedance. Keeping the electrode distance constant while increasing the electrode surface area causes both a reduction of R_{water} and R_{ceramic} . Consequently a generator with higher power i.e. lower impedance is required to drive such a reactor.

It is obvious that if the same generator is used to drive two reactors which just differ by their electrode surface areas the performance of the reactor whose impedance is better matched to generator will be superior. A special case is the coaxial reactor where the electric field at the anode which determines the number of streamers launched into the water depends on the anode radius. Therefore also reactor C (see Table 4.1) was better matched to the generator impedance than reactor A it resulted in a lower oxidant yield. This is demonstrated in Fig 4.40 and Fig. 4.41 where the $\cdot\text{OH}$ and H_2O_2 yields have been plotted.

4.2.8. Effect of dissolved and percolating gases: Gases dissolved in the water and small gas bubbles flowing through the zone of streamer formation can change the oxidant production. The effect of oxygen bubbles in pulsed corona discharges has been reported previously by other researchers. As expected, ozone was generated in the presence of oxygen bubbles [40]. Ozone can react with H_2O_2 accumulated in the bulk water and produce additional OH radicals.

We have extended the investigations to other gases like argon, N_2O , ozone and as a reference also applied oxygen. All experiments were performed under similar operating conditions. The water conductivity was kept constant at 400 $\mu\text{S}/\text{cm}$ and the experiments were performed at neutral pH.

As shown in Fig 4.42 the highest OH radical yield was obtained when ozone was bubbling through the solution. If ozone percolates through the reactor its concentration in the water increases up to the saturation concentration [at room temperature ozone has a saturation concentration of 12 mM] and reacts very fast ($k = 5.5 \times 10^6 \text{ M}^{-1}\text{s}^{-1}$) with the accumulated hydrogen peroxide (at neutral or higher pH) and produces OH radicals. This reaction is known as the peroxone process. [17]



The additional OH radicals, produced in the bulk, can be detected through their reaction with DNTA present in the water forming HTA. Therefore in this experiment a much higher OH radical yield was expected. However in contrary only a small increase of OH radicals was obtained.

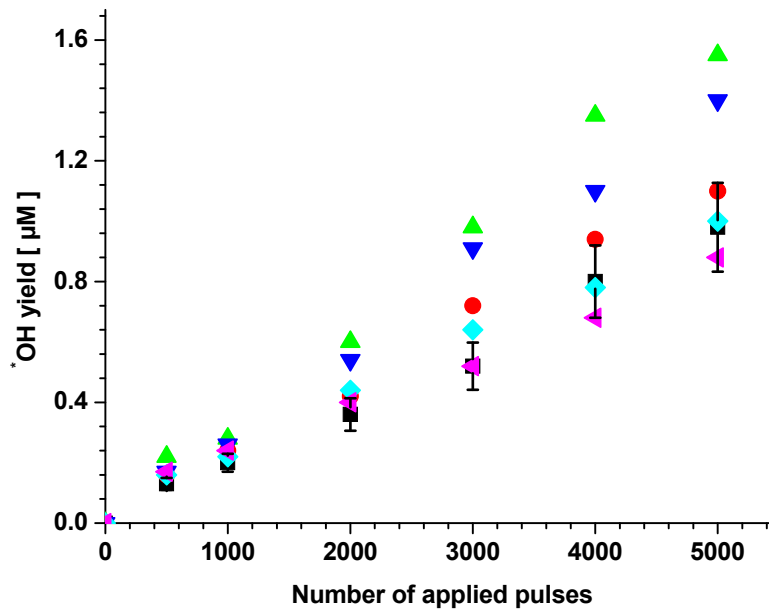


FIG. 4.42 Influence of percolating gases on the OH radical formation [▲ = ozone (8.36 J/pulse), ▼ = N₂O (8.7 J/pulse), ● = oxygen (9.05 J/pulse), ■ = without gases (fresh anode 7.98 J/pulse), ◆ = argon, ◄ = without gases (weary anode: 400,000 pulses, 8.8 J/pulse); water conductivity: 400 µS/cm, pH= 6.8]

Thus it is supposed that the HTA formed in this process might have been destructed by direct ozone attack [88]. At present direct reaction rate constants for hydroxylterephthalate ions with ozone are not available.

However in a pioneer work by Hoigné and Bader, different rate constants of ozone were determined for different phenolic compounds [109-110]. This study showed that the rate constants of some phenolate ions (with ozone) are sufficiently high to produce diffusion controlled reactions. A similar study on ozonolysis of phenols by Sonntag and his colleagues also confirmed these findings [111]. Because of similarity of HTA with phenolates we expect rate constants of similar magnitude for HTA. Of course the destruction and detection of HTA depends also upon the concentration of dissolved ozone, H₂O₂ and DNTA concentration.

In order to establish definite conditions in the experiments air dissolved in the water was removed by flowing argon through the solution. This was especially required to investigate the effect of N₂O gas bubbles in the water. N₂O is of interest since it interacts with solvated electrons and thus exploits another source for the production of additional OH radicals:



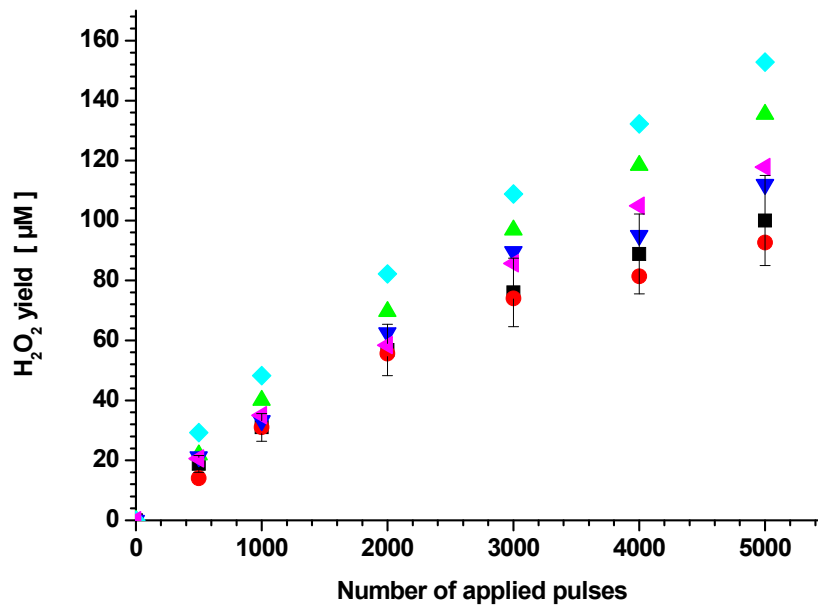


FIG. 4.43. Influence of percolating gases on the H_2O_2 production. [\blacklozenge = without gases (new anode), \blacktriangle = without gases (weary anode: 400,000 pulses), \blacktriangleleft = oxygen, \blacktriangledown = ozone, \blacksquare = argon, \bullet = N_2O ; water conductivity: $400 \mu\text{S}/\text{cm}$, $\text{pH} = 6.8$.]

It is also seen from Fig. 4.42 that in case of oxygen or argon percolating through the reactor there was only a marginal increase of the OH radical yield.

Without gas bubbling we obtained the highest yield of H_2O_2 . Percolating the different gases through the reactor does not show appreciable differences in the H_2O_2 yield (Fig. 4.43). The apparently observed increment in the H_2O_2 yield in case of ozone percolation with time can be attributed to reactions taking place between the increasing ozone concentrations in the water with Allen's reagent.

4.2.9. Distribution of oxidants: Since the streamer originates from the anode surface and remains confined in a limited radial zone around the anode, we expect that the initial radial distribution of oxidants produced inside the streamer or at its surface has a gradient towards the cathode. Without water circulation this radial distribution of concentrations should exist for times shorter than the diffusion time of molecules towards the cathode. Taking samples at different radial positions immediately after termination of the experiment should provide a higher concentration at the anode than at the cathode.

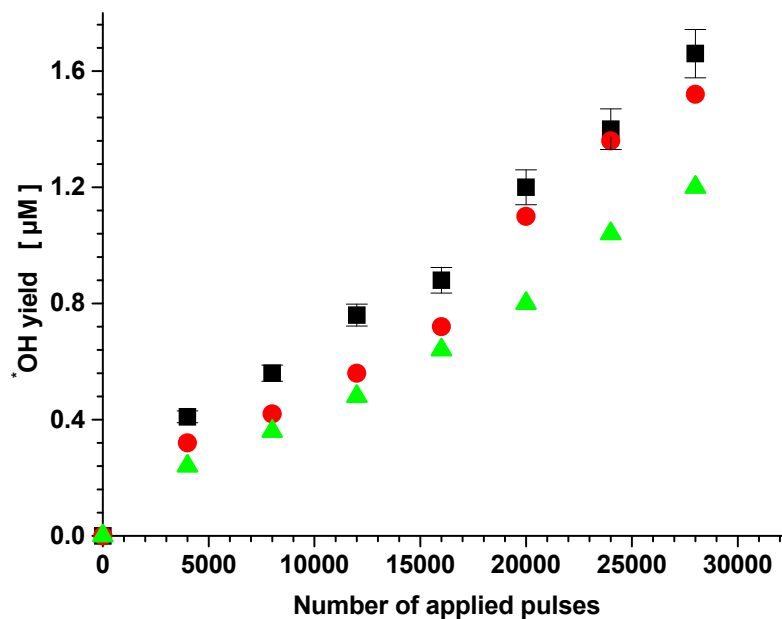


FIG. 4.44. Yield of OH radicals from samples taken at different radial positions. (■ = anode surface, ● = 15 mm from the anode surface, ▲ = cathode surface = reactor wall; Water conductivity: 400 µS/cm, pH= 6.8)

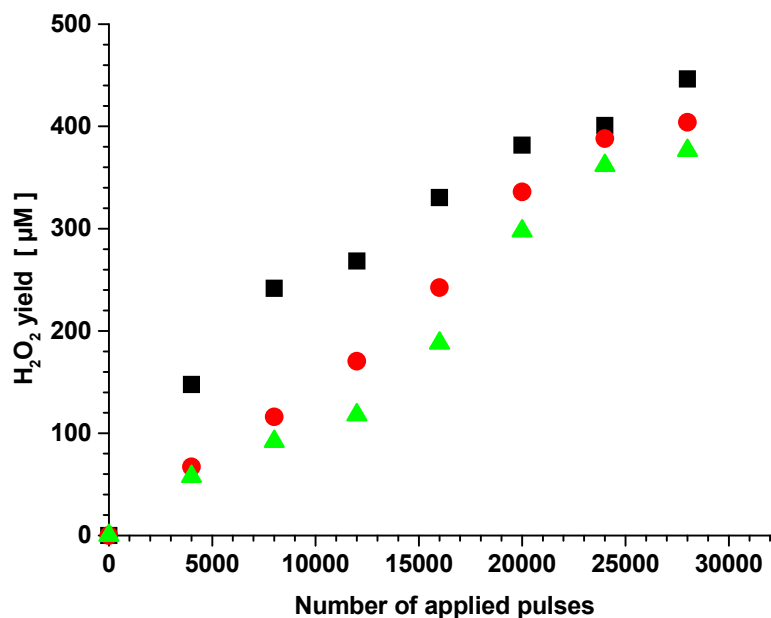


FIG. 4.45. Yield of H₂O₂ from samples taken at different radial positions. (■ = anode surface, ● = 15 mm from the anode surface, ▲ = cathode surface = reactor wall; Water conductivity: 400 µS/cm, pH= 6.8)

To verify this; experiments have been conducted with the larger diameter reactor ($\Phi=70$ mm). Sampling of the OH radicals and H_2O_2 was performed at three different radial positions: close to the anode surface, and 15 and 30 mm away from it (Fig. 4.44 and Fig.4.45).

The samples were collected within 30 seconds after experiment termination. Evidently diffusion also occurs during the experimental run which lasted 30 minutes (4000 pulses). To estimate the diffusion distance in the available time the diffusion constants are presented in Table: 4.4.

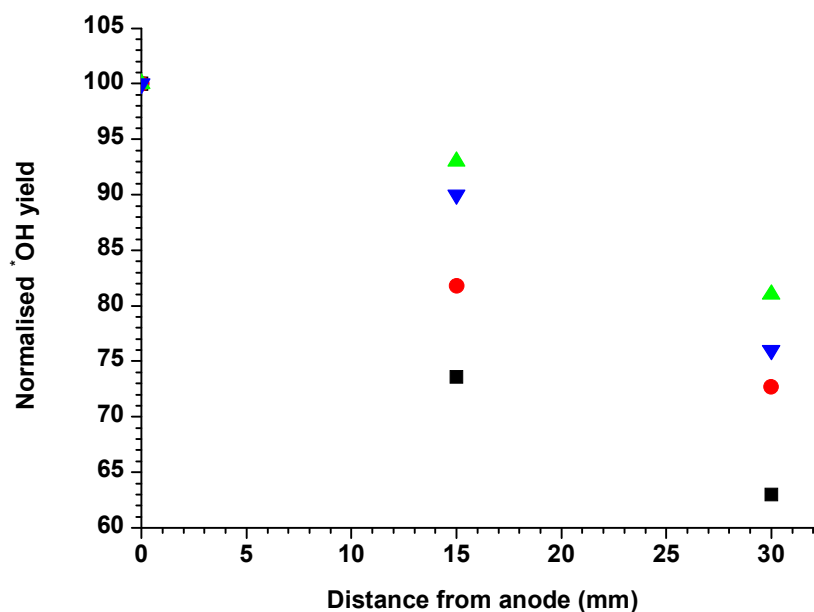
Table 4.4. Diffusion constants D for the relevant molecules created in the streamer channel or at its surface [112]

Species	D ($10^{-5} \text{ cm}^2 \text{ s}^{-1}$) @30° C
•OH	2
e^-_{aq}	5
H	8
H_2O_2	1.18

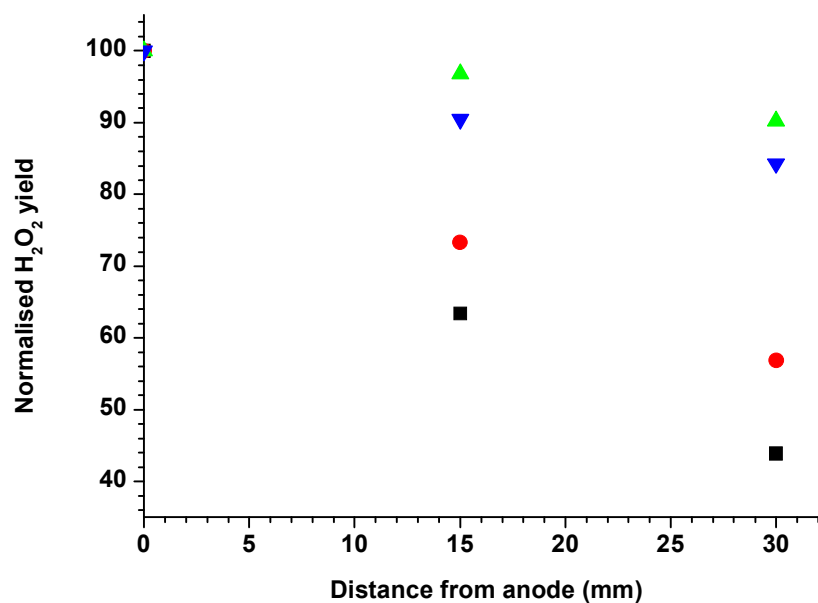
The distance λ that the produced oxidant will move within a time τ can be estimated from the following formula [112]:

$$\lambda = \sqrt{6 \tau D}$$

Normalizing the radial yields to that at the position closest to the anode should show a steeper gradient for shorter operation periods. This is shown in Fig. 4.46- [A] and [B] for the yields of OH radicals and H_2O_2 respectively. As expected the radial distribution becomes flatter as operation time progresses. Apparently the OH radical distribution follows the H_2O_2 distribution. However this merely reflects that the diffusion of H_2O_2 and the •OH indicator HTA diffuse similarly. After 1800 s the mean diffusion distance of H_2O_2 is estimated to be 3.5 mm. The results suggest that turbulent mixing of the water in the treatment section of the reactor is necessary to achieve an equal remedy of contaminants in the flow.



[A]



[B]

FIG. 4.46-[A].Radial distribution of OH radicals. [B]. Radial distribution of H₂O₂ (samples taken at different radial positions). (■ = 12000 pulses ● = 16000 pulses ▲ = 24000 pulses ▼ = 28000 pulses; water conductivity: 400 μS/cm, pH= 6.8)

4.2.10. Combination with Fenton's reaction: It is well known that the addition of [FeCl₂·4H₂O] salt to water containing H₂O₂ enhances the production of OH- radicals due to Fenton's reaction [113].

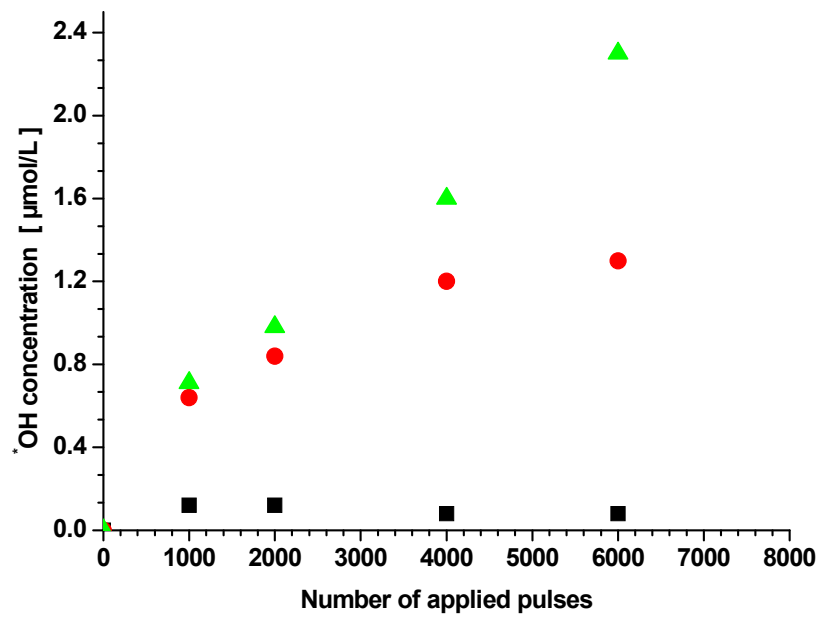


FIG. 4.47. OH radical yield in presence of ferric salt. Here DNTA has been used as the diagnostic probe. (■ = 0.5 mM DNTA with Fe salt, ● = 2.0 mM DNTA with Fe salt, ▲ = 2.0 mM DNTA without Fe salt [$\text{FeCl}_2 \cdot 4\text{H}_2\text{O}$])

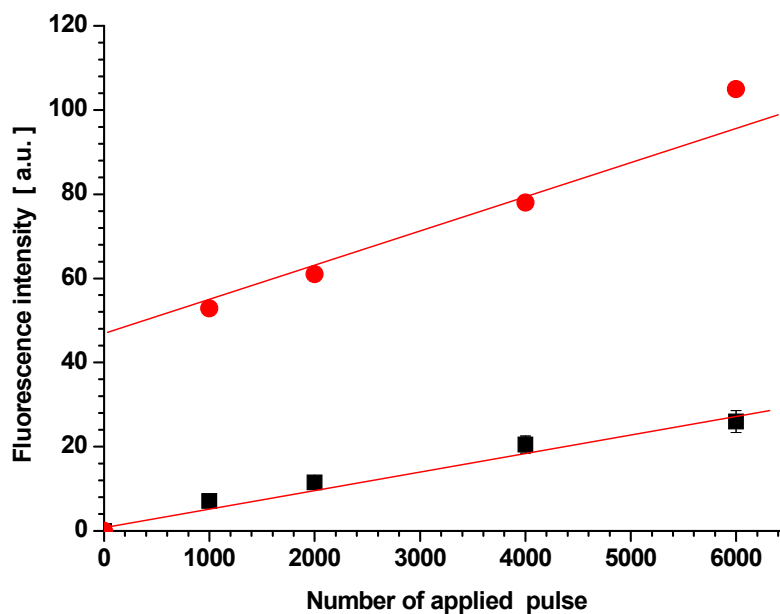


FIG. 4.48. OH radical yield with and without the addition of ferric salt to the corona chamber. The fluorescence intensity of the diagnostic probe coumarin is proportional to the OH-yield. (■ = coumarin without Fe salt, ● = coumarin with Fe salt [$\text{FeCl}_2 \cdot 4\text{H}_2\text{O}$])



To investigate this reaction in connection with streamer discharges it was not possible to use DNTA as a diagnostic probe because iron precipitated if DNTA was present. Fig. 4.47 shows that with this diagnostic probe we apparently recorded a lower yield of OH with ferric salt than without. It was therefore decided to use coumarin [C₉H₆O₂], which is an OH scavenger forming the fluorescent compound 7 hydroxy coumarin [77]. Adding 1 mM of the ferric salt to the treatment solution in the reactor chamber increased the fluorescence intensity of coumarin by more than 3 times compared to the case without iron (Fig. 4.48).

4.2.11. Oxidation of organic molecules: Oxidants have been used to remove organic pollutants from waste water [41, 42, 61, 70, and 114-116]. In textile industries chemical dyes like indigo constitute a major group of pollutants in wastewater. To demonstrate that such pollutants can be removed from water with underwater corona discharges an experiment with indigo has been carried out. Since we had found the highest OH radical yield by using copper anodes we chose an alumina coated copper anode and for comparison also a titanium anode with the same coating. The degradation of indigo achieved with both anodes is shown in Fig. 4.49.

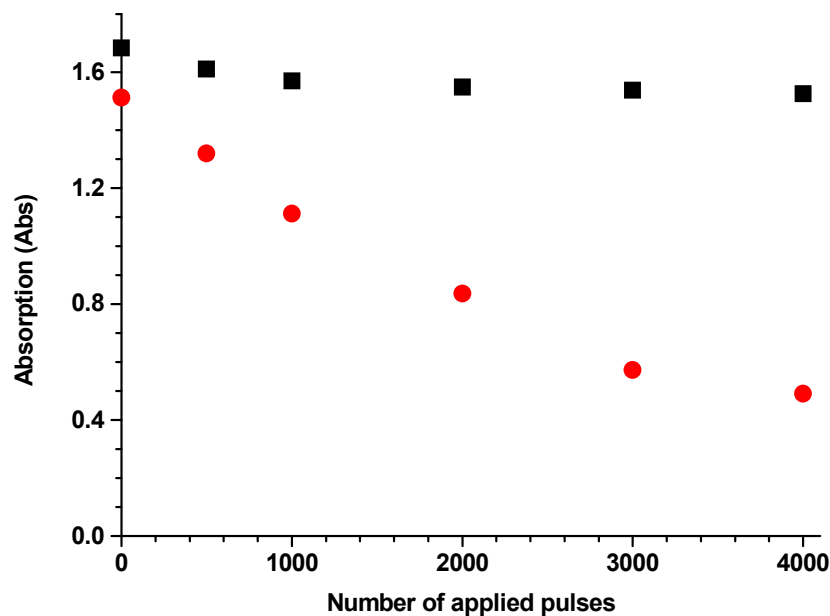


FIG. 4.49. Destruction of indigo dye determined from the spectral absorbance at 600 nm wavelength. (■ = almandine coated titanium anode, ● = alumina coated copper anode)

Because of the inhibition of streamer formation from alumina coated anode surfaces after longer operation, which has been described in section 4.2.5, saturation in the

deterioration was observed in both cases. Nevertheless, as expected a much faster degradation was achieved with the Cu + Al₂O₃ anode. It has also been observed that using a Ti+ Al₂O₃ anode the destruction of indigo by went much faster into saturation., This is probably due the fact that in case of a Cu + Al₂O₃ anode the release of Cu⁺ ions continues during the application of high voltage pulses, even though the streamer formation stops. The Cu⁺ ions react with the H₂O₂ molecules accumulated previously in the water and release OH radicals.

4.2.12. Comparison of H₂O₂ yields: As described in chapter 3 the methods described by Eisenberg [90] and by Allen [92] were applied to determine the formation of H₂O₂ in the corona reactor. Therefore it was desirable to compare the results achieved with both methods. It was found that the measured values deviated by less than 5%. As shown in Fig. 4.50 they commonly proved an initially linear increase of the H₂O₂ yield but for larger pulse numbers evidenced saturation. It is believed that the indicated saturation is due an increased decomposition of H₂O₂ at elevated temperatures. Typically, for a temperature rise of 10° C, the decomposition rate of H₂O₂ increases by a factor of 2.3. At higher repetition rates the water temperature in the corona reactor rises by more than 5°C after 15000 pulses.

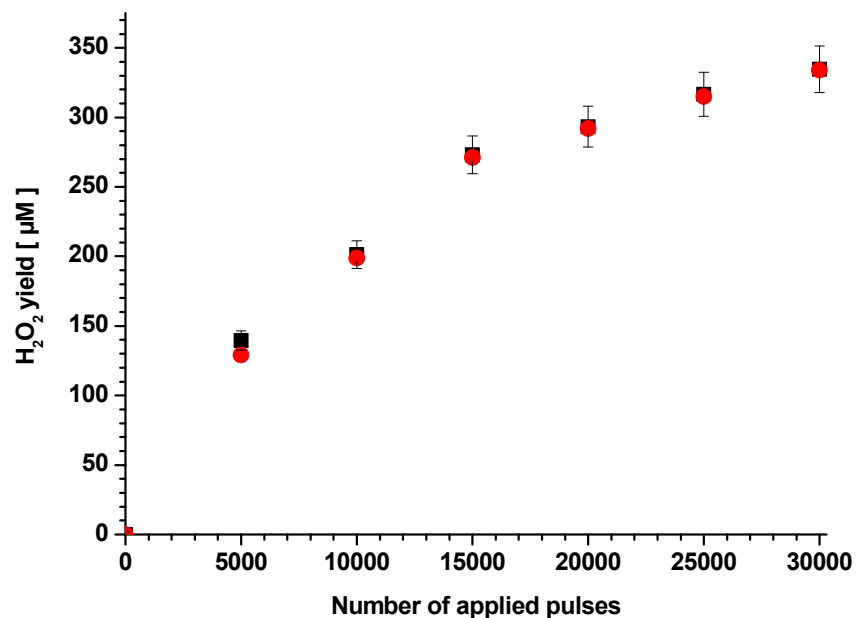


FIG. 4.50. Comparison of H₂O₂ yields determined from Eisenberg's and Allen's method. (■ = Eisenberg's (TiSO₄) method; ● = Allen's reagent; conductivity = 380 µS/cm, pH = 6.8)

4.2.13. Dependence of H₂O₂ production on conductivity and pH: In wastewater the conductivity varies over a large range of values. It has been found that an increase of the

water conductivity from 200 – 1600 $\mu\text{S}/\text{cm}$ resulted in a reduction of the H_2O_2 production from 562.6 μM to 146.8 μM (Fig. 4.51). We attribute this result to the reduction of streamer length with increasing water conductivity. The reason for the shortening of the streamer length has been described in section 4.1. As discussed in section 4.2.3 there is a linear relation between streamer length and H_2O_2 production.

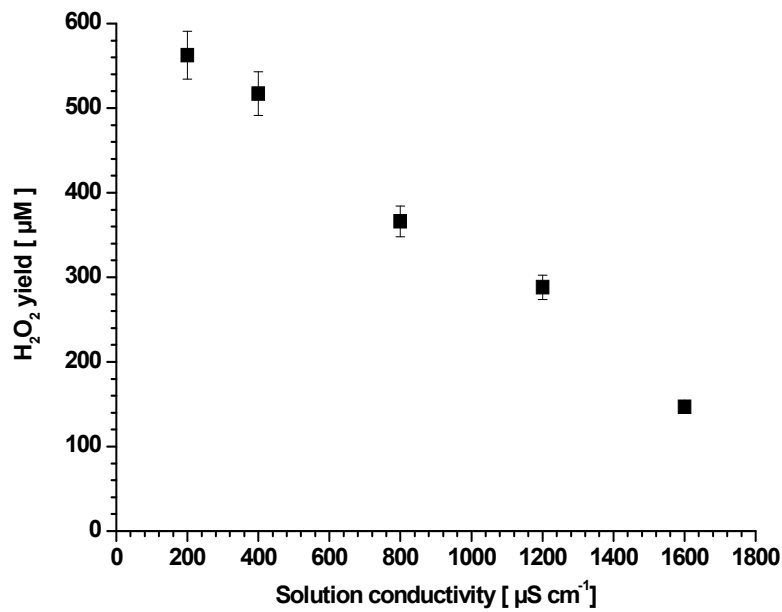


FIG. 4.51. H_2O_2 production vs. water conductivity. (Pulse voltage: 35 kV; number of applied pulses: 8000 for all data points).

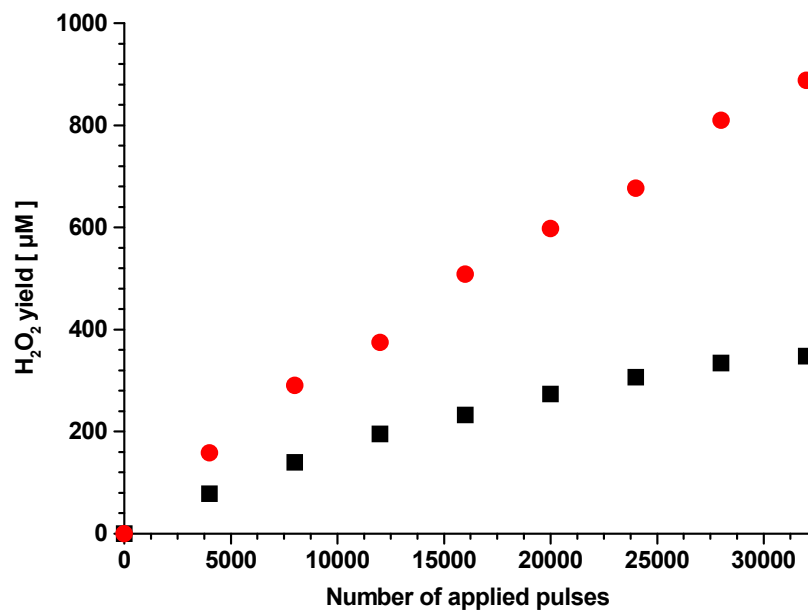


FIG. 4.52. Effect of pH on H_2O_2 production. (● = solution pH = 6.2, ■ = solution pH = 8.38)

The pH values in a wastewater treatment plant typically vary between 6 and 8. Experiments have been performed to determine the influence of the pH-values on the H_2O_2 production in this range. To increase the pH value of the solution, NaOH was added to the water which caused an increased conductivity as well. The results that were attained are presented in Fig. 4.52. At pH = 6.2 the H_2O_2 production was up to a factor of 4 higher than at pH = 8.4. One reason for this result is certainly the reduced streamer length at higher conductivity.

4.2.14. Ozone yield: Ozone is a powerful oxidant, second only to hydroxyl radicals and it is very commonly, used in water treatment processes. In limited quantities ozone is soluble in water. Typically in water disinfection treatment plants the applied ozone mixture is far from 100% ozone. This is a result of the low efficiency of ozone generators which in most cases use air as the feed gas. The ozone concentration used for water treatment is typically below 14% of its saturation value. Consequently, the actual concentration of ozone in water treatment stays below few hundred μM [88]. In water, ozone decomposes spontaneously and generates hydroxyl radicals. This hydroxyl radical production increases if ozone is exposed to UV radiation or is combined with H_2O_2 . Also a higher pH value leads to an augmented production of OH radicals. Though the reaction mechanism is not fully understood the most commonly accepted model is that developed by Hoigne and Bader [17, 109, 110]. In this model it is believed that hydroxyl radicals [1.5 mole OH radical / 1 mole ozone] are intermediate products, which react with any species (such as H_2O_2) present in the water.

For water treatment plants ozone is produced by dielectric barrier discharges (DBD). A small dissolved ozone concentration of 0.6 $\mu\text{g/L}$ was found to be sufficient to reduce the level of E-coli bacteria by 4 logs. When a pulsed corona discharge is performed in an oxygen saturated solution or when oxygen is bubbled through the reactor during the discharge process then ozone is produced. Because H_2O_2 is always formed in corona discharges it can produce OH radicals in the bulk solution. In this section the experimental results of absolute measured value of ozone in liquid (dissolved) phase as well as in gas phase are presented.

Ozone measurement in the liquid phase: The measurement of ozone production in pulsed corona discharges has been carried out in an oxygen-saturated aqueous solution. At fixed pulse intervals the samples were drawn from the corona reactor and the dissolved ozone concentration was monitored by the Indigo method. In Fig. 4.53 the absolute concentration of ozone in 1000 mL water has been plotted as a function of increasing pulse counts. The pulse energy was 9 joule. As H_2O_2 was also present in the solution and the experiments were performed at neutral pH, a reaction between the ozone and the

accumulated H_2O_2 cannot be ruled out. Therefore with increasing pulse counts a non-linear increment of the dissolved ozone concentration was observed.

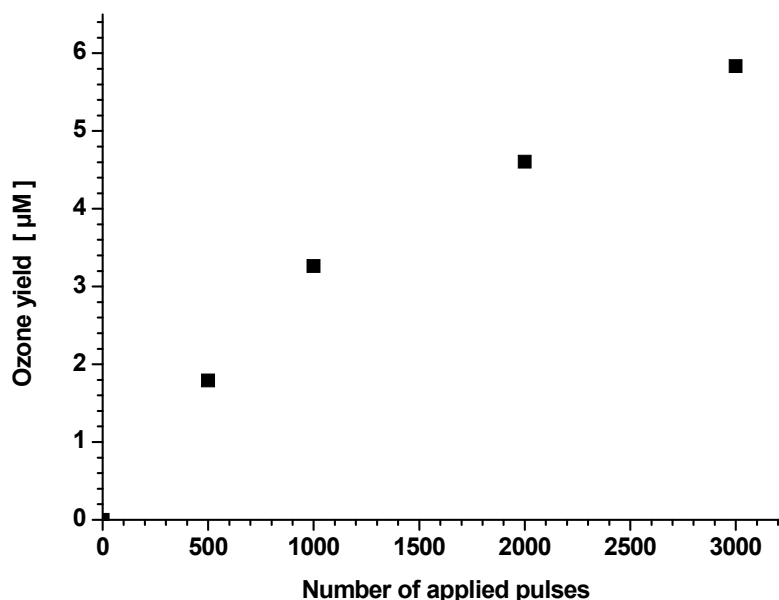


FIG. 4.53. Formation of ozone in dependence of the number of applied pulses. (solution conductivity: 400 μS , neutral pH; pulse energy: 9 J)

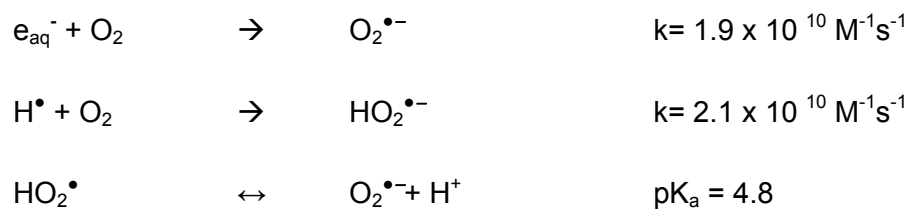
4.3 Reductive species

Apart from oxidative species, reductive species such as atomic hydrogen ($\cdot\text{H}$), super oxide radical anions ($\text{O}_2^{\cdot-}$), and solvated electrons (e_{aq}^-) are also produced in the pulsed underwater corona discharges. In this section experimental results, confirming the formation of super oxide radical anions ($\text{O}_2^{\cdot-}$), and aqueous electrons (e_{aq}^-) are presented. As far as available knowledge, the H radical quantification in the liquid phase is difficult because no direct chemical probes are available at present. However since main source of both OH radicals and H -atoms results from collisional disintegration of water molecules we can assume that the production of H -atoms is equivalent to that of OH radicals. Therefore in this section only experimental results, confirming the formation of super oxide radical anions ($\text{O}_2^{\cdot-}$), and aqueous electrons (e_{aq}^-) are presented.

4.3.1 Aqueous electrons: The detection of aqueous electrons (e_{aq}^-) is performed by percolating N_2O gas through the solution. As described in chapter 3, N_2O serves as a scavenger of solvated electrons (e_{aq}^-), forming additional OH radicals in the corona reactor. To see this effect OH radical detection was performed with and without N_2O in the solution. It has already been described in section 4.2.8 that in water saturated with N_2O the OH radical

yield was 1.5 times higher. This higher detection of OH radical with N₂O saturated solution can be due to the reaction between N₂O and solvated electrons, which are produced in pulsed corona discharge process; this is a highly exothermic reaction. At the N₂O saturation concentration the reactions leading to additional OH occur within a few nanoseconds. The results prove the presence of aqueous electrons (e_{aq}⁻) in corona reactor.

4.3.2 Super oxide ions (O₂^{•-}): If sufficiently large amounts of oxygen are present in the water aqueous electrons (e_{aq}⁻) can interact with it producing super oxide ions (O₂^{•-}). Similarly atomic H can also react with oxygen forming hydroperoxyl radicals. At neutral pH these hydroperoxyl radicals convert into super oxide ions(O₂^{•-}) by the following reactions:



The pKa value (acid dissociation constant) of HO₂[•] introduced above describes the limit of pH values above which it transforms into super oxide ions (O₂^{•-}) [117].

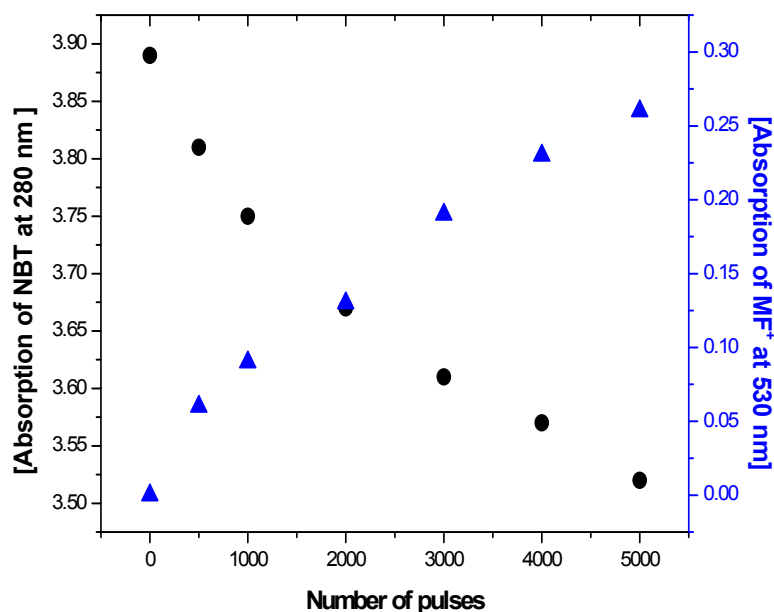


FIG 4.54. Formation of MF⁺ (mono formazan) and degradation of NBT [▲ formation of formazan; ● degradation of NBT; (neutral pH, water conductivity: 400-μS/cm)]

The reduction of NBT to purple formazan is used to evidence the generation of $O_2^{\bullet-}$ in biological systems. As described in section 3.7 the reactivity of $O_2^{\bullet-}$ with NBT can be monitored by observing the absorbance changes of the reactant. The original compound (NBT) and the product (formazan) are detected by measuring the absorbance at different wavelength. As shown in Fig. 4.54 the formation of formazan increases as a function of increasing pulse numbers and at the same time NBT gets destructed proportionally.

4.4 UV measurements

4.4.1. Spectroscopy: Using the spectroscopic set-up described in chapter 3.7 the time and space integrated emission spectra from the corona reactor have been measured. A typical spectrum is presented in Fig. 4.55. This spectrum covers a broad range from UV-C (microbicidal UV) to infra-red. The different peaks indicate the presence of hydrogen, nitrogen and oxygen emission lines confirming the disintegration of water and dissolved gas molecule by the pulsed corona discharge.

From the point of view of disinfection applications it is of interest to determine the radiant power emitted in the UV range and to estimate the average dose in the reactor. To derive the radiant UV power the emission from a known section of reactor volume (which is filled with plasma channels) is considered.

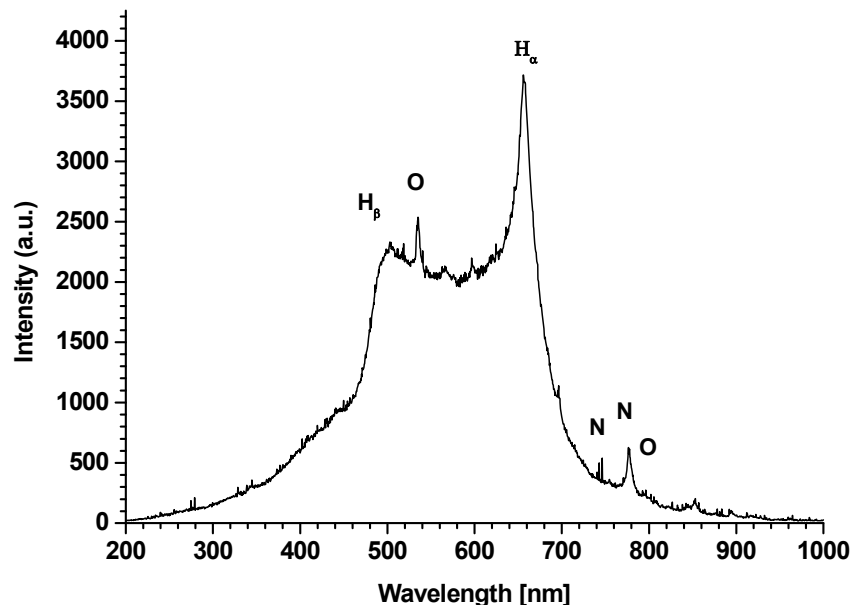


FIG. 4.55. Emission spectrum from the corona reactor; pulse amplitude = 60 kV.

The most effective wavelength for water disinfection is at 262nm. At this wavelength the DNA shows the highest absorption. Since the UV source results from individual streamer discharges distributed inside the reactor only a small fraction of the emitted UV light couples into the diffuser mounted above the corona reactor. Each volume element contributes with a different factor to the irradiance at the position of the diffuser depending on its geometric distance from the diffuser and on the wavelength dependent absorbance along the optical path-length in the water. Using the calibration described in section 3.7.1 the UV energy from the corona reactor at the entrance of the fibre optics (1.5 cm distant from the anode surface) is presented in Table 4.5 for different wavelength intervals.

Table 4.5. UV energy of plasma channels for different wavelength

λ	(UV energy) ($\mu\text{J}/\text{pulse}$)
210	0.32
220	0.26
230	0.06
240	0.04
250	0.03
260	0.02
270	0.02
280	0.02
290	0.02
300	0.02

4.4.2. Actinometry: UV measurements were also performed, by using uridine as a chemical actinometer, as described in chapter 3. For that purpose four different set-ups were applied:

- Uridine homogeneously dissolved in the corona reactor.
- Uridine filled in a suprasil (Heraus) cuvette placed inside the reactor. (see chapter 3.7)
- Uridine filled in cuvettes of normal glass and plastic
- Uridine filled in a suprasil (Heraus) cuvette with a high concentration of OH scavenger (2-propanol) placed inside the reactor. (see chapter 3.7)

The main advantage of set-up 1 is that a spatially and temporally integrated UV dose can be derived without complex geometrical calculations. Results obtained with this configuration are shown in Fig. 4.56.

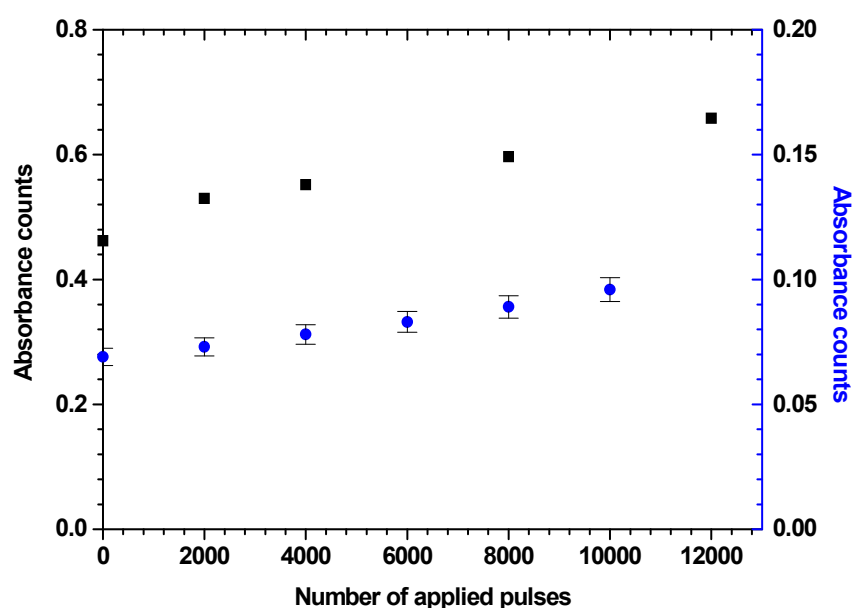


FIG. 4.56. Absorbance measurements of different uridine probes. ■ =uridine solution in Millipore water directly exposed to pulsed underwater corona discharges ● = uridine filled in a suprasil quartz cuvette placed inside the corona reactor.

When uridine is transformed into its photohydride form by UV irradiation the absorbance at 262 nm should drop. Surprisingly instead of an absorption decreasing with the number of applied pulses an increase was observed (Fig. 4.56). It is assumed that this was caused by interactions with other oxidants produced in the discharges disturbing the photohydride formation. This effect is prevented by the second set-up.

Uridine indirectly exposed to UV: To avoid the interference with other oxidants produced in the pulsed underwater corona discharges, uridine was filled into a spherical cuvette of suprasil quartz glass placed inside the corona reactor. It was assumed that turbidity did not effect the measurement and that the UV dose reaching the cuvette could be calculated from the decrease in absorbance. Unfortunately once again a similar behaviour was observed as with set-up 1 (Fig 4.56). An increase in absorption instead of a decrease was observed with exposure duration. This result shows that apart from UV some other reaction is taking place in the uridine solution. It was suggested that oxidants could have been formed inside the suprasil cuvette. To investigate this effect further the experiment was repeated with normal glass and plastic test tubes non-transparent for UV-light. However also in these cases an increase in absorbance was obtained. Therefore it has been concluded that shock waves penetrating the test assemblies are probably producing OH radicals disturbing the uridine measurements.

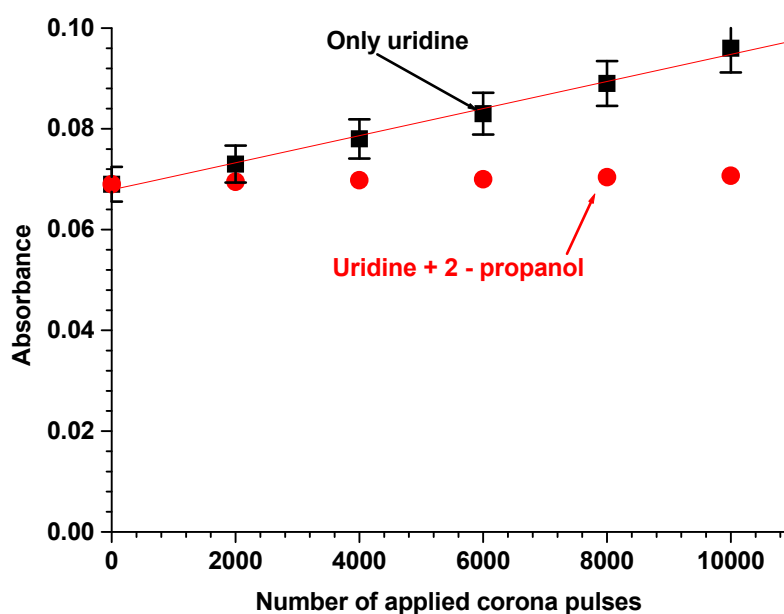


FIG. 4.57. Comparison of uridine absorbance with and without OH radical scavenger

To support this conclusion a high concentration 2-propanol which is a strong $\cdot\text{OH}$ scavenger was added to the uridine solution.

It was noticed, that in presence of 2-propanol the increase of uridine absorbance was reduced substantially. It is supposed that the OH radicals produced in the solution were scavenged by 2-propanol and thus only few were available to react with uridine. Still a noticeable decrease in absorbance was not observed (Fig.4.57). Therefore we must conclude that the sensitivity of the uridine probe for UV radiation in the present setup was not high enough. Consequently uridine actinometry cannot be used to quantify the UV flux if intense shock waves are present.

4.5 Cavitation effects

Many researchers have described the generation of shock waves in pulsed streamer discharges [32, 33, 65 and 116]. In previous work the presence of shock waves was detected by using shock wave transducers or interferometric methods. Here we used chemical reagents.

Measurement of OH radicals produced due to cavitation effects: As described before cuvettes of quartz, normal glass and plastic were placed inside the corona reactor near the anode surface. A 2 mM DNTA solution was filled into both the reactor and the cuvette. Samples were drawn from the reactor and from the cuvette at different pulse intervals and the OH radical as well as the hydrogen peroxide yields were determined.

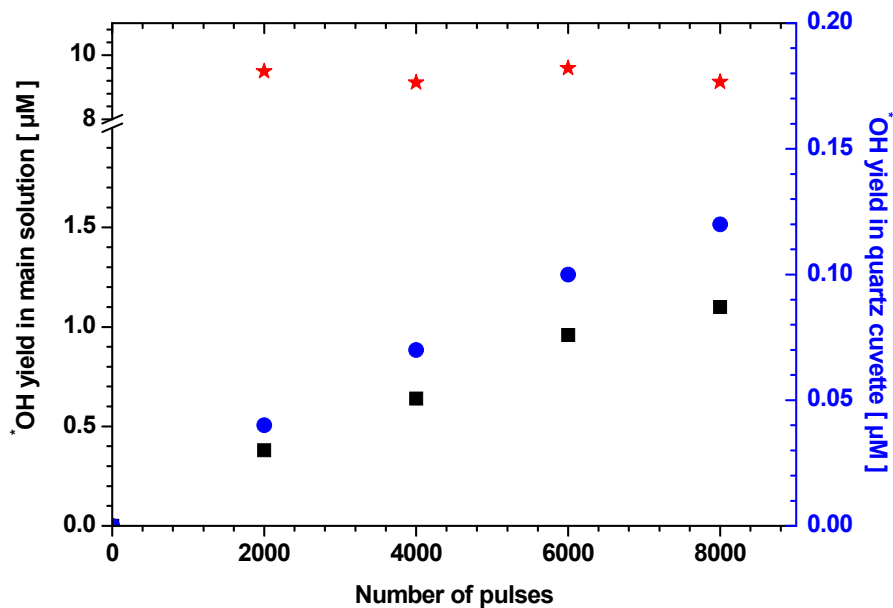


FIG. 4.58. Dependence of OH radical yield on the number of applied pulses in the corona reactor and in a quartz cuvette. (■ = corona reactor; ● = quartz cuvette * = ratio of both yields)

It was found that the OH radical yield inside the cuvette increased with pulse numbers although it was not in direct contact with the streamer channels (Fig 4.58). Similar to our earlier findings in section 4.2 the ratio between both yields remained constant suggesting that both effects are proportional to the number of pulses.

Using the normal glass and plastic cuvettes which are non-transparent to UV-radiation formation of OH radicals was also proven applying the DNTA diagnostic probe. This strongly supports our assumption that shock waves and the resulting cavitation are causing this radical formation.

Among the cuvettes the OH radical yield is highest in case of plastic material (Fig 4.59). It is assumed that this is due to the better matching between the acoustic impedances of water and plastic. The acoustic impedance of glass being much higher than that of water leads to larger reflections of the pressure waves at the cuvette surface. A simultaneous measurement of the H_2O_2 yield shows the same trend. For the same material a spherical cuvette results in a higher yield than a cylindrical one. This is probably due the fact that the refraction of waves at the spherical surface ends in an amplification of wave amplitudes in the interior of the cuvette.

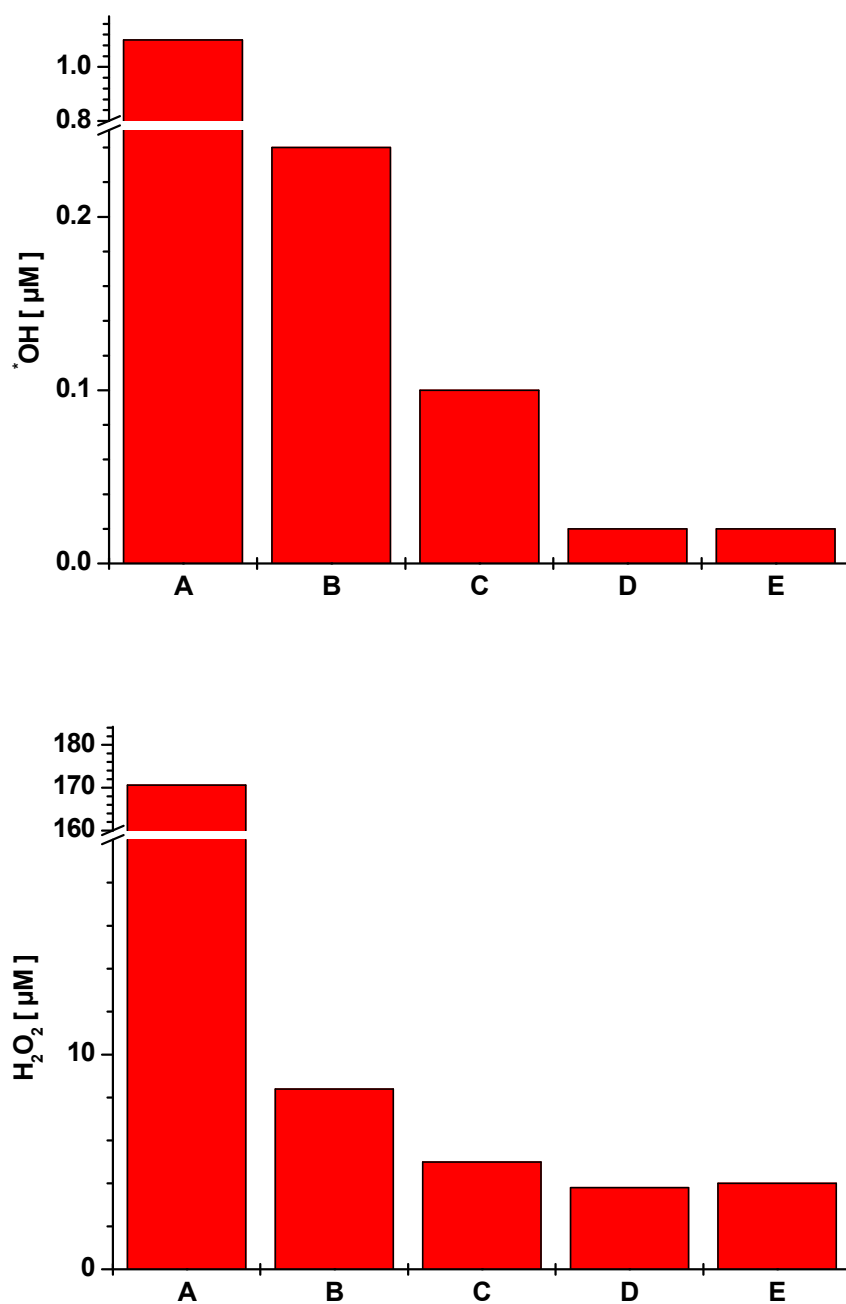


FIG. 4.59. OH radical and H_2O_2 yields in the corona reactor and in different cuvettes after 8000 pulses: A = corona reactor, B = plastic tube, C = spherical quartz tube, D = cylindrical quartz tube E = cylindrical glass tube

Summarizing, these results are strong evidence that cavitation effects produced by the propagation of shock waves launched from the streamer channels contribute to the production of oxidants.

4.6 Disinfection experiments

4.6.1 Epifluorescence microscopy: A chain of experiments was performed with known concentrations of *Pseudomonas putida*, a non-pathogenic and gram-negative bacterium, suspended in the corona reactor. The method of preparation of the water suspension has been described in chapter 3. For each experiment a fresh suspension of 200mL volume was taken from a stock solution. After a selected number of pulses the samples were evaluated by the epi-fluorescence and the heterotrophic plate count method. Results obtained from epifluorescence microscopy are shown in Fig.4.60 and Fig.4.61 before pulsing and after 250 pulses respectively.

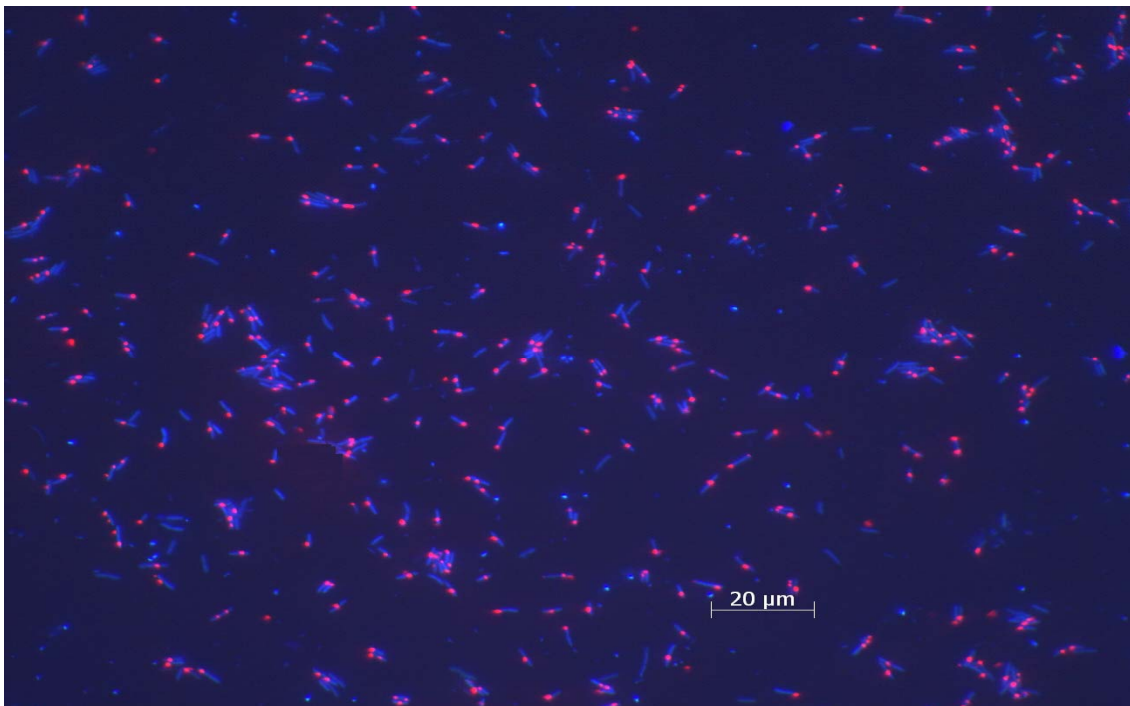


FIG. 4.60. Epifluorescence microscopy image of *Pseudomonas putida* bacteria stained with DAPI and CTC. The image shows the bacteria before pulsing. (Blue exemplifies all cells, red identifies active cells only)

A comparison of active cells counted before and after pulsing gives the killing rate. The cells stained red in the image identify the active ones showing metabolic activity. Due to inherent limitations of the manual counting method epifluorescence is accurate only for killing rates up to 3 log steps. The results are summarized in Table 4.6. Epifluorescence is a fast diagnostic method which is especially useful for exploratory studies.

Table 4.6. Bacterial destruction after different numbers of streamer discharges.

Initial <i>p. putida</i> concentration	Number of pulses	Specific energy J/mL	CTC/DAPI Epi-fluorescence counts
4×10^6	2000	158	> 3 log
4×10^6	1000	78	> 3 log
4×10^6	500	39	> 3 log
4×10^6	250	20	> 1.5 log

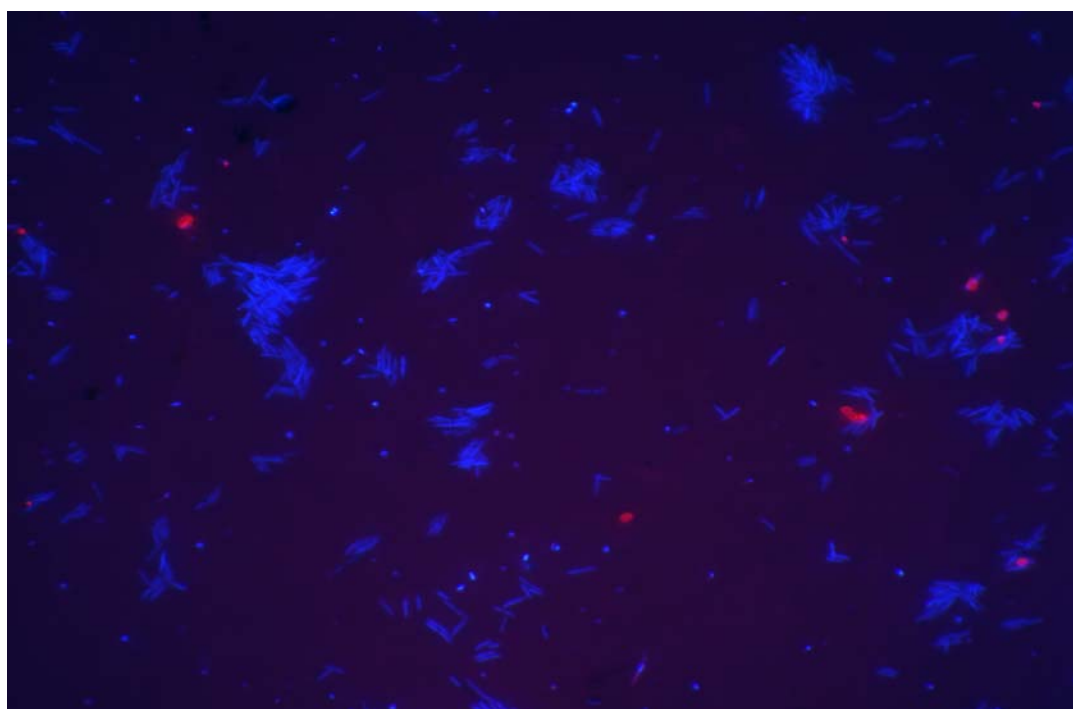


FIG. 4.61. Epifluorescence microscopy image of *Pseudomonas putida* bacteria stained with DAPI and CTC. The image shows the bacteria after 250 pulses. (Blue exemplifies all cells, red identifies active cells only)

4.6.2 Heterotrophic plate counting (HPC): Samples from the same series of experiments were also evaluated using petri dish plate counting. The results from this diagnostic are presented in Table 4.7. They demonstrate that a reduction of more than 6 log steps was achieved for all samples with a minimum specific energy deposition of 20 joule/mL (> 250 pulse).

In the preceding experiments the bacterial inactivation rate was always more than 6 log steps. As shown in Fig. 4.62 a specific pulse energy of 1.6 J/mL is required to achieve a bacterial inactivation of 0.63 log steps.

Table 4.7. Results obtained by heterotrophic plate count methods

Initial <i>p. putida</i> concentration	Number of pulses	Specific energy J/mL	Heterotrophic plate count (HPC)
4×10^6	2000	158	> 6 log
4×10^6	1000	78	> 6 log
4×10^6	500	39	> 6 log
4×10^6	250	20	> 6 log

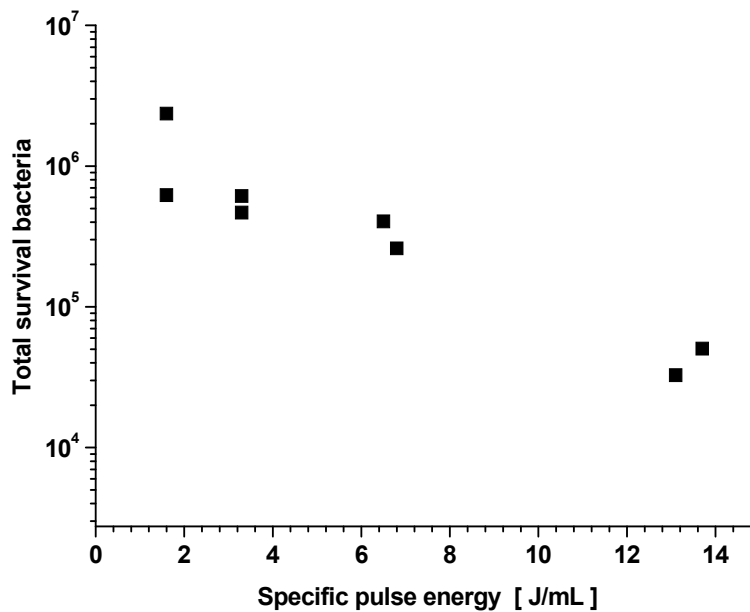


FIG. 4.62. Reduction of cells with reproduction capability vs. applied specific energy. (HPC method)

Effect of pulse energy (for wastewater): To apply pulsed underwater streamer discharges for waste water disinfection it is necessary to determine the efficiency for mixtures of bacteria present in this environment. Our earlier findings have proven that the use of copper anodes results in higher OH yields than with other anodes. Therefore two different anodes (almandine coated titanium and alumina coated copper) were implemented to detect the specific energy necessary for a two log reduction. A sample collected from the Karlsruhe (Neureut) municipal wastewater treatment plant was chosen for these measurements. The conductivity of this sample was rather high, i.e. 1200 $\mu\text{S}/\text{cm}$. The results are shown in Fig. 4.63.

To achieve a 2 log reduction of active bacteria between 89 and 180 J/mL were required. There are two reasons for these large numbers: First, the very high conductivity of the waste water samples and second the large variety of different bacterial species. To understand this in more detail an individual study of the different bacteria seems necessary which was not performed. Among these various species some are non pathogenic and some are pathogenic. In the present series of experiments we did not distinguish between both types. Therefore to get a reliable statement about the effectiveness of pulsed corona discharges for waste water disinfection studies of individual species present in the water are needed. Such studies are beyond the scope of this work.

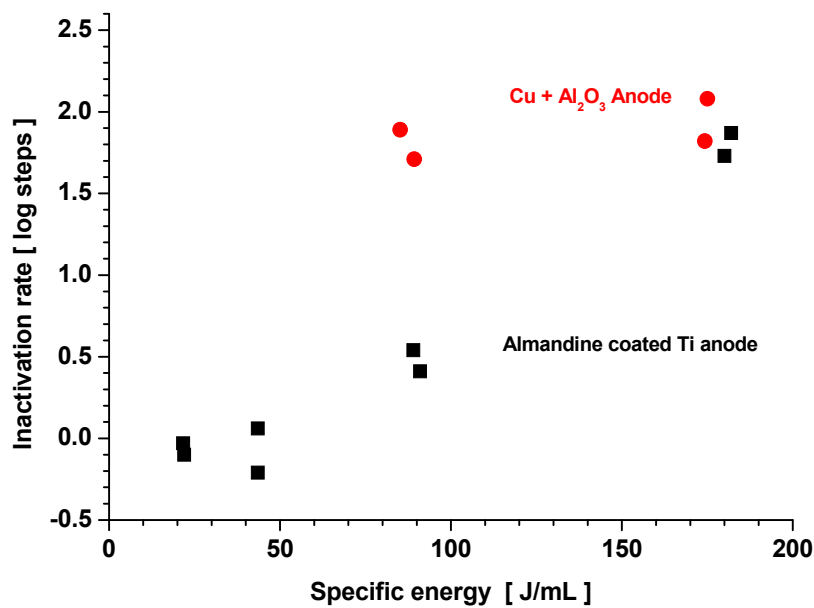


FIG 4.63. Bacterial inactivation of waste water samples vs. specific pulse energy for two different anode configurations. (● = Cu + Al₂O₃, ■ = Ti + almandine, wastewater conductivity: 1200 μS/cm).

Applying the alumina coated copper anode 89 J/mL are needed to achieve a 2-log bacteria inactivation. At this amount of energy deposition we obtain only a 0.5 log reduction with an almandine coated Ti anode. To reach a 2-log reduction 180 J/mL are requested. The reason for the saturation evident in Fig. 4.63 has been discussed previously: It is connected with the degradation of streamers in case of an alumina coated anode.

5. Discussion

Streamer channel formation: To initiate streamers from a metallic surface an electric field of the order of 1 MV/cm is required. Such high electric fields can be achieved by various methods (section 2.1), but considering industrial applications of underwater pulsed corona discharges, anodes covered with a thin layer of porous ceramic seem to be the most promising choice. This is supported by the results of our chemical and microbiological diagnostics which show additional advantages: Using such anodes a multitude of streamer channels homogeneously distributed over the entire anode surface can be obtained with moderately high voltage pulses. Two further advantages of these anodes exist: first there is no geometrical limitation on their size and second they are easy to prepare and cheap.

High voltage pulses can be produced by various ways. Earlier attempts to energize pulsed corona discharges comprise of simple capacitor discharges. From our experiments it was inferred that the number of streamers launched from the anode surface increases if the pulse rise time is reduced and if the pulse voltage is augmented. Simultaneously the streamer length grows if the voltage or the pulse width is enlarged. This is ultimately limited by a sufficiently large margin below arc breakdown. It has been found that the yields of OH radicals and of H₂O₂ grow linearly with the number and the length of streamers. To optimise the overall system efficiency the pulse generator impedance should match the impedance of the corona reactor. The latter depends upon the water conductivity; the electrode gap and the thickness and the porosity of the ceramic layer. However it is independent of the anode voltage.

High voltage pulse generator: To generate the required high voltage pulses a repetitively operating Blumlein generator built of discrete capacitances and inductances seems an adequate choice. It can be easily modified to match the reactor impedance and to achieve the desired pulse width. Besides this the output pulse voltage is equal to the input DC voltage. To generate fast rising pulses a gas filled pressurised spark gap switch has been selected. Spark gap switches are simple, robust and therefore inexpensive devices. In addition they have a large power handling capacity and a sufficiently small recovery time. At the required power levels of a few GW the electrode wear is small and their operational lifetime is adequate for industrial applications. However, any other switch is suitable if it allows fast rise times and if it is economic. Selecting the LC values of the Blumlein generator one has to keep in mind that the value of the inductance has a major influence on the pulse rise time too and thus should be selected as small as possible.

Electric field enhancement: The water and the ceramic layer in the corona reactor act as parallel resistive and capacitive dividers. When a fast rising high voltage pulse is

applied to the anode the voltage is divided capacitively for times shorter than the dielectric relaxation time $\tau = \epsilon\epsilon_0/\sigma$ and it becomes resistively divided for times greater than τ . Due to the very thin and porous ceramic layer an electric field enhancement occurs at the surface of this ceramic layer. At a porosity around 5% and for layer thickness between 200 and 300 μm typically half the voltage drops across the ceramic coating. Depending upon the porosity and the thickness of the ceramic layer rather low anode voltage (30-40 kV) is sufficient to attain a very high electric field strength ($> 1\text{MV/cm}$) independent of the reactor geometry. Such high field strengths fulfil the criterium for streamer formation and thus hundreds of homogeneously distributed plasma channels can be launched from the anode surface into the dense water medium. The corona onset voltage in a reactor is determined by the electric field actually established in the ceramic layer which depends on the factor of voltage division and the layer thickness. In addition it is influenced by the pulse duration.

A model of streamer initiation and propagation based on recent experimental findings has been adopted from the literature [12, 37 and 58]. In this model a primary streamer appears if the local electric field surmounts a value of 1MV/cm . It is assumed that electric field induced phase instabilities or gas bubbles cause the formation of primary streamer bushels. They have very low conductivity and do not disturb the local electric field distribution. Depending on statistically distributed heating and avalanching processes in one of the primary streamers the anode potential is transported to the tip of a certain primary streamer and a secondary streamer self-propagates if the potential is sufficiently high. The initial radius of the secondary streamer seems to be constant around $4\ \mu\text{m}$ leading to local electric fields of up to $100\ \text{MV/cm}$ sufficient to create dissociation and electronic breakdown in water. The self-propagation of secondary streamers stops when the potential at the streamer tip drops below a critical value at which the electric field is no longer sufficient to maintain the required level of dissociation and electronic breakdown. Therefore the length of a streamer channel is determined by the amplitude and the width of the anode pulse. The experimentally measured voltage drop along the streamer was $4\ \text{kV/mm}$ and the velocity of streamer propagating was found to be around $8\ \text{km/s}$. If the water conductivity increases the bypass current outside the streamer channel and through its surface increases too and reduces the potential at the streamer tip leading to an earlier stop of streamer propagation. Hence the streamer length shortens with increasing water conductivity. Since the production of oxidants is related to the streamer length it falls too. However in his study on streamer discharges Luke [101] has suggested that the UV emission increases under these conditions. At lower water conductivity the dielectric relaxation time constant increases and the capacitive voltage division between the water and the ceramic layer dominates for a longer time, which changes the field enhancement factor at the ceramic layer and therefore influences the initiation of streamers. Hence it is evident that the water conductivity strongly

affects the operation of a corona reactor and determines both, the choice of the pulse amplitude and pulse duration.

The secondary self-propagating streamer channels are the primary source of oxidants and other effects responsible for water disinfection. It is apparent from the measured optical spectra that H^I , OH , and O^I are present in the plasma channel. As the plasma channel cools down the different atomic and molecular species interact with each other, mainly reforming H_2O and creating H_2 , H_2O_2 , O_2 , O_3 , etc. During the active phase of the streamer large temperature and density gradients exist inside the streamer channel and the the described chemical reactions will also occur at the interface between the bulk water and the streamer channel and the products will diffuse into the water. In this process the most important oxidative species produced is the hydroxyl radical. It is the parent of several other oxidants and especially of H_2O_2 . Further OH radicals are produced in bulk solution due to the reaction between UV radiation and shock waves with other molecular species in the water.

Quantification of oxidants: It is extremely difficult and uncertain to quantify the production of OH radicals by spectroscopic methods. The only promising method seems to be the use of a selective chemical probe which leads to a characteristic product as a result of the reaction with OH radicals. As such a chemical probe compound DNTA was chosen to measure the OH radical concentration. This compound is easily soluble in water and does not react with most of the primary species produced in underwater corona discharges. In comparison with other compounds it is easy to handle (non toxic) and simple to measure. It has the advantage that the main reaction product, 2 hydroxyterephthalate, is the only product which shows fluorescence and thus it can be easily detected, even at lower OH radical concentrations. However, DNTA is probably destroyed inside the plasma channel and therefore cannot measure the OH radical concentration inside the channel during the active phase. Also it seems unlikely that any reactions between the probe component and OH radicals occur before the streamer channel collapses. A surprising result inferred from our measurements with DNTA in presence of another scavenger of OH radicals (t-Butanol) demonstrates that H_2O_2 , is mainly formed at the streamer water interface or after collapse of the channel. The results are compatible with an initial OH radical concentration of 30 mM (section 4.2).

Despite many differences there are some similarities between AOPs based on ultrasound, pulsed radiolysis, and pulsed underwater corona discharges. In all processes the formation of reactive species depends on the applied energy. In ultrasound systems radicals are produced inside of cavitation bubbles. Once the bubbles implode oxidants are liberated into the bulk solution. In pulsed radiolysis the oxidative species are directly produced in the

bulk water. Since their concentration along the radiation track is very high the recombination rate is very high too. A study of ultrasound processes by Hengelein and colleagues [72, 73] suggests that in pure water more than 80% of the OH and H radicals recombine to reform water.

It has already been mentioned that all results obtained in this thesis indicate that OH radicals are the prime source of H₂O₂ formation. Therefore a rough estimate of the OH radicals initially available outside the plasma channels can be derived from the H₂O₂ yield.

Table 5.1. Comparison of •OH production rates determined from reaction with DNTA and derived from H₂O₂ yields.

Experimental conditions	•OH production rate (from H ₂ O ₂)	•OH production rate (from DNTA)
Conductivity =400μS/cm		
Pulse energy 4.68 J/pulse	4.6 x 10 ⁻⁷ M s ⁻¹	1.5 x 10 ⁻⁹ M s ⁻¹
Pulse repetition rate 10 Hz		

In Table 5.1 we compare the •OH production rates derived from reactions with chemical probe DNTA with those calculated from the hydrogen peroxide production rates (2 OH radicals =1 H₂O₂ molecule). The values presented in Table 5.1 are the production rates averaged over the entire reactor volume. It is obvious that only a small fraction of the initially created OH radicals reaches the bulk water where it reacts with the probe DNTA. This can only be understood if we again assume a very high •OH concentration around the streamer. Since the reaction rate constants of •OH with •OH and •OH with DNTA are comparable the •OH-•OH reaction dominates if the local •OH concentration is much higher than the local DNTA concentration.

Comparison of G Values: In radiation chemistry the efficiency is expressed by the G value. It represents the number of molecules formed (or destroyed) per 100 eV of absorbed energy. A comparison of G values for the formation of OH radicals and H₂O₂ by sonolysis, radiolysis and pulsed corona discharges is summarized in Table 5.2. They are based on the total amount of energy deposited into the system. The G value for the formation of H₂O₂ in underwater corona discharges is very close to that obtained in radiation chemistry and much higher than that achieved in sonochemistry. It is important to note that in pulsed underwater corona discharges part of the applied energy is transformed into UV radiation and shockwaves. In addition other effective oxidants like ozone are produced.

Table 5.2: Comparison of G values (molecules/100 eV) for OH radical and H₂O₂ formation in various advanced oxidation processes.

G value	Pulsed streamer discharges [This thesis]	Sonolysis [71,88]	Radiolysis ⁶⁰ CO-γ-rays or 3 MeV electrons [117]
G_{•OH}	0.3 - 0.88 x 10 ⁻³	(1 - 3) x 10 ⁻³	2.7
G_{H2O2}	70 - 81 x 10 ⁻³	1 - 6 x 10 ⁻³	0.7
G_{Ozone}	3.8 x 10 ⁻³	Not determined	Not determined
$\frac{G_{H_2O_2}}{G_{•OH}}$	92 - 270	2.5 - 6.6	0.25

Comparing the relative values $\frac{G_{H_2O_2}}{G_{•OH}}$, we can conclude that in the pulsed streamer discharges a much larger fraction of OH radicals reacts to form H₂O₂ than in the other AOPs.

Anode materials: Experimentally it was observed that during the streamer discharges metal ions were released from the anode surface. The releases of these metal ions are of the order of a few μM per 5000 pulses. These metal ions can react with the H₂O₂ present in the bulk solution producing further hydroxyl radicals. Among the different anode materials that were tried, copper showed the highest hydroxyl radical yield. This effect is caused by copper ions catalysing Fenton's reaction (Section 4.2.5). This is reflected by the higher removal rate of organic chemical compounds and the larger disinfection rates.

Anode coatings: The porous ceramic layer on the anode affects the radical formation in two ways: First the structure and the distribution of pores determine the number and the distribution of streamers. Second the coating material can release ions that enhance the Fenton's reaction. Among the different coating materials tried almandine showed the best performance. It supports the formation of large numbers streamers homogeneously distributed over the surface and does not suppress streamer formation due to surface charges even after long operation. Moreover it releases Fe ions that contribute to Fenton's reaction. The adhesion of all coatings needs to be improved which probably requires a suitable bonding layer between the metallic anode and the ceramic. A necessary condition for good adhesion is an equal thermal expansion coefficient of the metal and the ceramic. In this respect the combination of titanium and almandine is the best choice. A systematic study to select suitable metal ceramic combinations was beyond the scope of the present study. An important criterion for the selection of adequate ceramic layers is the pH value of its

isoelectric point which should be much below the pH of the solutions to be treated (see section 2.1).

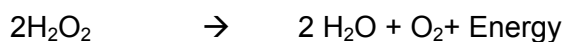
Dissolved and percolating gases: Previous studies have demonstrated that oxygen flowing through the corona reactor produces ozone. It seems unlikely that many streamers incorporate bubbles in the discharge channel. Therefore the probability of a direct interaction between a gas bubble and the discharge channel is small. It is more qualified to assume that the water becomes saturated with oxygen which then appears in the plasma channels with the same fraction as in the water. Since the binding energy of O₂ (2.6 eV) is smaller than that of H₂O it will dissociate to a large degree into atomic oxygen which can further react with molecular oxygen forming ozone. As the plasma channel cools down ozone will diffuse into the bulk solution where it can react with accumulated hydrogen peroxide and initiate the peroxone process which is a well established AOP and widely used in the industry. Besides oxygen N₂O, Argon and ozone were used in the experiments. Among these gases only N₂O resulted in a higher yield of OH radicals. This is most likely caused by the interaction between N₂O and solvated electrons producing additional OH radicals in the bulk water. However considering the relatively small increase of the OH radical yield we must conclude that only a small fraction of the electrons in the streamer channel becomes solvated. One important observation made during an experiment where ozone flew through the reactor was that it destructed HTA.

Spatial distributions: Radicals and other atomic and molecular species are produced inside and around the plasma channels. Once the plasma channels collapse the concentration of these species remains higher in the region of streamer formation i.e. near the anode surface. Depending upon their diffusion constant and their concentration these oxidants slowly diffuse towards the cathode. The time for complete equilibration can take several minutes. Therefore to achieve homogeneous removal of contaminants across the entire flow cross section an external turbulent mixing system is required for any industrial reactor.

Addition of Fe salt: Pulsed corona discharges can be combined with Fe²⁺ ions to take advantage of Fenton's reaction. It is observed that the addition of Fe salts raises the hydroxyl radical yield by up to three times improving the disinfection efficiency.

Oxidation of organic molecules: The destruction of toxic organic contaminants in water is an attractive field of application for pulsed underwater corona discharges. These capabilities have been demonstrated by oxidizing indigo tri sulfonate.

H₂O₂: Hydrogen peroxide is a safe and easy to use chemical oxidant, which has a high oxidation potential (1.78 V). Depending upon environmental conditions it decomposes exothermically into water and oxygen. Raising the pH of the solution to values greater than 6-8 or increasing the concentration of transition metal ions like iron or copper accelerates its decomposition rate dramatically. The same effect occurs under UV radiation or in presence of ozone.



A result of this decomposition is the formation of OH radicals which are much more oxidative. The OH radicals are an intermediate product in the decomposition process. Therefore a combination of H₂O₂ with UV, ozone or iron salts (Fenton's reactions) is often used in industrial disinfection plants. As discussed earlier only few OH radicals migrate directly from the plasma channels into the bulk water. Many recombine with hydrogen or form H₂O₂. Therefore the interaction between UV radiation and H₂O₂ accumulated in the water becomes a major path of OH radical production in the bulk solution.

Ozone: The effect of ozone on micro organism is not well understood. Some studies for bacteria suggest that ozone alters the proteins and unsaturated bonds of fatty acids in the cell membrane, leading to cell lysis, while other studies suggest that ozone affects the DNA in the cell [17]. Its bactericidal efficiency increases if it interacts with H₂O₂ or UV because OH radicals are produced in this reaction. As described before, ozone is especially created if the solution has been saturated with oxygen.

Reductive species: Besides oxidative species reductive species can also contribute to the disinfection efficiency. The main reductive species produced in pulsed corona discharges are H atoms, super oxide radical anions and a small quantity of solvated electrons. The effects of reductive species have well been studied in pulsed radiolysis. Some of the results from these studies can be transferred to pulsed corona discharges. In an oxygen atmosphere H radicals can react with oxygen forming HO[•]₂.



The reaction depends on the pH value and in a neutral solution O₂^{•-} ions dominate. For some contaminants (e.g. chlorinated compounds containing nitro groups) these reductive species are even more effective than hydroxyl radicals. The presence of O₂^{•-} ions has been proven with the help of nitroblue tetrazolium chloride (NBT) salt (section 3.6). It is therefore

supposed that these reductive species can also contribute to the overall disinfection mechanism.

UV emission: Next to oxidative and reductive species UV radiation from the plasma channels plays a key role in the disinfection process based on pulsed underwater corona discharges. The streamer channel emits a broad spectrum ranging from 200 – 1000 nm. Below 200 nm almost all UV radiation is absorbed within a few μm in water. The photon energy at these wavelengths is sufficient to dissociate water molecules directly into OH and H radicals. UV-C (200-280 nm) radiation causes damage to the DNA and leads to inactivation of bacteria. Dissociation of H_2O_2 molecules into OH radicals also appears in this wavelength range. The DNA shows a maximum of absorption at 200 nm and 262 nm. The main emission of low pressure UV lamps used for water disinfection occurs at 254 nm. Most of the absorption at 200 nm takes place in the ribose and phosphate molecules forming the backbone of the DNA [14, 15 and 19]. At 262 nm the absorption appears mainly in the nucleotide bases. Several studies have shown that microbial DNA is capable to repair the damage after irradiation with the spectrum from low pressure UV lamps. Pulsed corona discharges emit a broad spectrum of UV radiation which not only damages the DNA but also causes damage to other molecules thus making it more difficult for cells to recover their viability. e.g. it has been demonstrated that UV-B (280 nm – 315 nm) and UV-C are absorbed by proteins. Thus a broader UV spectrum can more effectively lead to irreparable DNA damage. The degree of damage to the cell depends on the received dose. Typically, to achieve a 4 log reduction of reproducible cells a dose of 400 J/m^2 is required.

As described in section 3.7.2 actinometry is a suitable method to measure the effective UV dose in a certain volume element of the reactor. Using ferrioxalate as an actinometric substance, Lukes has measured the UV emission from under water corona discharges [101]. Since ferrioxalate is very sensitive to visible light and requires a dark room for the experiments, uridine was selected as an actinometer in our experiments. Unfortunately we found that uridine actinometry is not applicable under the conditions of pulsed corona discharges. It has been shown that cavitation effects producing OH radicals even inside a UV transparent quartz cuvette destroyed the photochemical products created by the UV radiation in the first place. Thus any actinometry compound which reacts with OH radicals is unsuitable for UV measurements in pulsed corona discharges. This conclusion can be extended to other disinfection systems like those based on a combination of UV and ultrasound where OH radicals and UV radiation appear simultaneously.

Pressure waves: It is well known that shock waves can effectively destroy bacterial cells. In pulsed streamer discharges shock waves are produced due to the rapid expansion

of the discharge channel into the water. Nanosecond pressure pulses with amplitudes of up to 50 kbar have recently been inferred from time resolved interferometric studies of single streamers [37]. These pressure waves can influence the disinfection process in two ways: First, bacteria flocs can be deagglomerated by mechanical shear stresses; second propagating strong shock waves impacting on the cell membrane can rupture it, leading to cell death by lysis. Cavitation effects can reduce the turbidity of waste water [24, 25]. Hence if pressure waves are combined with UV radiation the UV penetration into water can be improved. Pressure waves generated from the streamer channels also advance the mixing in the water to be treated and thus accelerate the homogenisation of reactive chemical species. Cavitation effects resulting from reflected shock waves can also contribute to the formation of OH radicals. Using $\cdot\text{OH}$ sensitive chemical probes in thin walled cuvettes nontransparent for UV radiation we have proven that OH radicals are created. Moreover it was found that the OH radical yield increased if the matching between the acoustic impedances of the cuvette wall material and water was improved.

Disinfection: The effect of strong pulsed electric fields on bacteria has first been studied by Sale and Hamilton (1967) [120]. They correctly interpreted their results as a nonthermal field induced perforation of the cell membrane leading to cell death by lysis. For the *E-coli* bacteria treated by them they found a threshold for the field strength around 10 kV/cm and keeping the pulse width constant a killing rate growing exponentially with the field strength above the threshold. Later the observed phenomenon was termed electroporation. Many experimental and theoretical studies have appeared since the early work of Sale and Hamilton. They aimed at improving the understanding of the formation of pores in the cell membrane and at advancing the energy efficiency. At present, the specific energy required for a 3 log bacterial (*Pseudomonas putida*) reduction by electroporation is 120 J cm^{-3} . Recently it has been found that ultrashort pulses with field strength above 100 kV/cm do not create pores in the cell membrane but interact directly with organelles and molecules in the cell interior, inducing stress reactions which can also lead to cell death [118, 119]. Since the electric fields at the streamer tip are extremely high (up to 100 MV/cm) but of ns or even sub-ns duration inducing reactions in the cell interior is the only mechanism through which electric field effects can contribute to the destruction of bacteria in pulsed corona discharges.

However, it is assumed that the other phenomena of pulsed streamer discharges namely the appearance of free radicals, UV radiation and shock waves are more important for their disinfection efficiency. We have found that a 3 log reduction of bacteria counts requires a specific energy of 13 J cm^{-3} which is much less than for electroporation. Even 6 log reductions were achieved with a specific energy deposition of 20 J cm^{-3} . It is expected that the efficiency grows as oxidants accumulate in the water.

A solid comparison of the effectiveness of pulsed corona discharges with that of other methods, for specific bacteria and equal environmental conditions requires a broader data base. However based on our present experimental results and using published data a rough comparison with ozone and UV will be presented.

Only the ozone dissolved in the liquid phase becomes effective for disinfection. Ozone trapped in gas bubbles does not contribute to the disinfection process. Further the solubility of ozone in water depends upon the environmental conditions. In pure water at 20° C the ratio of converting ozone from the gas phase to the liquid phase is approximately 3:1. i.e. at this temperature only one third of the injected ozone becomes dissolved in the water. At higher temperatures the ozone solubility in water falls dramatically. Increasing the external pressure, the solubility can be increased but on the expense of additional energy. Any impurities present in the water also affect the ozone solubility in the water. All these factors reduce its disinfection efficiency. Ozone is produced by gas discharge methods which have a poor efficiency. Approximately 90% of the applied electrical energy is transformed into heat. To remove the heat from the electrodes of the ozonizer additional cooling arrangements are required.

The effectiveness of any disinfection process is determined by the concentration of the disinfectant and the contact time. It can be described by a relationship first derived by Chick and Watson in 1908 [121, 122].

$$\frac{dN}{dt} = -A C^d N$$

$$\ln \frac{N}{N_0} = -A C^d t$$

where

N_0 =number of microorganisms in the system at $t=0$

N =number of microorganisms in the system at time t

t =contact time

A = specific coefficient of lethality

C =disinfectant concentration

d = exponent of order 1 depending on the specific disinfectant

In many cases d is very close to 1. Hence the logarithmic decrease of the relative deactivation of microorganisms is simply a linear function of the ct product. The effectiveness of ozone increases with temperature (although its solubility decreases). For *E -coli* bacteria we have $A=102$ L/mg s at 15°C and $A=130$ L/mg s at 20°C. Therefore to reduce the *E -coli* concentration by 6 logsteps ct products of 0.13 mg s/L and 0.11 mg s/L are required at 15°C

and 20°C respectively. In a flow through reactor the contact time depends upon the length of the system, and the flow velocity of water. In a water distribution network the flow rate can vary depending on water consumption. Typically the applied ozone concentrations are of the order of 0.4 µg/L requiring contact times between 4 and 10 minutes. Using pulsed corona discharges for disinfection we have found that contact times of a few seconds were sufficient to achieve a deactivation by more than 6 logsteps. Of course the required contact time depends on the pulse repetition rate.

Considering a deactivation reactor with a throughput of 3 m³/ hour and assuming ideal conditions (room temperature, clean water) an ozone based system requires an energy input of approximately 1.5 kWh while an equivalent pulsed corona based system need 12 kWh.

Water disinfection systems based on UV-radiation or a combination of UV and H₂O₂ are also very commonly used. As described previously combining UV with H₂O₂ can produce OH-radicals. From the results of their experiments (using a photoferrioxalate photochemical method) Cho et al. [81] concluded that OH radicals are the prime species responsible for *E. coli* inactivation. However the molar extinction coefficient of H₂O₂ at the emission peak of the UV-lamps around 254 nm is rather low (19.6 M⁻¹ cm⁻¹). Therefore a high concentration of H₂O₂ is needed to generate sufficient OH radicals.

In pulsed corona discharges a broader UV spectrum is emitted moreover rather high concentrations of H₂O₂ accumulate in the water. The broad UV spectrum produces more favourable conditions for effective absorption in H₂O₂ and therefore higher OH contributions to the disinfection efficiency are expected.

UV based disinfection systems are of limited value for the disinfection of water with high turbidity. Since the disinfection capabilities of corona discharge based systems rely on several rather different effects they can become an attractive alternative in this case. For laboratory reactor (volume =1 L) used in this dissertation the specific energy costs for a deactivation of microorganisms by 6 logsteps amount to 50 cent/m³. As described in the present work, there are many possibilities like gas percolation, combination with Fenton reagents, etc to further improve the system efficiency and thus to reduce the cost further.

6. Conclusions

The aim of this work was twofold first to develop the concept for a scalable pulsed corona based water disinfection system, and second to establish suitable diagnostic methods for the quantitative measurement of various oxidants and other effects produced in this process. It has been shown that pulsed underwater corona discharges have a great potential as a water disinfection method. Without using any additional chemicals this method has a more powerful effect than many other conventional technologies. It was found that the production of reactive oxidants like OH radicals and H₂O₂, combined with the appearance of UV radiation, shock waves, and strong electric field enhances the disinfection efficiency. Mainly by using suitable chemical probes it has been possible to improve our knowledge about the mechanism and the locations of the formation of OH radicals and H₂O₂.

To generate a multiplicity of underwater streamer discharges an easily scalable reactor of coaxial geometry has been used. It comprises a central metallic anode covered by a thin layer (200-300 μm) of porous ceramic. Applying a pulsed voltage of 30-50 kV for a duration of 200-400 ns to the anode a large number of streamers is launched homogeneously from the ceramic surface extending up to 10 mm into the anode cathode water gap. Thus the streamers occupy a large fraction of the reactor volume. Different ceramic materials were tried for the anode layer. However the best results were obtained with almandine. It allows continuous operation in a large range of pH values and promotes the formation of OH radicals from H₂O₂ in the bulk water through the release of Fe²⁺ ions.

An *L-C* chain in a Blumlein configuration has been selected as the pulse generator. By changing the number and the values of the *LC* elements the impedance of the generator and its pulse width could easily be adapted to the requirements of the experiment. Streamer initiation is governed by the electric field at the surface of the porous ceramic layer, while streamer propagation is determined by the potential at the streamer tip. Since both the anode cathode water gap and the ceramic layer through its porosity filled with water are conductive the voltage at the ceramic surface is determined by the resistances and capacitances of the layers. For times greater than the dielectric relaxation time of the water ($\tau = \epsilon\epsilon_0/\sigma$) resistive voltage division dominates and the electric field at the ceramic layer can be more enhanced than in the case of capacitive voltage division. The onset of streamer formation had little influence on the reactor impedance which was mainly determined by the water conductivity. As the anode voltage increases both the number and the length of streamers are enlarged.

A linear relation was found between the number-length-product of streamers and the oxidant production. It is believed that oxidants play a dominant role in the disinfection process. Therefore suitable chemical diagnostic methods were established and the

conditions of their applicability were studied. Spectroscopic methods are difficult to interpret quantitatively. Also the results obtained with selectively sensitive chemical probes need to be considered with care. Certainly, initially OH and H radicals are produced in the core of active streamer channels by electron collisional dissociation of water molecules. This process is energetically preferred since it requires only half the energy of collisional ionisation of water molecules. However OH radicals cannot form any stable secondary products until they reach the streamer surface or until the streamer cools down and collapses. Many of the OH and H radicals will recombine to reform water other will interact with themselves creating either H₂O₂ or H₂. OH radicals cannot be detected by chemical probes until they reach a cold environment. It is assumed that the chemical probes will not survive the conditions in the hot streamer channels. Using a simple kinetic model for the relevant chemical reactions and the chemical probe DNTA for OH detection in combination with another •OH scavenger of varying concentration it was possible to determine the average initial •OH concentration at the position of cold streamer channels. There the OH radical concentration was found to be about 30 mM. A large fraction of it reacts to produce H₂O₂ which accumulates in the bulk water. More sophisticated models are required to get more precise results. They should combine the zero dimensional kinetic equations with a solution of the diffusion equation. Comparing the large local OH concentration of 30 mM with the mean concentration of 2 mM of the applied chemical probe DNTA it is obvious that it can detect only a small fraction of it. Consequently the chemical probes recorded mainly the OH radicals produced in the bulk water by secondary reactions like the interaction of UV radiation with H₂O₂. In all measurements using DNTA for OH detection and simultaneously a suitable diagnostic for H₂O₂ it was found that the ratio of both yields remained independent of the number of applied pulses. Besides OH radicals and H₂O₂ solvated electrons can diffuse into the bulk water. Solvated electrons (e_{aq}⁻) are a most powerful reducing agent (E= -2.9 V) and except for the alkali metal cations most of the others are reduced by e_{aq}⁻. Solvated electrons also attach to compounds with electron affinity (such as O₂ and carbonyl containing compounds) producing radical anions (such as O₂^{•-}) which also participate in the disinfection process. In this work we have proven for the first time that solvated electrons appear in the bulk solution. Nitrous oxide is efficiently reduced to form OH radical by solvated electrons. Saturating the water with nitrous oxide we obtained a higher OH radical yield confirming the production of e_{aq}⁻ during pulsed corona discharges. The formation of ozone dissolving in the bulk liquid after the streamer discharges was also detected in the experiments. The reaction of dissolved ozone with hydrogen peroxide accumulated in the water also leads to additional production of OH radicals. Moreover the dissolved ozone is very germicide and contributes to the deactivation of microorganisms in the water.

In addition to the diagnostics of oxidative and reductive species, measurements were also performed to quantify the UV emission from streamers and to assess the effects of pressure pulses. Band spectra from OH radicals have been identified in the general emission spectrum from the streamer channels confirming the existence of OH radicals in the streamer core. For applications in water disinfection the emission intensity in the UV-C band (200-280 nm) is most relevant. We tried to measure the UV radiation dose in this wavelength range by applying uridine actinometry. However no assessable signal could be obtained. We believe that this result can be attributed either to an insufficient sensitivity of the uridine actinometer or to the formation of hitherto undiscovered radicals interfering with this diagnostic. It was indeed confirmed by a series of experiments that uridine actinometry can not be applied in the presence of OH radicals. During the propagation of streamer channels into the water pressure pulses of ns duration with amplitudes of up to 50 kbar are produced launching shock waves into the water. These shock waves can disintegrate flocs of suspended particles in water improving the UV efficiency. In addition they can damage the membrane of bacterial cells. Using water filled cuvettes immersed into the reactor thus preventing the direct contact with streamers and the exposure by UV radiation we have been able to show that the shockwaves also contribute to the production of OH radicals and H₂O₂. It has been found that the OH radical yield inside the cuvettes increases if the acoustic impedance of the wall material matches that of water.

The final goal of this work was to study the disinfection efficiency of pulsed underwater streamer discharges. Exposing *pseudomonas putida* bacteria to underwater corona discharges it was demonstrated that a reduction by more than 6 log steps could be achieved with an energy consumption of 20 J/cm³ which is much less than the energy required for disinfection by electroporation. A lower disinfection rate was obtained for waste water containing many different bacterial species. To classify this result more detailed studies are required identifying the different species present in the waste water. Most important would be to determine the disinfection rate for pathogenic bacteria. There is still much room to improve the disinfection efficiency of underwater streamer discharges. e.g. using copper or steel anodes increases the production of OH radicals in the bulk solution due to the release of metal ions which promote Fenton's reactions creating OH radicals from H₂O₂ accumulated in the water.

Some complex organic chemical compounds are toxic and not easily degradable by biological methods. Treating indigo as a substance representative for this category of chemicals we have demonstrated the capability of pulsed corona discharges to decompose such compounds into non-toxic parts which are digestible by bacteria in a biological sewage plant.

The presented experimental results confirm that pulsed underwater corona discharges have the potential for an alternative water disinfection technology free of problematic chemicals.

7. References

- [1] United state environmental protection agency (USEPA), "Microbial and disinfection by-products rules simultaneous compliance guidance manual," Report No. EPA- 815-R-99-015 (1999).
- [2] K. Waller, S. H. Swan, G. De Lorenze, and B. Hopkins, "Trihalomethanes in drinking water and spontaneous abortion," *Am J. Epidemiol.* 9 pp. 134-140 (1998).
- [3] K. P. Cantor, C. F. Lynch, M. E. Hildesheim, M. Dosemeci, J. Lubin, M. Alavanja, and G. Craun. "Drinking water source and chlorination byproducts I. risk of bladder cancer," *Am J. Epidemiol.* 9, pp. 21-28 (1998).
- [4] S. H. Swan, K. Waller, B. Hopkins, G. Windham, L. Fenster, C. Schaefer, R. Neutra, "A prospective study of spontaneous abortion: relation to amount and source of drinking water consumed in early pregnancy," *Am J. Epidemiol.* 9, pp.126-133 (1998).
- [5] D. A. Savitz, P. C. Singer, A. H. Herring, K. E. Hartmann, H. S. Weinberg, and C. Makarushka, "Exposure of drinking water disinfection by products and pregnancy loss," *Am J. Epidemiol.* 164, pp.1043-1051 (2006).
- [6] W. H. Glaze, J. W. Kang, and D. H. Chapin, "The chemistry of water treatment processes involving ozone, hydrogen peroxide, and ultraviolet radiation," *Ozone Sci. Eng.* 9, pp. 335-352 (1987).
- [7] United state environmental protection agency (USEPA), "Alternative disinfectants guidance," Report No. EPA- 815-R-99-014 (April 1999).
- [8] I. Hua and J. E. Thompson, "Inactivation of *E-coli* by sonication at discrete ultrasound frequencies," *Water Res.* 34, pp. 3888-3893 (2000).
- [9] I. Hua and M. R. Hoffmann, "Optimization of ultrasonic irradiation as an advanced oxidation technology," *Environ. Sci. Technol.* 31, pp. 2237-2243 (1997).
- [10] W. J. Cooper, M. G. Nickelsen, D. E. Meacham, T. D. Waite and C. N. Kurucz, "High energy electron beam irradiation: an advanced oxidation process for the treatment of aqueous based organic hazardous wastes," *Wat. Poll. Res. J. Canada* 27, pp. 69-95 (1992).
- [11] A. K. Pikaev, "New data on electron beam purification of water," *Radiat. Phys. Chem.* 65, pp. 515-526 (2002).
- [12] P. Šunka, "Pulse electrical discharges in water and their applications," *Phys. Plasmas.* 8, pp. 2587-2594 (2001).
- [13] H. Zhou and D. W. Smith, "Advanced technologies in water and wastewater treatment," *J. Environ. Eng. Sci.* 1, pp. 247-264 (2002).
- [14] C. von Sonntag, A. Kolch, J. Gebel, K. Oguma, R. Sommer, "The photochemical basis of UV disinfection," in the proceedings of the European conference on UV radiation, effects and technologies (UV Karlsruhe 2004), Karlsruhe, Germany, (on CD) , September 22-24, (2004).
- [15] R. Sommer, M. Lhotsky, T. Haider, A. Cabaj, "UV inactivation, liquid –holding recovery and photoreaction of *Escherichia-coli* O157 and other pathogenic *Escherichia-coli* strains in water," *J. Food Prot.* 63, pp. 1015-1020 (2000).

-
- [16] J. Baron, M. M. Bourbigot, "Repair of *Escherichia coli* enterococci in sea water after ultraviolet disinfection quantification using diffusion chambers," *Wat. Res.* 30 pp. 2817-2821 (1996).
- [17] United state environmental protection agency (USEPA) "Waste water technology fact sheet, ozone disinfection," Report No. EPA- 832-F-99-063 (1999).
- [18] E. Koltunski and J. Plumridge, "Ozone as a disinfecting agent in the reuse of wastewater," <http://www.ozonia.com>.
- [19] C. von Sonntag, G. Mark, R. Mertens, M. N. Schuchmann and H. P. Schuchmann, "Chemical principles behind the use of UV-radiation and/or oxidants (ozone and hydrogen peroxide) in water pollution control," *J. Water SRT-Aqua.* 42, pp. 201-211 (1993).
- [20] B. S. Oh, S. J Park, H. G. Lee, K. S. Kim, and K. H. Lee, J. W. Kang, "Application of ozone/UV process for reclamation of sewage treatment plant effluent," *Journal of water and environmental technology*, 1, pp.141-153 (2003).
- [21] J. C. Kruithof, P. C. Kamp, N. W. Lute, M. Belosevic and G. Williams, "Implementation of UV/H₂O₂ treatment for inactivation of microorganisms and pesticide control" in proceedings of the 2nd international congress on ultraviolet technologies, Vienna, Austria, (on CD), July 9-11, (2003).
- [22] C. Sato, A. M. Asce and Steve M. Ogle, "Modeling tetrachloroethylene decomposition in photosonolysis reactor," *Journal of environmental engineering* 129, pp.136-146 (2003).
- [23] P. C. Fung, K. M. Sin, S. M. T. Sui, "Decolorization and degradation kinetics of reactive dye wastewater by a UV/ultrasound/peroxide system," *Coloration Technology.* 116, pp. 170 (2000).
- [24] T. Blume, I. Martinez, U. Neis, "Wastewater disinfection using ultrasound and UV light," *TU Hamburg-Harburg reports on sanitary engineering*, 35, pp. 117-128 (2002).
- [25] <http://www.svarog-uv.ru/English/disinf.htm>
- [26] C. N. Kurucz, T. D. Waite, W. J. Cooper, "The miami electron beam research facility: a large-scale wastewater treatment application," *Rad. Phys. Chem.* 45, pp. 299-308 (1995).
- [27] N. A. Strokin, "Electron beam treatment of drinking water in an industrial system," *High Energy Chemistry* 41, pp. 1-4 (2007).
- [28] M. H. O. Sampa, S. I. Borrely, B. L. Silva, J. M. Vieira, P. R. Rela, W. A. P. Calvo, R. C. Nieto, C. L. Duarte, H. E. B. Perez, E. S. Somessari, A. B. Lugao, "The use of electron beam accelerator for the treatment of drinking water and waste water brazil," *Rad. Phys. Chem.* 46, pp. 1143-1146 (1995).
- [29] United state environmental protection agency (USEPA), "Membrane filtration guidance manual," Report No. EPA 815-R-06-009 (2005).
- [30] J. R. Bolton, K. G. Bircher, W. Tumas and C. A. Tolman, "Figures of merit for the technical development and application of advanced oxidation processes," *J. Adv. Ox. Technol.* 1, pp. 13-17 (1996).
- [31] A. M. Anpilov, E. M. Barkhudarov, N. Christofi, V. A. Kop'ev, I. A. Kossyi, M. I. Taktakishvili, Y. Zadiraka, "Pulsed high voltage electric discharge disinfection of microbially contaminated liquids," *Lett. Appl. Microbiol.* 35, pp. 90-94 (2002).

-
- [32] H. Y. Lee, H. S. Uhm, H. N. Choi, Y. J. Jung, B. K. Kang, H. C. Yoo, "Underwater discharge and cell destruction by shockwaves," *J. Korean Phys. Soc.* 42, pp. S880-S884 (2003).
- [33] H. Y. Lee, Y. S. Ko, J. P. Lim, J. G. Kang, H. S. Kim and H. S. Uhm, "Application of pulsed high-voltage discharge to algae elimination in freshwater," in proceedings of the XXVIIth international conference on phenomena in ionized gases, Eindhoven, The Netherlands, (on CD), July 17-22, (2005).
- [34] J. C. Metsa, G. E. Mullins, and W. S. Sottile, "Biological disinfection of water using pulsed corona discharge," in proceedings of the 4th Int. symp. on non thermal plasma technology for pollution control and sustainable energy development (ISNTPT-4), Panama City, Florida, United States, pp. 104-108. May 10-14, (2004).
- [35] B. E. J. M. van Heesch, G. A. J. M. Pemen, P. A. H. J. Huijbrechts, P. C. T. van der Laan, K. J. Ptasiński, G. J. Zanstra and P. de Jong, "A fast pulsed power source applied to treatment of conducting liquids," *IEEE Trans. Plasma Sci.* 28, pp. 137-143 (2000).
- [36] H. Bluhm, "Pulsed power systems," Springer-Verlag Berlin, (2006).
- [37] W. An, K. Baumung, and H. Bluhm, "Underwater streamer propagation analyzed from detailed measurements of pressure release," *J. Appl. Phys.* 101, pp. 053302-1-10 (2007).
- [38] A. T. Sugiarto, M. Sato, and J. Skalny, "Transient regime of pulsed breakdown in low conductive water solutions," *J. Phys. D: Appl. Phys.* 34, pp. 3400-3406 (2001).
- [39] A. K. Sharma, B. R. Locke, P. Arce, and W. C. Finney, "A preliminary study of pulsed streamer corona discharge for degradation of phenol in aqueous solutions," *Hazard. Waste Hazard. Mater.* 10, pp. 209-219 (1993).
- [40] J. S. Clements, M. Sato, and R. H. Davis, "Preliminary investigation of prebreakdown phenomena and chemical reactions using a pulsed high voltage discharge in water," *IEEE Trans. Ind. Appl.* IA-23, pp. 224-235 (1987).
- [41] W. F. L. M. Hoeben, "Pulsed corona-induced degradation of organic materials in water," Ph. D. Thesis, Technical University Eindhoven, The Netherlands, (2000).
- [42] L. R. Grabowski, E. M. van. Veldhuizen, A. J. M. Pemen, A. Pokryvailo, Y. Yankelevich, W. R. Rutgers, "Gas-phased pulsed corona for wastewater treatment- comparative study," in proceedings of the 17th international symposium on plasma chemistry (ISPC-17), Toronto, Canada, (on CD), August 07-12, (2005).
- [43] M. J. Kirkpatrick, and B. R. Locke, "Hydrogen, oxygen, and hydrogen peroxide formation in aqueous phase pulsed corona electrical discharge," *Ind. Eng. Chem. Res.* 44, pp. 4243-4248 (2005).
- [44] M. Monte, F. De Baerdemaeker, and C. Leys, "Experimental study of a diaphragm discharge in water," *Czech J. Phys.* 52, pp. D724-D730 (2002).
- [45] F. De Baerdemaeker, M. Šimek, and C. Leys, "Efficiency of hydrogen peroxide production by ac capillary discharges in water solution," *J. Phys. D: Appl. Phys.* 40, pp. 2801-2809 (2007).
- [46] T. Iijima, Y. Okita, K. Kubo, R. Makise and T. Murata, "New oxidation technology by using OH radical with long life time in plasma," in proceedings of the Ozone and related oxidants: Innovative and current technologies, 17th world congress of the international ozone association, Strasbourg, France, (on CD), August 22-25. (2005).

-
- [47] N. I. Kuskova, "Mechanism of leader propagation in water," *Sov. Phys. Tech. Phys.* 28, pp. 591 (1983).
- [48] N. Kuskova, "Mechanism of electrical breakdown in water," *Sov. Phys. Tech. Phys.* 32, pp. 1215 (1983).
- [49] H. M. Jones, and E. E. Kunhardt, "Pulsed dielectric breakdown of pressurized water and salt solutions," *J. Appl. Phys.* 77, pp. 795-805 (1995).
- [50] R. P. Joshi, J. Qian, K. H. Schoenbach, E. Schamiloglu, "Microscopic analysis for water stressed by high electric fields in the prebreakdown regime," *J. Appl. Phys.* 96, pp. 3617-3625 (2004).
- [51] A. Denat, "High field conduction and pre breakdown phenomena in dielectric liquids," in proceedings of the 15th IEEE international conference on dielectric liquids (ICDL 2005), Coimbra, Portugal, (on CD) , June 26-July 01, (2005).
- [52] I. V. Lisitsyn, H. Nomiya, S. Katsuki, and H. Akiyama, "Streamer discharge reactor for water treatment by pulsed power," *Rev. Sci. Instrum.* 70, pp. 3457-3462 (1999).
- [53] D. R. Lide, "Handbook of chemistry and physics," CRC press, (2004).
- [54] S. Siegmann, Swiss federal laboratories for materials testing and research (EMPA), Thun, Switzerland, Private communication.
- [55] H. Akiyama, "Streamer discharges in liquids and their applications," *IEEE Trans. Dielectr. Electr. Insul.* 7, pp. 646-653 (2000).
- [56] T. J. Lewis, "Breakdown initiating mechanisms at electrode interfaces in liquids," *IEEE Trans. Dielectr. Electr. Insul.* 10, pp. 948-955 (2003).
- [57] T. J. Lewis, "A new model for the primary process of electrical breakdown in liquids," *IEEE Trans. Dielectr. Electr. Insul.* 5, pp. 306-315 (1998).
- [58] P. Lukeš, M. Clupek, V. Babický, P. Šunka, "Role of plasma-solid interactions in pulsed corona discharge generated in water using ceramic-coated wire electrodes," in proceedings of the 5th international symposium of non-thermal plasma technology for pollution control and sustainable development (ISNTPT-5), St. Pierre, Ile d'Oléron, France (on CD), June 19-23, (2006).
- [59] D. R. Grymonpre, W. C. Finney, R. J. Clark, and B. R. Locke "Suspended activated carbon particles and ozone formation in aqueous-phase pulsed corona discharge reactors," *Ind. Eng. Chem. Res.* 42, pp. 5117-5134 (2003).
- [60] M. A. Malik, "Synergistic effect of plasmacatalyst and ozone in a pulsed corona discharge reactor on the decomposition of organic pollutants in water," *Plasma Sources Sci. Technol.* 12, pp. S26-S32 (2003).
- [61] B. Sun, M. Sato, and J. S. Clements, "Use of a pulsed high-voltage discharge for removal of organic compounds in aqueous solution," *J. Phys. D: Appl. Phys.* 32, pp. 1908-1915 (1999).
- [62] P. Lukeš and B. R. Locke, "Plasmachemical oxidation processes in a hybrid gas-liquid electrical discharge reactor," *J. Phys. D: Appl. Phys.* 38, pp. 4074-4081 (2005).
- [63] M. Sato, T. Ohgiyama and J. S. Clements, "Formation of chemical species and their effects on microorganisms using a pulsed high-voltage discharge in water," *IEEE Trans. Ind. Appl.* 32, pp. 106-112 (1996).

-
- [64] A. A. Ghazala, S. Katsuki, K. H. Schoenbach and K. R. Moreira, "Bacterial decontamination of water by means of pulsed-corona discharges," *IEEE Trans. Plasma Sci.* 30, pp. 1449-1453 (2002).
- [65] P. Šunka, V. Babický, M. Člupek, J. Beneš, and P. Poučková, "Localized damage of tissues induced by focused shock waves," *IEEE Trans. Plasma Sci.* 32, pp. 1609- 1613 (2004).
- [66] A. A. Joshi, B. R. Locke, P. Arce, W. C. Finney, "Formation of hydroxyl radicals, hydrogen peroxide and aqueous electrons by pulsed streamer corona discharge in aqueous solution," *J. Hazard. Mater.* 41, pp. 3-30 (1995).
- [67] P. Lukeš, A. T. Appellton, and B. R. Locke, "Hydrogen peroxide and ozone formation in hybrid gas-liquid electrical discharge reactors," *IEEE Trans. on Ind. Appl.* 40, pp. 60-67 (2004).
- [68] B. Sun, M. Sato, J. S. Clements, "Optical study of active species produced by a pulsed streamer corona discharge in water," *J. Electrostatics* 39, pp.189-202 (1997).
- [69] P. Šunka, V. Babický, M. Člupek, P. Lukeš, M. Šimek, J. Schmidt and M. Černák. "Generation of chemically active species by electrical discharges in water," *Plasma Sources Sci. Technol.* 8, pp. 258–265 (1999).
- [70] M. Sahní, "Analysis of chemical reactions in pulsed streamer discharges: an experimental study," PhD thesis, Florida state university, (2006).
- [71] G. Mark, A. Tauber, R. Laupert, H. P. Schuchmann, D. Schulz, A. Mues, C. von Sonntag, "OH-radical formation by ultrasound in aqueous solution – Part II: Terephthalate and Fricke dosimetry and the influence of various conditions on the sonolytic yield," *Ultrasonics Sonochem.* 5, pp. 41-52 (1998).
- [72] C. H. Fischer, E. J. Hart, and A. Henglein, "H/D Isotope exchange in the D₂-H₂O system under the influence of ultrasound," *J. Phys. Chem.* 90, pp. 222-224 (1986).
- [73] C. H. Fischer, E. J. Hart, and A. Henglein, "H/D Isotope exchange in the HD-H₂O system under the influence of ultrasound," *J. Phys. Chem.* 90, pp. 3059-3060 (1986).
- [74] B. Sun, S. Kunitomo, and C. Igarashi, "Characteristics of ultraviolet light and radicals formed by pulsed discharge in water," *J. Phys. D: Appl. Phys.* 39, pp. 3814-3820 (2006).
- [75] A. M. Anpilov, E. M. Barkhudarov, Y. B. Bark, Y. V. Zadiraka, M. Christofi, Y. N. Kpzlov, I. A. Kossyi, V. A. Kop'ev, V. P. Silakov, M. I. Taktakishvili, and S. M. Temchin, "Electric discharge in water as a source of UV radiation, ozone and hydrogen peroxide," *J. Phys. D: Appl. Phys.* 34, pp. 993-999 (2001).
- [76] K. Yan, "Corona plasma generation," Ph.D. Thesis, Technische Universiteit Eindhoven, (2001).
- [77] S. B. Gupta, H. Bluhm, "Pulsed underwater corona discharges as a source of strong oxidants: OH and H₂O₂," *Water Science and Technology.* 55, pp. 7-12 (2007).
- [78] Y. Manevich, K. D. Held and J. E. Biaglow, "Coumarin 3- carboxylic acid as a detector for hydroxyl radicals generated chemically and by gamma radiation," *Rad. Res.* 148, pp. 580-591 (1997).
- [79] Y. Pi, J. Schumacher, and M. Jekel, "The use of para-chlorobenzoic acid (pCBA) as an ozone/hydroxyl radical probe compound," *Ozone Sci. Eng.* 27, pp. 431-436 (2005).

-
- [80] M. S. Elovitz and U. von Gunten, "Hydroxyl radical/ozone ratios during ozonation processes. I. The R_{ct} concept," *Ozone Sci. Eng.* 21, pp. 239-260 (1998).
- [81] M. Cho, H. Chung, W. Choi, J. Yoon, "Linear correlation between inactivation of *E. coli* and OH radical concentration in TiO_2 photocatalytic disinfection," *Wat. Res.* 38, pp. 1069-1077 (2004).
- [82] J. S. Park, H. Choi, and J. Cho, "Kinetic decomposition of ozone and para - chlorobenzoic acid (pCBA) during catalytic ozonation," *Wat. Res.* 38, pp. 2285-2292 (2004).
- [83] M. Heinley, Institute of Technical Chemistry Forschungszentrum Karlsruhe, Germany, private communication.
- [84] R. W. Matthews, "The radiation chemistry of the terephthalate dosimeter," *Radiat. Res.* 83, pp. 27-41 (1981).
- [85] X. Fang, G. Mark, C. von Sonntag, "OH radical formation by ultrasound in aqueous solutions Part I: the chemistry underlying the terephthalate dosimeter," *Ultrasonics Sonochem.* 3, pp. 57-63 (1996).
- [86] X. Qu, L. J. Kirschenbaum and E. T. Borish, "Hydroxyterephthalate as a fluorescent probe for hydroxyl radicals: Application to hair melanin." *Photochem. Photobio.* 71, pp. 307-313 (2000).
- [87] Y. T. Didenko and K.S. Suslick, "The energy efficiency of formation of photons, radicals and ions during single-bubble cavitation," *Nature.* 418, pp. 394-397 (2002).
- [88] C. von Sonntag, Mühlheim, Germany, private communication.
- [89] T. J. Mason, J. P. Lorimer, D. M. Bates, Y. Zhao, "Dosimetry in sonochemistry: the use of aqueous terephthalate ion as a fluorescence monitor," *Ultrasonics Sonochem.* 1, pp. S91-S95 (1994).
- [90] G. M. Eisenberg, "Colorimetric determination of hydrogen peroxide," *Ind. Eng. Chem. Anal. Ed.* 15, pp. 327-328 (1943).
- [91] G. Uher, E. Gilbert, U. Siegfried, H. Eberle, "Determination of hydrogen peroxide in presence of organic peroxides" *Vom Wasser*, 76, pp. 225 - 234 (1991).
- [92] A. O. Allen, C. J. Hochanadel, J. A. Ghormley and T. W. Davis, "Decomposition of water and aqueous solutions under mixed fast neutron and gamma radiation," *J. Phys. Chem.* 56, pp. 575-586 (1952).
- [93] E. Gilbert, D. Schulte-Frohlinde, "Photolyse von 5-Ioduracil in wässriger, sauerstoffgesättigter Lösung" *Z. Naturforsch.* 25b, pp. 492-495, (1970).
- [94] H. Bader, J. Hoigne', "Determination of ozone in water by the indigo method," *Water Res.* 15, pp. 449-456 (1981).
- [95] U. von Gunten, Eawag - Swiss Federal Institute of Aquatic Science and Technology, Dübendorf, Switzerland, private communication.
- [96] D. Head and D. C. Walker, "Nitrous oxide as a scavenger in the radiolysis of water," *Nature.* 207, pp. 517-518 (1965).
- [97] A. Kovács, M. Baranyai, L. Wojnárovits, A. Moussa, I. Othman, W.L. McLaughlin, "Aqueous-ethanol nitro blue tetrazolium solutions for high dose dosimetry," *Rad. Phys. Chem.* 55, pp. 799-803 (1999).

-
- [98] B. H. J. Bielski and H. W. Richter, "A study of the super oxide radical chemistry by stopped flow radiolysis and radiation induced oxygen consumption," *J. Am. Chem. Soc.* 99, pp. 3019-3323 (1977).
- [99] B. H. J. Bielski G. G. Shiue, and S. Bajuk, "Reduction of nitroblue tetrazollum by CO_2^- and O_2^- radicals," *J. Phys. Chem.* 84, pp. 830-833 (1980).
- [100] H. Goto, Y. Hanada, T. Ohno, and M. Matsumura, "Quantitative analysis of superoxide ion and hydrogen peroxide produced from molecular oxygen on photo irradiated TiO_2 particles," *J. Cata.* 225, pp. 223-229 (2004).
- [101] P. Lukeš, "Water treatment by pulsed streamer corona discharge," Ph. D. Thesis, Institute of chemical technology, Institute of plasma physics, Prague, (2002).
- [102] M. G. Gonzalez, E. Oliversons, M. Wörner, A. M. Braun, "Vacuum-ultraviolet photolysis of aqueous reaction systems," *J. Photochem. Photobiol. C: Photochem. Reviews.* 5, pp. 225-246 (2004).
- [103] J. R. Bolton, and M. I. Stefan, "Fundamental photochemical approach to the concepts of fluence (UV dose) and electrical energy efficiency in photochemical degradation reactions," *Res. Chem. Intermed.* 28, pp. 857-870 (2002).
- [104] C. von Sonntag, and H.P. Schuchmann, "UV disinfection of drinking water and by-product formation-some basic considerations," *J Water SRT-Aqua.* 41 pp. 67-74 (2002).
- [105] J. Y. Zhang, "Photochemische modifizierung von Oberflächen durch Excimer-UV-Strahlung" PhD Thesis. Karlsruhe University (1993).
- [106] T. Schwartz, S. Hoffmann, and U. Obst, "Formation of natural biofilms during chlorine dioxide and UV disinfection in a public drinking water system," *J. Appl. Microbiol.* 95, pp. 591-601 (2003).
- [107] W. Yu, W. K. Dodds, M. K. Banks, J. Skalsky, and E. A. Strauss, "Optimal staining and sample storage time for direct microscopic enumeration of total and active bacteria in soil with two fluorescent dyes," *Appl. Environ. Microbiol.* 61, pp. 3367-3372 (1995).
- [108] J. W. Moffett and R. G. Zika, "Reaction kinetics of hydrogen peroxide with copper and iron in sea water," *Environ. Sci. Technol.* 21, pp. 804-810 (1987).
- [109] J. Hoigne, H. Bader, "Rate constants of reaction of ozone with organic and inorganic compound in the water-I non-dissociating organic compounds," *Water Res.* 17, pp. 173-183 (1983).
- [110] J. Hoigne, H. Bader, "Rate constants of reaction of ozone with organic and Inorganic compound in the water-II dissociating organic compounds," *Water Res.* 17, pp. 185-194 (1983).
- [111] E. Mvula and C. von Sonntag, "Ozonolysis of phenols in aqueous solution," *Org. Biomol. Chem.* 1, pp. 1749-1756 (2003).
- [112] J. E. Turner, "Atoms, radiation, and radiation protection," Pergamon press, (1986).
- [113] H. J. Fenton, "Oxidation of tartaric acid in the presence of iron," *J. Chem. Soc. Trans.* 65, pp. 899-910 (1894).
- [114] M. A. Malik, A. Ghaffar, and S.A. Malik, "Water purification by electrical discharges," *Plasma Sources Sci. Technol.* 10, pp.82-91 (2001).

- [115] A. T. Sugiarto, T. Ohshima, M. Sato, "Advanced oxidation processes using pulsed streamer corona discharge in water," *Thin Solid Films*. 407, pp.174-178 (2002).
- [116] B. R. Locke, M. Sato, P. Šunka, M. R. Hoffmann, J. S. Chang, "Electrohydraulic discharge and nonthermal plasma for water treatment," *Ind. Eng. Chem. Res.* 45, pp. 882 - 905 (2006).
- [117] C. von Sonntag, "Free radical induced DNA damage and its repair a chemical perspective," Springer Verlag, (2006).
- [118] K. H. Schoenbach, R. P. Joshi, J. F. Kolb, N. Chen, M. Stacey, P. F. Blackmore, E. S. Buescher, S. J. Beebe, "Ultrashort electrical pulses open a new gateway into biological cells," in proceedings of the 31st International conference on plasma science (IEEE 2004), Baltimore, United States, pp. 1122 – 1137, June 28-July 01 (2004).
- [119] R. P. Joshi, Q. Hu and K. H. Schoenbach, "Modeling studies of cell response to ultrashort, high-intensity electric fields – implications for intracellular manipulation," *IEEE Trans. Plasma Science* 32, pp.1677-1686, (2004).
- [120] A. J. H. Sale, and W. A. Hamilton, "Effect of high electric fields on micro-organisms. I. Killing of bacteria and yeast," *Biochimica et Biophysica Acta*. 148, pp. 781–788 (1967).
- [121] H. Chick, "An investigation of the laws of disinfection," *Journal of Hygiene*. 8, pp.92-157 (1908).
- [122] H. E. Watson, "A note on the variation of the rate of disinfection with change in the concentration of the disinfectant," *Journal of Hygiene*. 8, pp. 536-542 (1908).

ANNEXURE

CHEMICALS: Following table shows a list of chemical used for the various experiments. These chemicals were used without further purification. All compound solutions were prepared with Millipore water (resistivity = $18.2 \text{ M}\Omega\text{-cm}^{-1}$).

Compound	Formula	CAS no.	F.W. (g/mol)	Manufacturer
2 Propanaol	$\text{C}_3\text{H}_8\text{O}$	67-63-0	60.1	Merck KGaA
2-bromo-terephthalic acid	$\text{BrC}_6\text{H}_3\text{-1,4-}(\text{CO}_2\text{H})_2$, or $\text{C}_8\text{H}_5\text{BrO}_4$	586-35-6	245.03	Sigma-Aldrich
4-chlorobenzoic acid	$\text{ClC}_6\text{H}_4\text{CO}_2\text{H}$	74-11-3	156.57	Sigma-Aldrich
7 Hydroxy coumarin	$\text{C}_9\text{H}_6\text{O}_3$	93-35-6	162	Acros organics
Ammoniumheptamolybdat Tetrahydrat	$(\text{NH}_4)_6\text{MO}_7\text{O}_{24}\cdot 4\text{H}_2\text{O}$	12054-85-2	1235.86	E-Merck
CCA	$\text{C}_{10}\text{H}_6\text{O}_4$	531-81-7	190.155	Sigma-Aldrich
Coumarin	$\text{C}_9\text{H}_6\text{O}_2$	91-64-5	146.14	Sigma-Aldrich
Deuterium oxide atom 99% D	D_2O	7789-20-0	20.03	Sigma-Aldrich
Di-sodium hydrogen phosphate dihydrate	$\text{Na}_2\text{HPO}_4\cdot 2\text{H}_2\text{O}$	10028-24-7	177.99	Merck KGaA
Di-sodium hydrogen phosphate dodecahydrate	$\text{Na}_2\text{HPO}_4\cdot 12\text{H}_2\text{O}$	7558-79-4	358.20	Merck KGaA
Hydrochloric acid	HCl	7647-01-0	36.46	Sigma-Aldrich
Hydrogen hexachloriridate (IV) hexahydrate 40% Iridium	$\text{H}_2\text{IrCl}_6\cdot n\text{H}_2\text{O}$	16941-92-7	515.02	Acros organics
Hydrogen peroxide	H_2O_2 30%	7722-84-1	34.02	Merck KGaA
Indigo trisulfonate potassium salt redox	$\text{C}_{16}\text{H}_7\text{K}_3\text{N}_2\text{O}_{11}\text{S}_3$	67627-18-3	616.73	Riedel-de Haen
Iron (II) chloride tetrahydrate	$\text{FeCl}_2\cdot 4\text{H}_2\text{O}$	13478-10-9	198.83	Merck KGaA
Methanol lichrosolv	CH_3OH	67-56-1	32.05	Sigma-Aldrich
Ortho phosphoric acid	H_3PO_4	7664-38-2	98.00	E Merck
Oxalic acid	$\text{C}_2\text{H}_2\text{O}_4$	6153-56-6	126.07	E Merck
Phenolphthalein	$\text{C}_{20}\text{H}_{14}\text{O}_4$	77-09-8	318.32	Sigma-Aldrich
Potassium dihydrogen phosphate monobasic puriss p.a.	KH_2PO_4	231-913-4	136.09	E-Merck
Potassium hydrogen phthalate	$\text{C}_8\text{H}_5\text{KO}_4$	877-24-7	204.23	E Merck
Potassium hydroxide (5%)	KOH	1310-58-3	56.11	Sigma-Aldrich
Potassium Iodide	KI	7681-11-0	166.00	Carl Roth GmbH
Sodium acetate	CH_3COONa	127-09-3	82.03	Sigma-Aldrich

Sodium chloride	NaCl	7647-14-5	58.44	E-Merck
Sodium dihydrogen phosphate dihydrate	NaH ₂ PO ₄ ·2H ₂ O	13472-35-0	156.02	Merck KGaA
Sodium dihydrogen phosphate monohydrate	NaH ₂ PO ₄ ·H ₂ O	10049-21-5	137.99	Merck KGaA
Sodium hydroxide	NaOH,	1310-73-2	40.00	Merck KGaA
Sodium sulphate anhydrous	Na ₂ SO ₄	7757-82-6	142.04	E-Merck
Starch soluble ACS reagent	C ₁₂ H ₂₂ O ₁₁	9005-84-9	342.3	Sigma-Aldrich
Sulphuric acid	H ₂ SO ₄	7664-93-9	98	Riedel–de Haen
Terephthalic acid	C ₈ H ₆ O ₄	100-21-0	166.13	Sigma-Aldrich
Terephthalic acid di sodium salt 96%	C ₈ H ₆ O ₄ Na	10028-70-3	210.09	Sigma-Aldrich
Tert.-Butyl alcohol (2 Methyl-2-Propanol, Trmethylcarbinol)	(CH ₃) ₃ COH	75-65-0	74.1	Fluka
Titanium oxide sulfate hydrate (titanyl sulfate)	TiSO ₄ ·xH ₂ O		159,94	Riedel–de Haen
Unstabilized hydrogen peroxide	H ₂ O ₂ (not stabilized)30%	7722-84-1	34.02	Fluka chemie GmbH
Uridine	C ₉ H ₁₂ N ₂ O ₆ ,	58-96-8	244.20	Sigma-Aldrich
